ABSTRACT

GARDNER, TIFFANY LYNNE. Climate Warming Impacts on Precipitation in Strongly and Weakly-Forced Composite-Based Simulations in the Southern United States. (Under the direction of Dr. Gary M. Lackmann).

Extreme precipitation events result in annual damage in excess of $2B USD, and 127 deaths per year in the US. Here, we investigate the question of how weakly and strongly-forced extreme precipitation events would change in a warmer climate. Previous studies have found that in a warmer climate, extreme precipitation events could increase in intensity. The water vapor content of the atmosphere is expected to increase with increasing temperatures, potentially leading to more intense heavy rainfall along with an increased risk of severe floods. For this study, we focus on the synoptically-forced events over the southern United States during the cool season and spring season. We classify extreme events as those in which three or more inches of precipitation occurred within 24 h at three or more stations located at least 10 miles apart. A composite of these events is generated using North American Regional Analysis (NARR) data.

We use the Weather Research and Forecasting (WRF) model to simulate this composite event. The purpose of using WRF for this simulation is to enable the application of thermodynamic changes derived from the IPCC AR4 GCM data. We then compare the current to the future WRF simulated composite events to examine changes in intensity and structure of the precipitation systems. By using this method, we determine how current strongly and weakly-forced events in this region could change in a warmer climate, as well as identify environmental parameters that have a significant influence on the observed change. We find that the weakly-forced precipitation event decreases in intensity in the warmer

climate, while the strongly-forced precipitation event increases in intensity. In the strongly-forced precipitation event, the low level jet, large CAPE, and strong synoptic forcing play a large role and the increase in precipitation shows a super Clausius-Clapeyron relationship.

Climate Warming Impacts on Precipitation in Strongly and Weakly-Forced Composite-Based Simulations in the Southern United States

by
Tiffany Lynne Gardner

A thesis submitted to the Graduate Faculty of
North Carolina State University
in partial fulfillment of the
requirements for the degree of
Master of Science

Marine, Earth and Atmospheric Sciences

Raleigh, North Carolina

2012

APPROVED BY:

_____ _____

Dr. Gary M. Lackmann
(Chair of Advisory Committee)

Dr. Walter Robinson

_____

Dr. Fredrick Semazzi

BIOGRAPHY

Tiffany was born in Charlotte, North Carolina on August 8, 1988, and graduated from North Mecklenburg High School in May 2006. Tiffany has had a passion for weather since she was very young. Her parents have pictures of her when she was three years old, lying beside the window and watching the thunderstorms roll by until she fell asleep. When she was 10 years old, her family made plans to go on a cruise to the Bahamas. Their flight from Charlotte to Miami had been cancelled last minute due to an approaching tropical storm, so instead they flew into West Palm Beach and drove to Miami. While her family members spent the 70 mile drive chatting about the cruise, Tiffany spent the time watching and observing the rising flood waters that were taking over the roadways as the rain began to fall harder and harder. When they finally arrived in Miami, her family boarded the cruise ship only to find out the ship had been ordered to remain in the port for the next day while the tropical storm passed over. That night over dinner, as the passengers around her and her family complained and commented on the frustration of being stuck in Miami for an extra 24 hours, Tiffany was overjoyed with excitement as she ran from one window to the next, cupping her hands around her eyes trying to see how rapidly the flags were waving and how hard the rain was falling. Seeing her excitement, her dad took her hand, held onto it tightly, and took her outside on the balcony to feel the wind and watch the storm. While all of the other passengers were sulking in their aggravation because of the tropical storm, Tiffany was as happy as could be with the wind and rain beating against her face as she stood holding onto her dad, taking everything in around her. Her dad looked at her beaming face once they

got back inside and half-jokingly said, “You should really think about majoring in Meteorology.”

In high school, Tiffany favored math, science and chemistry over all other subjects, and when it came time to decide on what she wanted to major in during college, there was no question about it; meteorology it was! She attended the University of North Carolina at Charlotte for her undergraduate career and made the Chancellor’s List every semester, finishing with a four-year cumulative 4.00 GPA. She was selected to be the Commencement Speaker at her graduation in front of 9,000 people, as well as the student speaker for the university’s donor event. During her time at UNC Charlotte, Tiffany was fortunate to have the opportunity to perform undergraduate research with her advisor, Dr. Matthew Eastin. A research article titled “Surface Cold Pools in the Outer Rainbands of Tropical Storm Hanna (2008) Near Landfall” is published with Tiffany as a coauthor in the February 2012 edition of the Monthly Weather Review. Tiffany enjoyed her undergraduate research experience and during her senior year decided to continue her education and attend graduate school. She graduated in May 2010 and accepted the offer from North Carolina State University to attend graduate school and pursue her M.S. of Atmospheric Science beginning in August 2010. Tiffany has had the honor of working with Dr. Gary Lackmann, who has encouraged and pushed her to reach her goals while offering his advice and guidance every step of the way.

ACKNOWLEDGMENTS

I would like to first thank my advisor, Dr. Gary Lackmann. His unwavering support, guidance and encouragement greatly contributed to the completion of this research study. I would also like to thank Drs. Semazzi and Robinson for their feedback and advice. I have learned valuable skills from all of these professors, as patience, persistency and hard work have been required and praised. Through them, I have learned how to be a better scientist and reach my research and educational goals.

Support for this research was provided by the U.S. National Science Foundation (NSF) grant AGS-1007606 and the U.S. Department of Energy (DOE) grant ER64448 awarded to North Carolina State University. I would like to express my great appreciation and gratitude for the funds provided to complete this project. I would also like to thank the National Center for Atmospheric Research (NCAR) for making available the Weather Research and Forecasting (WRF) model, which was used extensively throughout this study. A special thank you also goes to the Program for Climate Model Diagnosis and Intercomparison (PCMDI) for collecting and archiving the CMIP3 model output, as well as the World Climate Research Program's (WCRP) Working Group on Coupled Modeling (WGCM) for organizing the model data analysis activity.

The majority of the data collected was acquired from the Dartmouth Flood Observatory, directed by Dr. G. Robert Brakenridge. His dedication to this active archive of large floods contributed greatly. The rain gauge data provided by the National Climatic Data Center (NCDC) was also used, and my sincere appreciation goes out to them as well.

My labmates, Briana Gordon, Whitney Rushing, Megan Mallard, Chris Marciano, Jordan Dale, Michael Graves, and Allison Camras, have been always been there for support, brainstorming, and friendship, and am I very fortunate to have landed in such a tightly-knit and determined research lab. I would also like to thank my friends and fellow graduate students in the NCSU MEAS department, specifically Jeff Willison, Michelle Cipullo, Sofia Montalvo, and Katie Costa, for their unwavering help, laughter and friendship along the way.

Lastly, I would like to thank my family and friends. Their kind words have given me confidence and their encouragement has pushed me toward success. Through love, devotion, consolation and inspiration, they have been there every step of the way and I am very blessed to have such a strong support system behind me.

TABLE OF CONTENTS

LIST OF TABLES

LIST OF FIGURES

1. Introduction

1.1 Motivation

Extreme precipitation events are widely studied because they impact many facets of our society and are yet still fairly challenging to predict (Lenderink and Meijgaard 2010). This research focuses on individual extreme precipitation events that resulted in large floods, which is one of the biggest problems associated with these extreme events. In the United States, floods are the number one cause of deaths associated with thunderstorms, overshadowing deaths caused by lightning, tornadoes, wind and hail (NWS 2011). According to the National Weather Service, as of 2011 the average number of deaths caused by flooding in the past 30 years is about 94 deaths per year. In 2011, the total damage caused by flooding in the United States was approximately $8 billion USD (NWS 2011). These statistics are just two of many, and over the years many researchers have taken on the task of studying these events. Despite the challenge in predicting them though, there is a broader understanding today of extreme precipitation events in the present-day climate, however, the question still remains as to how they will change in a warmer climate.

Extreme precipitation events cause flooding, erosion, and damage to life and property. With warmer temperatures and the increase in water vapor content, if extreme precipitation events intensify, there is a greater risk of flooding (Milly et al. 2002). The runoff associated with this extreme precipitation intensification can cause additional consequences to the infrastructure and environment (Christensen and Christensen 2004). These impacts will be discussed further in sections below. Understanding not only extreme precipitation events, but how they could change in a changed climate is necessary in order to

react and mitigate impacts.

Light precipitation events are also of great interest because they have implications for droughts. If the light precipitation decreases in a warmer climate, areas that see little precipitation could experience a further decrease. The previous literature associated with light precipitation events and climate change is discussed below, but a decrease in light precipitation events could affect the agriculture, water supply, and human health, and it is necessary to understand the impacts of a warmer climate on these as well.

There are two main questions associated with this better understanding for both light and extreme events. First of which, what does the atmospheric pattern look like prior to these precipitation events? This could be useful for forecasters. Secondly and more importantly, how could these events change in a warmer climate? This is important for city planners and water management companies, among others. A main question that researchers strive to understand is whether or not in a future climate with warmer temperatures, will the extreme events be more extreme and if so, will positive feedback loops between precipitation and another factor result in an increase in precipitation that exceeds the increase in moisture content?

There are many methods used to estimate the amount of precipitation, including rain gauge, satellite and radar data. Modern Numerical Weather Prediction (NWP) systems employ data assimilation techniques where observations are combined with results from a short-term forecast to provide the best analysis for a given time. The WRF model is used extensively in this research, and is also widely used across the world for atmospheric research and operational forecasting. This computationally efficient and versatile model

allows researchers to run case study or idealized simulations over the continental United States. A more detailed description of this model and its application will be discussed in Chapter 2.

Using the WRF model to study precipitation events and how they could change in a changed climate is not unusual, however, the method used in this study has not been widely used in previous research studies. Here, a composite is created from individual extreme precipitation events, so instead of running either a case study or idealized simulation, it is a combination of both, resulting in a pseudo-idealized-case study simulation. This method is unconventional but it allows for a highly representative simulation of a certain type of event; in this case, cool season synoptically-forced extreme precipitation events.

Using a composite to initialize a model is a new approach and has been done in only a handful of other studies that will be discussed further in the next section on previous literature. This upcoming section will also examine the previous studies that have researched the effects of climate warming on mean and extreme and light precipitation events, the impacts in changing the thermodynamic or dynamic components, different future scenarios that can be applied, and possible feedback loops between the projected changes in precipitation and other factors.

1.2 Literature Review

Section 1.2.1 covers the climatology of the southern United States and present-day precipitation patterns. Section 1.2.2 discusses the future implications of climate change projections and the subsections examine in further depth the approaches and results found in

previous studies on this matter. Section 1.2.3 analyzes the composite approach used here with examples from recent studies.

1.2.1 Southern United States Climatology

The climatology today in the southern United States can be described as rainy and temperate with hot summers. There is no dry season as rain falls throughout the year, and the majority of the rain falls in the summer mainly from thunderstorms and tropical systems (Bailey 2009). There are many different atmospheric forcings that cause precipitation, and a few in particular that cause extreme precipitation. In 1979 Robert Maddox studied 150 heavy rainfall events and determined there are three primary types of systems that cause heavy rainfall; frontal, meso-high, and synoptic patterns. Maddox excluded tropical events from this research however, for this study, tropical events were included.

Meso-high events are convective and develop near the axis of an upper level ridge. They are common where the shear and the winds are weak (Fig. 2.1). In this type of event, the greatest threat of heavy rainfall is in the southern or western portions of the meso-high (Maddox 1979). The frontal events often occur near a 500mb ridge as well where the mid-level flow is fairly weak. This type of event primarily occurs at night, and the greatest threat of heavy precipitation is to the east of the warm moist tongue of air reaching up from the south (Maddox, 1979). Synoptic events were the last type Maddox studied. These generally occur in the spring and early summer, or fall and early winter. They are associated with a strong 500mb trough that is moving to the east or northeast and frontal boundary oriented from the southwest to the northeast. In this type, the heavy precipitation is usually located in

the warm sector however, it can also be collocated near an old frontal boundary or under the right entrance region of an upper level jet streak (Maddox, 1979).

Finding that these are the type of atmospheric patterns that result in heavy precipitation was a great advancement in the understanding of extreme precipitation events, however, one of the main concerns today is how will these patterns, and the resulting extreme precipitation events, may change in the future. An understanding in the changes in the frequency, intensity, location, type and total amount of precipitation in a warmer climate is essential, and studying all of these in relation to extreme events is necessary. The next subsections will discuss in more depth research performed on these topics and their findings.

1.2.2 Future Projections and Implications

The Clausius-Clapeyron equation states that the water vapor increases by about 7% for every 1°C temperature increase,

$$\ln\frac{e_s}{6.11} = 5.42\text{x}10^3\left(\frac{1}{273} - \frac{1}{T}\right) \qquad (1.1)$$

where P is the saturation vapor pressure, T is the temperature, L is latent heat, and v is the volume. So with future warming, the atmospheric water vapor content also increases. If the relative humidity remains constant, then the atmospheric vapor content must increase.

Trenberth (1998, 1999, 2003), Allen and Ingram (2002), Chou and Neelin (2004), Emori and Brown (2005), Held and Soden (2006), Chou et al (2011), and many more have performed extensive research on this topic of how precipitation events could change in a future warmer climate. In terms of where the precipitation will fall in a warmer climate, Neelin and Chou in 2004 found that wet areas will get wetter and dry areas will get dryer in

the tropics. With the increase in atmospheric water vapor, more moisture will be available and the moisture transport increases from the subtropics to convergence zones resulting in "the rich get richer and the poor get poorer" (Chou and Neelin 2004).

On top of this, because of the increase in moisture the winds can be less in magnitude and still accomplish the same moisture transport, giving rise to the phrase "more bang for your buck" (Held and Soden 2006). With the increase in moisture and resulting intensification of extreme precipitation events, there is a greater risk of flooding in a warmer climate. In 2002, Milly et al. found that the frequency of great floods increased significantly in the twentieth century due to the intensification of the global hydrologic cycle caused by climate change, and that this significantly increasing trend is expected to continue. The intensification of heavy precipitation events and the surface runoff associated with it can have disastrous consequences, such as irreparable property damage and loss of life (Christensen and Christensen 2004).

Compared to the mean precipitation, studies have found that while the mean increases in future simulations, the extreme events increase more (Allen and Ingram 2002; Kharin and Zwiers 2005; Emori and Brown 2005; Shiogama et al. 2008). The reason for this can be found in the energy budget. The large-scale mean precipitation events are constrained by the atmospheric energy budget, however, the extreme precipitation events are associated with increases in the atmospheric moisture content. Because of this, the nonlinear relationship between the extreme precipitation events and the the Clausius-Clapeyron equation make it such that for a specific temperature increase, the intensification of the extreme precipitation events can be larger than the mean precipitation events (Allen and Ingram 2002).

The great majority of studies show that in a warmer climate, the mean precipitation will increase. As mentioned above, many also suggest that the extreme precipitation will intensify more than the mean, but the question now is will the extreme precipitation increase at the same rate as the Clausius-Clapeyron equation or will the extreme precipitation events intensify at a faster rate, and more importantly, why? This will be discussed in more detail in the next subsection. To study this, Emori and Brown in 2005, Seager et al. in 2010, and Chou et al. in 2011 examined the effects of changing the thermodynamic and/or dynamic components in their future simulations to see how the precipitation was affected. This same method is applied in this research and will be discussed in section 1.2.2.2.

1.2.2.1 Extreme Events and the Clausius-Clapeyron Relation

The Clausius-Clapeyron relation, named after Rudolf Clausius and Benoît Paul Émile Clapeyron, is an equation that relates saturation in water vapor content to temperature. Mathematically, it shows that the change in the saturation vapor pressure by the change in temperature is equivalent to the latent heat of evaporation divided by the product of the temperature and the change in the volume. In other words as the temperatures rise, the vapor capacity increases, and more specifically, for every degree Celsius increase, the low level vapor capacity increases by roughly 7% for the range of temperatures in question (Soden et al. 2005). The question today though is whether or not the extreme precipitation events will increase at this Clausius-Clapeyron rate, or will the extreme precipitation events intensify at a faster rate? Based on previous literature it is expected to increase at a faster rate, which will be discussed more in section 1.3, but more importantly the question to be answered is why

would it increase at this faster rate?

Some studies suggest that the precipitation will increase by the Clausius-Clapeyron relation, while others suggest the precipitation could increase faster than this relation. With the relative humidity held constant and the specific humidity and atmospheric moisture increasing exponentially with increases in temperature, it is argued that the heaviest precipitation events are expected to increase with the Clausius-Clapeyron equation acting as a constraint (Frei et al. 1998; Hennessey et al. 1998; Pall et al. 2007). Other studies however, suggest that a super Clausius-Clapeyron relation is expected for the extreme events (Allen and Ingram 2002; Held and Soden 2006; Allen and Soden 2008; Lenderink and van Meijgaard 2010).

A super Clausius-Clapeyron relationship exists when the precipitation increases at a faster rate than 7% per degree Celsius. Allen and Soden in 2008 found in their study that in a warmer climate the frequency of intense precipitation events increases while the frequency of light to moderate precipitation events decreases. It is also suggested that the extreme precipitation events will be more localized in a warmer climate, and instead of widespread heavy precipitation events, there will be more short duration events with larger amounts of precipitation over a smaller area (Lenderink and van Meijgaard 2010).

The reason this super Clausius-Clapeyron relationship occurs is important to understand in order to have a better understanding of how the extreme precipitation events will differ in a changed climate. This super relation occurs because although the increase in atmospheric moisture plays a large role in the increase of precipitation, dynamical factors also influence the intensity of precipitation events. Lenderink and Meijgaard, who found a

14% increase in precipitation extremes per degree Celsius, point to the physics in a convective cloud as the main driving dynamical factor responsible for the amplified rate of precipitation intensity. With more rainfall there is more latent heating, which creates stronger updrafts and a possible increased rate of condensation formation in the cloud and ultimately a higher rainfall rate (Lenderink and Meijgaard 2010). This is one type of positive feedback loop that could be playing a role. This, as well as another positive feedback loop examined in this study as a possible mechanism will be discussed in more 1.2.2.3. Before looking at positive feedbacks though it is important to better understand first what atmospheric factors have a strong influence on the intensification of extreme rainfall events. One way to do this is to separate the thermodynamic and dynamic components in order to determine to what extent do each impact the precipitation events.

1.2.2.2 Thermodynamic and Dynamic Component Impacts

As mentioned above, the majority of studies show that the extreme precipitation events are projected to intensify more than mean precipitation events in a warmer climate, but what specifically causes this intensification is still not clearly understood. To test this, researchers have examined the thermodynamic and dynamic components impacts on extreme precipitation events by isolating one or the other to determine which has the greater impact on this projected intensification. Atmospheric dynamics are associated with the change in atmospheric motion and the thermodynamic components are associated with the change in temperature or the atmospheric moisture content (Emori and Brown 2005; Seager et al.

2010). By isolating one of these two types, researchers can determine how much of an impact that certain type has on the projected changes, thereby getting one step closer to a better understanding of the mechanism behind the intensification of extreme events.

One study by Emori and Brown in 2005 did this very experiment. They separated dynamic and thermodynamic components of projected mean and extreme precipitation changes from 6 climate model experiments to explore how the increase in atmospheric moisture affects the changes in both mean and extreme precipitation. All of the data was spatially interpolated to a ~2.81° grid. They found that the dynamic component is limited to the lower latitudes and plays a secondary role between mean and extreme precipitation changes, whereas the thermodynamic component has the largest impact on changes in the mean and extreme precipitation. The last finding was that the increases in the mean and extreme precipitation were comparable in magnitude to the increase in the thermodynamics (Emori and Brown 2005). Another study in 2005 by Meehl et al. pointed out that while the thermodynamic properties play a large role in the intensification of precipitation events, changes in the atmospheric circulation also impact the location and intensity changes of precipitation.

In the current study, the thermodynamic properties are changed but the synoptic-scale properties are kept the same. The end result is a future simulation that has a synoptic pattern similar to the present day run but warmer temperatures. The advantage of using this approach is that changing the thermodynamics and keeping the synoptic-scale dynamics the same, it is possible to see how the meso-scale dynamic components respond to the thermodynamic change. This is important to see how certain feedbacks, such as the low level jet, might

amplify the extreme events by bringing more moisture into a certain region. A large part of the analysis focuses on the low level jet as well as the vigor of the convection, and this will be discussed in more detail in the section below.

1.2.2.3 Extreme Precipitation and the Low Level Jet: The Positive Feedback Loop

Low level jets are elongated areas of wind maxima that are essential to the transport of warm air and moisture into certain regions of the world. Numerous studies suggest there is a positive relationship between precipitation and these low level jets (Mo and Paegle 1994; Stensrud 1996; Paegle et al. 1996; Hu and Feng 2001; Lackmann and Gyakum 1999; Lackmann 2002). This study focuses specifically on the southerly low level jet that pumps warm, moist air into the southern and central states from the Gulf of Mexico. The jet transports moisture from the tropics to these states, creating additional instability from the warmer temperatures, and precipitation, making the jet a vital ingredient in the development, evolution, and sustainability of floods over the southern and central United States (Mo et al. 1995; Paegle et al. 1996).

In section 1.2.2.1 a possible dynamical feedback was mentioned pertaining to the relationship proposed by Lenderink and Meijgaard (2010) between precipitation and convective clouds. This study examines a possible feedback between the low level jet and extreme precipitation events. Low level jets transport moisture into areas which amplifies precipitation events. Condensation and precipitation release latent heat which acts to strengthen surface low pressure systems including the southerly flow to the east of the system and the northerly flow to the west of the system. This intensification of the low pressure

system and southerly flow can strengthen the low level jet, which in turn can transport even more moisture into the area resulting in more condensation and precipitation, and so on and so forth, making this a positive feedback loop between the low level jet and precipitation (Brennan et al. 2008). In a warmer climate, with more moisture and potentially more condensation, the question examined in this study is will there be a stronger low level jet?

The implications associated with a stronger low level jet have dire impacts on extreme precipitation events because it is that extra dynamical ingredient that could contribute to a super Clausius-Clapeyron relation. When the temperatures are warmed and the water vapor content increases at a rate of 7% per degree Celsius, it is expected that the precipitation amounts will increase as well. When another forcing, such as the low level jet or enhanced convection, is thrown into the mix though, the precipitation amounts can increase at a rate faster than the vapor. This is analyzed in detail in this research to first determine if the low level jet or the convective updraft strength does indeed intensify, and secondly, if the precipitation increases at a faster rate than the vapor by means of a super Clausius-Clapeyron relation.

1.2.3 Composite Approach

A composite approach is used in this research to streamline the results of numerous individual event simulations. A composite is an aggregate of different elements; in this case, those elements are extreme precipitation events. The events in this study were selected based on a rigorous classification process, which will be discussed in Chapter 2. Particular variables are combined from these individual events together, creating one "event" that

represents the whole group ideally. This approach uses the composite event to drive a simulation of a present-day case and a future case, in which the composite datasets are used as the initial and boundary conditions for the model runs. This approach is unconventional as most of the model runs today are either case study or idealized simulations; by combining variables from numerous events, the composite is somewhat of an idealized-case study simulation and the number of studies that have used composites to initialize a model are far and few between. Ideally, the composite-based simulations, though, are highly representative, pseudo-idealized simulations of these extreme precipitation events and by using this composite approach, only two simulations total are analyzed as opposed to two per event (present-day and future). Although this is a fairly new technique to use, it has been done before in a handful of other studies (Nachamkin et al. 2005; Lackmann 2007; Mahoney 2012; Zhao 2012). A couple of these studies will be touched on briefly in the subsections below to show how composites were used for other events.

1.2.3.1 Case Study #1: Changes in Hail and Flood Risk

In 2012, Mahoney et al. studied the impacts of climate change on the frequency and intensity of hailstorms in Colorado's mountains. The authors state that although hailstorms are generally associated with the property and crop damage that they cause, hailstorms are very useful in the prevention or delaying of floods; since hail takes a certain amount of time to melt before it turns into runoff, floods do not occur right away as opposed to heavy rainstorms (Mahoney et al. 2012).

For their study, the authors used composites to represent the top ten largest

precipitation events from June to August from 1971 to 2000 for the present-day simulation and 2041 to 2070 for the future simulation. The North American Regional Climate Change Assessment Program (NARCCAP) regional climate models (RCMs) are used for this first step and they span 30 years in the past and 30 years in the future. They are used with a 50 kilometer grid spacing and the A2 scenario, and the extreme precipitation events from NARCCAP are downscaled further using the WRF model. The WRF model version 3.1.1 was employed for the high-resolution model runs and it was initialized about 6 hours before the largest 3 hour precipitation total of the event. The duration of the simulations was 24 hours and the output from the model was hourly.

The authors found that most of the simulations showed a significant decrease in hail near the surface in the future simulation. The reason determined for this near-elimination of surface hail is due to the increased height of the environmental melting level in the warmer climate. The results from the study are not relevant to this work however, the use and application of the composite method in it is important.

For the composites events, the temperature, moisture and winds are all vertical levels were averaged together from the top ten heavy events for the present-day and then again for the future, and these composites were used as the initial and boundary conditions for the simulations. The authors state that for "clarity and conciseness", the composite approach was used in their research because instead of comparing twenty simulations all at once, they have the choice to only compare two (Mahoney et al. 2012).

1.2.3.2 Case Study #2: Lake-Effect Precipitation

Also in 2012, Zhao et al. used the composite approach to evaluate the impact of remotely sensed lake surface temperature and lake ice cover over the Great Lakes region on precipitation simulations using the WRF model version 3.2 in order to make improvements. The composite was created from eleven typical lake-effect events at Buffalo, New York. The authors first used hourly observations from Buffalo to determine which events lasted more than six hours. Secondly, radar reflectivity images were used from the National Climatic Data Center (NCDC) to see in which of the events did the reflectivity develop over Lake Erie and Lake Ontario but was not a result of the synoptic set up; this determined a typical lake-effect event over Buffalo. The events were then divided into two stages, the first being the initial stage when the first precipitation amount was recorded at Buffalo and the second being the demise stage when last time the precipitation amount was recorded.

The authors found that integrating Moderate Resolution Imaging Spectroradiometer (MODIS) lake surface temperature (LST) and National Ice Center (NIC) lake ice cover (LIC) improved simulations of lake-effect precipitation over the Great Lakes region. The results from the study, as in the previous section, are not pertinent to this work however, the use of the composite approach is relevant. The variables from these eleven events were averaged together from the initial stage to the demise stage to create the composite lake-effect precipitation event. As in the previous example, the composite here was used to show a more direct depiction of this type of event for clearer cut results and analyses.

1.2.3.3 Potential Problems and Benefits

There are a few concerns associated with using the composite approach. Since a composite is an aggregation of variables from individual events, it is possible to smear some of the data and weaken the forcings of interest. For example, if one wants to use a composite to study the intensity of the polar jet, using a time period of all twelve months is not efficient or accurate, and the composite will show a very weak representation of the intensity of the jet. The reason for this is that the polar jet shifts north and south depending on the time of year due to the temperature gradients. In the winter the jet reaches farther to the south and is more intense, and in the summer when the temperature differences are not as great, the polar jet is farther north and weaker. Because of this, when one is averaging together the most southern extent of the jet when it is at its peak intensity, and the most northern extent of the jet when it is weakest, the two will cancel each other out and the product will be somewhere in the middle with an average intensity. Unless the intention is to have a yearly average of the jet, a better representation of the polar jet would be to create seasonal composites that show the average positions and intensities of the polar jet during the different times of the year.

As noted above, there are many benefits to using the composite approach if it is done correctly. Composite simulations are highly representative, pseudo-idealized simulations. They essentially filter out small-scale details giving a clearer signal, such as the low level jet or low pressure system, to analyze. A rigorous method to determine what events are being composited is necessary to ensure the composite is the very best representation of that certain event. Using composites allows researchers to show very compact and to-the-point results without overwhelming the audience with numerous plots that would show the same findings.

As Mahoney et al. prefaced the composite approached in their 2012 study, the composites show clear and concise results. Instead of displaying and comparing over twenty present-day and future simulations at one time, with the composite approach there is only one present-day simulation and one future simulation to compare.

1.3 Hypothesis

The aim of this study is to determine how cool season strongly-forced precipitation events and springtime weakly-forced precipitation events in the southern United States will change in a warmer climate. To do this, we change the thermodynamic components to see how the dynamic components respond, specifically the low level jet and the convective updraft strength, to get a better understanding of what is behind the observed changes in precipitation. Many studies have investigated the impacts of climate change on extreme and light precipitation events however, this study is different in that it uses composites in conjunction with a model as the approach to identify these changes. We create a composite event from previous extreme precipitation events and run a simulation of the composite using the WRF model. The details on the configuration of the model will be discussed in Chapter 2.

There is one main hypothesis for this study but before discussing that it is important to bring attention to a few points. First of all, the light precipitation events are expected to see a decrease of the precipitation in a warmer climate. This result has been found in other studies (Allen and Ingram 2002) and for the next two points to be correct due to the water budget restrictions, the light precipitation is expected to decrease. Secondly, more precipitation is expected in a warmer climate. As mentioned above, with warmer

temperatures and an increase in the water vapor content, the precipitation should increase as well but we are analyzing the rate at which it increases; is it constrained by the Clausius-Clapeyron relation of 7% per degree Celsius or does it increase at a faster rate showing a super Clausius-Clapeyron relation? So for our hypothesis, with increased water vapor content, we expect there to be an increase in the strength of condensationally-driven dynamical factors which serve to amplify precipitation increases beyond the Clausius-Clapeyron implied vapor increase. With potentially more condensation and more latent heat being released, the low level jet, for example, can strengthen resulting in a positive feedback loop with the precipitation (Fig. 1.1). Nonlinear factors contribute greatly to super Clausius-Clapeyron relationships as they serve as an extra forcing that can produce even more precipitation than there would be already.

1.4 Thesis Outline

Chapter 2 will cover the methods involved in this research. It will explain in detail the approach used for classifying the precipitation events, the creation of the composite event, the configuration of the WRF model, and the application of climate change. Chapter 3 discusses and analyses the results of the light and extreme precipitation composites, present-day simulations and future simulations. Plots are used to show similarities and differences between the simulations in terms of the precipitation totals and spatial extent and the dynamical responses. Chapter 4 summarizes the findings and relates them back to the main hypotheses. This chapter also discusses the implications behind the findings and outlines advisable future work.

2. Methods

The first section below describes the classification process for the extreme precipitation events. The second section entails the creation of the composite event, and the third section discusses the configuration of the WRF model. Finally, the fourth section details the application of climate change parameters to the composite.

2.1 Extreme Precipitation Event Classification

The data for the precipitation events used in this research were obtained from the Dartmouth Flood Observatory and NCDC. The North American Regional Reanalysis (NARR) grib data were collected from two days prior to, the day of, and one day after each event. The reason for this is to capture and understand the synoptic pattern leading up to the event. Prior to gathering the data though, a classification process was carried out to determine which events were indeed extreme precipitation events. This selection process is discussed in the subsections below.

2.1.1 Data Collection

The first step in this process is to use the Dartmouth Flood Observatory to identify when and where large floods occurred in the United States. The Dartmouth Flood Observatory is an active global archive of large floods from 1985 to the present. In the current research, the years 1985 through 2011 are used. On the Dartmouth Flood Observatory website, all the floods are recorded in a spreadsheet with the cause for the flood, the region and time it occurred, the severity, and the number of fatalities among other factors.

For this research, the floods that occurred in the United States and were caused by heavy rains are selected.

The next step is to narrow down these large floods caused by heavy rains to determine which rain events were the most extreme. To do this, NCDC rain gauge data are used. NCDC rain gauge data shows both hourly and daily precipitation totals, however, for this study only the daily totals are used. For each flood event, every state listed in the Dartmouth Flood Observatory as being affected is searched in the NCDC database and the total daily precipitation is examined. Here, we define extreme events as those in which the total daily precipitation was three or more inches at two or more stations separated by at least ten miles. The reason behind using two or more stations is to minimize error in the rain gauge data. For example, if one location had a very high precipitation total and no others around it did, it could possibly be an error in the data. If there was a very large value at a neighboring location on the same day though, there is a greater probability it is correct.

In summary, the extreme precipitation events chosen for this research underwent a selection process and consist of every individual heavy rainfall event that, according to the Dartmouth Flood Observatory, caused a great flood that occurred in the United States between 1985 and 2011 where at least three inches of precipitation fell in twenty four hours or less at two or more stations separated by at least ten miles. After performing this process, 136 extreme precipitation events are identified. The next step is to categorize these extreme precipitation events by meteorological pattern, and this categorization will be discussed in the subsection below.

2.1.2 Extreme Event Categorization

Once the extreme precipitation events are identified, the next step is to arrange them by season, region, and synoptic pattern. Each of the four seasons consists of three months. The regions examined are the south, southwest, southeast, east, northeast, northwest, north, west, and central United States (Fig. 2.1). The separation of the states into each region was based on the geographical area they fall in. The regions and seasons are based on geography and climatology, but the flooding type category is based on a study by Maddox et al. (1979).

Maddox et al. studied 150 heavy rainfall events and came to the conclusion that three primary types of systems cause this heavy precipitation; meso-high, frontal, and synoptic atmospheric set ups. Although Maddox et al. excluded tropical events from their research, tropical events are examined in this study. Here, we define tropical events as any event in which a tropical cyclone crossed over an area, as seen in the North American Regional Reanalysis (NARR) four-panel plots in conjunction with the National Hurricane Center (NHC) archives, at the time the heavy rainfall was recorded. Out of the three Maddox heavy precipitation inducing systems, each has characteristics differentiating them from the others.

Meso-high, or convective, systems develop near the axis of an upper level ridge where the winds and the shear are weak (Fig. 2.1a). In this system, the greatest threat of heavy precipitation is in the southern or western portions of the meso-high. Frontal systems also occur near an upper level ridge where the mid-level flow is fairly weak, but they are associated with a frontal boundary oriented from west to east and they primarily occur at night (Fig. 2.1b). In this type of system, the greatest threat of heavy precipitation is to the east of a warm, moist tongue of air reaching up from the south. Finally, the synoptic systems

are the third type and these systems differ greatly from the other two types. Instead of occurring near an upper level ridge, this type of system is associated with a strong upper level trough moving to the east or northeast with a frontal boundary oriented from the southwest to the northeast (Fig. 2.1c). They primarily occur in the spring and early summer or fall and early winter. In this type of system, the greatest threat of heavy precipitation is usually located in the warm sector however, it can also be collocated with an old frontal boundary or under the right entrance region of an upper level jet streak (Maddox et al. 1979).

Four panel plots of North American Regional Reanalysis (NARR) data are used to summarize the atmospheric pattern for all of the 136 extreme precipitation events is analyzed in order to determine what type of atmospheric pattern was dominant. The upper level plots are used to identify the location of the upper level ridge or trough in conjunction with the location of the extreme precipitation, and the surface map is used to identify frontal boundaries and their orientations. The extreme precipitation events are then separated into one of the three Maddox categories or the tropical category, which consists of tropical cyclones, based on the atmospheric pattern that caused the heavy precipitation.

To summarize the categorization process, all of the 136 events are categorized based on the season they occurred in, the region in, as well as the flooding type. The reason for differentiating and categorizing these events is because when making a composite, the most similar events must be used together and in order to do that it is best to identify these common characteristics at the very beginning. After categorizing all of these events in an Excel spreadsheet, the next step is to create the composite by using the congruent events.

2.2 Creation of the Composite Event

We created two composites using synoptic-type events. The reason for using this type was because the majority of the events were synoptic-type and we wanted to use the most number of cases possible for a better representation. The first composite is created using nine extreme precipitation events that occurred in March, April, and May in the southern states of Texas, Louisiana, Mississippi, and Alabama (Fig. 2.2a). This composite shows a strong synoptic forcing event with a pronounced upper trough. The details and results of the present-day and future simulations for this composite are discussed in Chapter 3 and it is in that chapter referred to as the strongly-forced event.

After creating this strong composite, we decide to create another composite that consists of more events in a more geographically confined area in hopes that the new composite would be an event better representation of this certain type of event. That being decided, an even larger composite is constructed. This composite consists of cool season events, or those occurring from September through May, within a box bounded by the latitude and longitude coordinates of 28°N to 37°N and 85°W to 94° W, respectively (Fig. 2.2b). This area covers the states of Louisiana, Mississippi, western and central Tennessee, and Arkansas. Originally there are seventeen events that fit these criterion but in order to ensure that the synoptic patterns are similar in the individual events, the events undergo one more process before being selected. The last part of the selection process is that each of the events must have a 500mb trough axis or closed low located over the western United States between 115°W and 90°W at 12Z with associated vorticity values greater than or equal to $20\text{x}10^{-5}s^{-1}$. This narrows the events down to thirteen, and these thirteen are the final events

used to create the composite. By narrowing down the areal coverage of the composite and increasing the number of months, the composite contains more extreme precipitation events however, the event showed weaker synoptic and mesoscale forcings than the first composite. We expected this new composite to have even stronger forcings, but the opposite happened. Even though we constrained the locations of the troughs in the individual extreme events, more smearing of the data occurred resulting in a weakly-forced event rather than an extreme one. The results from the present-day and future simulations run using this composite are discussed in Chapter 3, and in that chapter this is referred to as the weakly-forced event.

Once the events are selected to use for these composites, the first step is to gather the NARR grib data and convert it from grib files to GEMPAK files. Specific c-shell and Fortran programs are used for these conversions. The GEMPAK files created are hourly files, so a separate script is used to create daily files from the individual hourly files.

For each composite, all of the basic parameters at every level from the selected extreme precipitation events are combined together to create one highly representative composite event so that the composite can be used to initialize WRF. The first parameters composited are the temperatures, horizontal wind components, specific humidity, and geopotential heights at all vertical levels from all of the events. The relative humidity is computed using a different script for all of the levels as well. These variables show a good representation of the atmospheric pattern, but it is necessary to composite surface data as well. Three soil parameters at four layers were composited next, as well as the surface pressure, surface temperature and sea level pressure. The last variables composited are the horizontal wind components at ten meters, and the temperature, relative humidity, and

specific humidity at two meters. With all of the individual event variables composited into one event, it is important to examine the data in order to understand the synoptic setup, ensure it is representative of the Maddox et al. synoptic type event and that the winds are geostrophic aloft, and lastly to see that the progression of the synoptic pattern is reasonable.

Once these steps are carried out and it is reinforced these composites are a very realistic representation of these types of event, the composited gempak files are reconverted back to grib files, which are then used in the WRF Preprocessing System (WPS) and the WRF model. Configurations of the WRF model are discussed in the section below.

2.2.1 Individual Cases of the Composites

Before moving to the next subsection, it is important to first discuss the individual cases that created the composites. The first step was to use the Dartmouth Flood Observatory active archive that consists of "large flood events" from 1985 to the present. The floods are categorized based on the region in the world that they occurred, the dates they occurred on, the duration of the flood, the number of causalities, and the cause of the flood, among many other categories. Out of all of these flooding events, the floods that occurred in the United States and that were due to heavy rainfall were selected. These selected events were then narrowed down using the extreme precipitation event categorization, by which all events where three or more inches of rain fell in 24 hours or less at two or more NCDC rain gauge stations separated by at least ten miles were the extreme events used for this research.

Total, there are 136 extreme precipitation events from 1985 to 2011. These events are separated into tropical events and the three Maddox heavy precipitation categories; synoptic,

mesohigh, and frontal. Out of the 136 events, 4.4% are mesohigh, 5.1% are frontal, 23.5% are tropical, 67% are synoptic, with the total number of events for each category being 6, 7, 32, and 91, respectively (Appendix A). Because the majority of the events are synoptic, the synoptic-type events are used to create both composites in this research because this yields the most number of cases thereby, ideally, yielding a better representation of the events.

2.3 WRF Model Configuration and Application

For this study, the Weather Research and Forecasting model (WRF) version 3.2 is used. The WRF model was created by the National Center for Atmospheric Research (NCAR) to serve both operational forecasting and research demands. It is a nonhydrostatic, fully compressible regional numerical weather prediction model featuring many dynamical cores and a three-dimensional variational data assimilation system. The WRF model allows users to run idealized or case study simulations and it is applicable for many different applications across large spans of distances. For a more detailed description of the WRF model, refer to Skamarock et al. (2008).

For this study three domains are used with nest domain values of 36, 12, and 4 kilometers. The event is simulated for 72 hours with a 120 second time step, starting at 12Z on the first day of the composite and ending at 12Z on the last day. Because nine and thirteen events are used to create the strongly and weakly-forced composites, respectively, and each individual event falls on a different month and day, it is necessary to select one date from them to use for the WRF simulation in order to have the correct radiation. For the nine event composite, because all of the events fell in March, April or May, the dates of the events are

averaged together and the resulting date, April 14, is the date selected. For the thirteen event composite the number of days between the event and the winter solstice are calculated for each individual event, added together, and then the sum is divided by thirteen. The resulting number is 88, and when 88 days are added onto December 21 the date is March 19. So, for the nine event composite and the thirteen event composite, April 14 and March 19, respectively, are the date used for the composites and WRF simulations.

For both the weakly and strongly-forced events, the cumulus parameterization scheme used is Betts-Miller-Janjic for the first two domains. The WSM6 microphysics scheme is used for all three domains, which is a single moment, six-class scheme containing graupel. For the radiation schemes, RRTM is used for the longwave radiation and MM5 shortwave (Dudhia) is used for the shortwave radiation. RRTM is a spectral scheme with a specified profile of ozone and constant, well-mixed carbon dioxide. The Dudhia shortwave scheme contains a simple downward calculation and includes water vapor and cloud absorption and cloud albedo. For the surface schemes, the atmospheric surface layer scheme used is the Monin-Obukhov, and this is used as suggested with the Mellor-Yamada-Janjic (MYJ) Planetary Boundary Layer (PBL) scheme. The MYJ scheme was selected as it has the reputation of handling the low level jet with more accuracy over the YSU PBL scheme. With these, the Noah Land Surface Model is used, which includes heat and moisture fluxes from for the planetary boundary layer and predicts the soil moisture and soil temperature in four layers to determine the skin temperature. All of these schemes are used not only for all three domains, but they are used for all three domains in both the present-day and future simulations for both the strongly and weakly-forced event.

With these schemes, the present-day simulations are run using the composites for the initial and boundary conditions. The next step is to apply climate change parameters to the present-day composite event by altering the thermodynamic properties, through which the response of the dynamic components, such as the low level jet, is observed and analyzed. This technique is explained in more detail in the section below.

2.4 Application of Climate Change Parameters

The Intergovernmental Panel on Climate Change (IPCC) uses greenhouse gas emission scenarios, discussed in the Special Report on Emissions Scenarios (SRES), to identify possible future climate change projections. The scenario used for the application of climate change parameters in this research is the A2 scenario. There are four SRES scenario families with A2 showing the highest increase in temperature at the end of 2100 (IPCC 2007). The predicted increases in the future temperatures are based on an ensemble of models that make up one climate model, and several Earth System Models and Atmosphere-Ocean General Circulation Models (Fig. 2.3). The least extreme scenario, B1, shows an increase in the future temperature of 1.8°C with a likely range between 1.1°C and 2.9°C, followed by B2, which shows an increase of 2.4°C with a likely range between 1.4°C and 3.8°C. The A1B scenario, which is more extreme than B2 predicts an increase of 2.8°C with a range of 1.7°C to 4.4°C. Finally, the A2 scenario, which is used in this study and is the most extreme, shows an increase in the temperature by 2100 of 3.4°C with a range of 2.0°C to 5.4°C (IPCC 2007; Solomon et al. 2007). The A2 scenario also exhibits the sharpest increase in global carbon dioxide emissions with A1FI, which is a part of the A1 family,

being the only close contender (IPCC 2007).

Each of these scenario families are based on certain differing assumptions that result in the predicted temperatures mentioned above. The A2 scenario describes a world of self-reliance and independently operating nations. The local, and therefore global, population is growing continuously while the development of renewable energy grows much slower. In summary, the A2 scenario represents a more fractured world where regional economic development and growth overshadow the sustainability of the economy and environment (Solomon et al. 2007).

Using the SRES A2 scenario and IPCC Fourth Annual Report (AR4) Global Climate Model (GCM) simulations, the thermodynamic changes are applied. Since the dates selected as described above is April 14 and March 19 for the strongly and weakly-forced event simulations, the monthly temperature fields for April and March are computed using five GCMs that contained reliable temperature data at all vertical levels. Then using these monthly averages, the decadal averages are calculated for 1990-1999 and 2090-2099, which are interpolated to the same grid using the initial and lateral boundary conditions from the present-day simulations. For both the strongly and weakly-forced event, the difference between the present and future averages are computed for each grid cell and added to the present-day temperature fields, yielding the thermodynamic change for the future simulations. The relative humidity is kept constant so the relative humidity values computed for the present-day strongly and weakly-forced composites are used for the future composites. Although a recent study suggests this approach of maintaining a fixed relative humidity is not appropriate to use as the authors found that the relative humidity changes in a

warmer climate (Issac and Wijngaarden 2012), the majority of studies use the constant relative humidity approach. The reason behind this constant value is because even though the water vapor content is expected to increase with warmer temperatures, the amount of evaporation is expected to increase as well resulting in nearly constant relative humidity values in a warmer climate (Allen and Ingram 2002; Held and Soden 2006; Gettelman and Fu 2008).

Although the temperature is the only variable manually changed for the future composites, the other variables adjust to the increase as well. For example, in the future simulations the heights are higher because of the warmer air and increased vapor content. This response in the other fields shows how the dynamic components respond to the change in the thermodynamic components, ultimately allowing for an examination and analysis of our third hypothesis focusing on the low level jet, enhanced convection, and other positive feedback loops that could lead to a super Clausius-Clapeyron relationship between a certain forcing and the precipitation. In order to apply the climate change parameters and observe the dynamic response, the model must be used.

3. Results and Analysis

Rather than study the climate change impact on several different individual precipitation events, any one of which may not be representative of the broader phenomenon, there is some advantage to generating composites. By using composites for initial and lateral boundary conditions for high-resolution WRF simulations, we can treat these simulations as pseudo-idealized events which may be more representative of the events in question. In this thesis, two composites are created, one from nine extreme precipitation events characterized by strong upper-level forcing for ascent, and one from thirteen extreme precipitation events, but with a composite that is characterized by less organized forcing for ascent. Comparison of these two composites provides insight into climate impacts for generic events with strong versus weaker forcing.

The nine events were synoptic and occurred during March, April, and May in the states of Texas, Louisiana, Mississippi, and Alabama. The WRF model simulations based on the 9-event composite produced a precipitation event, with strong synoptic-scale forcing for ascent associated with an upper-level trough. The thirteen events were also of the Maddox (1979) synoptic type and occurred during the cool season from September through May between the latitude longitude bounds of 28°-37°N and 85°-94°W, respectively. The WRF model simulations based on this composite produced relatively light, due to less organized upper-level forcing for ascent.

The WRF model, which is initialized 48 hours before the extreme precipitation event, is run with 32, 12, and 4km grid spacings (Fig. 3.1). According to previous literature, weak and strong precipitation events will have different behaviors in a warmer climate; strong

events will get stronger and weak events may get weaker (Allen and Ingram 2002). Because of this, we focus our study on two events, each representing a strong or weakly-forced event. How these two types of events change in a changed climate have implications for the future, mainly how it will affect flooding intensities and frequencies.

Before getting in to the results, it is important touch on the reason why one composite is strongly-forced while the other is weakly-forced even though both composites are based on extreme precipitation events. The weakly-forced composite was created using 13 synoptic-type events during the cool season months. These 13 events met the criterion discussed in Section 2.2 and therefore had upper-level troughs in similar locations on the day of the extreme precipitation, however, this composite shows a weaker trough than in the strongly-forced composite. This is because although in both composites the troughs in the individual cases are in similar locations relative to each other, the strongly-forced composite has less smearing of the forcings from the individual cases resulting in stronger upper and low level systems.

In terms of the simulations, as mentioned before, the composite-based simulations are initialized two days prior to the precipitation, at a time when the troughs in the individual events do not necessarily align (Fig. 3.2). For this weakly-forced event, the location of the upper-level troughs in the individual events have a large spread two days prior and as a result, the upper-level trough in the simulation is weak due to more smearing of the forcings. The strongly-forced composite on the other hand, which was created using nine synoptic-type events during the spring months, shows strong forcings in the composite and simulation. Although this simulation is also initialized two days prior to the precipitation, the upper-level

troughs in the individual events are aligned better than those in the weakly-forced composite, resulting in a strongly-forced event in the simulation (Fig. 3.3). So, because the strongly-forced composite shows a better alignment of the troughs in the individual cases two days prior to the precipitation, the strongly-forced composite-based simulation sees a deeper trough and stronger system when compared to the weakly-forced composite-based simulation.

In Section 3.1 below we first discuss the 13-case composite-initialized precipitation event, which has weak synoptic and mesoscale forcings. In this section, the composite used to initialize the model is described, along with the results of both present-day and future simulations. The impacts of changing the thermodynamic components in a fashion consistent with climate warming are examined for this weakly-forced event.

In Section 3.2, the 9-case precipitation event is discussed. As in Section 3.1, the composite is discussed first, followed by the present-day and future WRF simulations based on that composite. After this, the impacts of changing the thermodynamic components for this strongly-forced event are examined. The final section, Section 3.3, discusses the differences between the climate change impacts for the strong and weakly-forced event.

Note that when talking about the composite, the times are referred to as “one day before the event”, “the day of the event”, etc., with the times associated with these being 1200UTC. When referring to the times in the simulation, though, it is the number of hours after the start of the simulation beginning at zero. Because the model was initialized at 1200UTC two days before the composite precipitation event, the very first hour, 00, corresponds to 1200UTC of the first day. So continuing this, the start of the second day is the

24^{th} hour which is also 1200UTC the day before the composite precipitation event (in terms of the composite), and so on and so forth. The plots are labeled using these different times so use this as a clarification when comparing composites and simulations.

3.1 The Weaker Event

3.1.1 The Composite Event

Once the thirteen events were selected as discussed in Chapter 2, a composite is created. The thirteen events occurred between the months of September through May; one in September, one in November, two in December, one in January, one in March, four in April, and three in May. The analysis of the composite starts with an understanding on the synoptic pattern prior to and during the composited event. Two days before the event, an upper level trough is located over the western part of the United States with a fairly weak upper level jet and small vorticity values maxing out at values less than $16\text{x}10^{-5}s^{-1}$ (Fig. 3.4). The jet maximum east of the trough axis is consistent with a lifting, weakening trough, and two shortwaves are evident, one east of the broader trough axis, and one to the west (Fig. 3.4a). The sea level pressure (Fig. 3.4d) and 850-hPa height (Fig. 3.4c) each show southerly geostrophic flow extending from the Gulf of Mexico into the southern U.S. This windflow is consistent with moisture transport into the area of interest prior to the precipitation event.

One day before the event, the trough has moved eastward and strengthened (Fig. 3.5a,b); however, some of this strengthening is likely a figment of reduced spread among the composite members as the "center time" of the composite is approached. A more pronounced upper level jet is evident as well as stronger vorticity in the axis of the trough (Fig. 3.5a).

The strongest winds remain east of the trough axis, consistent with a lifting trough signature. The implied lower-tropospheric winds are still blowing from the south and the amount of moisture over the area of interest has increased (Fig. 3.5c,d).

On the day of the extreme precipitation event, the right entrance region of the intensified upper level jet is positioned over the area where heavy rainfall fell in the composite event, and water vapor mixing ratio has increased, apparently in response to continued moisture transport from the Gulf of Mexico (Fig. 3.6d). The upper level trough is positioned in an area that matches the criteria used in selecting the individual events, indicating that the events selected do indeed preserve the Maddox (1979) synoptic-type pattern. As the system moves eastward, the day after the event the upper level trough has lifted, the jet has weakened, and the moisture content over the area has diminished (Fig. 3.7).

The total precipitation for the duration of the composite is shown in Figure 3.8. The heaviest precipitation is located mainly within the geographical boundaries set for the precipitation of the individual events, covering Louisiana, Alabama, Arkansas and Tennessee. The maximum amounts of precipitation fall just short of three inches, with smaller amounts located around the heaviest area and to the northeast.

Many different synoptic factors make this composite favorable for a heavy precipitation event. First of all, the right entrance region of the upper level jet is positioned over the latitude and longitude coordinates from where the precipitation data were collected for this composite, suggesting that the area where rainfall occurred is experiencing synoptic lift from the jet. The moisture feed from the Gulf of Mexico also acts to destabilize the environment by transporting warm, moist air in the lower troposphere. In order to have a

better understanding of the processes involved in this event, to determine how much precipitation fell, and to apply climate change parameters, a model simulation must be performed for this present-day composite. The present-day simulation will be discussed in Section 3.1.2, followed by the discussion of the future simulation in 3.1.3.

3.1.2 Present-Day Simulation

Using the thirteen event composite datasets for the initial and boundary conditions, the present-day 72 hour WRF simulation is run for the three domains (32, 12, and 4km grid spacing) discussed in Section 2. A comparison between the simulation and the composite is examined in the next subsection, followed by a detailed analysis of the present-day simulation. The majority of the plots shown in the following sections are from the 12 km grid spacing domain in order to show a larger view of the atmospheric conditions and simulation results.

3.1.2.1 Composite vs. Present-day Simulation

The large-scale synoptic evolution in the present-day simulation is very similar to the composite with only a few differences separating the two. We expect there to be some differences as only the very first time should be the same, although the lateral boundary conditions on the outermost domain are also provided by the composite. Therefore, this section is not a verification of the simulation, but rather just to make note of the differences between the two. Note that a central composite date of March 19 was assigned to the composite-based simulation in order to give solar radiation values consistent with the average

of the composite events.

The synoptic system in the composite is much stronger than the simulation during the course of the simulation (Figs. 3.10, 3.11, 3.12). The upper level trough is much more defined and intense in the composite, stretching further to the south than it does in the simulation. The magnitude of the vorticity increases in the simulation as the upper level trough makes the transition to become oriented from the northwest to the southeast (negatively tilted), enhancing the cyclonic spin, whereas the composite trough remains oriented from the southwest to the northeast. However, the upper trough and strong forcing for ascent are centered to the north of the area of heavy precipitation in the simulation. As for the upper level jets, they occur in the same locations in the composite and simulation however, the composite shows a larger and stronger upper level jet (Figs.3.6a, 3.11a). As expected, there are some differences between the composite, and the simulation initialized with it. Some of the differences are due to the higher resolution of the WRF simulation plots shown here, but the general character of the trough is broadly consistent with the composite. Note that because the initial time for the composite simulation was two days before the event, at a time when the upper forcing was less focused due to greater composite member spread, we might expect that the WRF event would be weaker than the individual events that went into the composite.

Focusing the comparison near the surface, the amount of moisture is fairly similar at 900mb with the present-day simulation showing specific humidity values of about 3 g/kg more than the composite (Figs. 3.5d, 3.10d). The surface plots are similar with the main differences being that the simulation shows a warming at 850mb in the Gulf of Mexico after

the first twenty-four hours and the sea level pressure plots look very different (Figs. 3.5c,d, 3.10c,d).

To reiterate what was mentioned before, the composite and the present-day simulation are not supposed to be identical. Overall there are differences between the simulation and composite as expected but the simulation is a reasonable representation of the composite because it preserves the synoptic evolution and maintains the weak forcings that acted to create the environment in which the weakly-forced precipitation event occurred. Because the model was initialized at a time when the upper forcing in the composite was still disorganized, and because cancellation within the composite led to a weaker forcing environment with the strongest ascent to the north of the area used for the precipitation composite, simulation precipitation is lighter than the composite average, as discussed in the following subsection.

3.1.2.2 Main Features: Present-day WRF Simulation

Two days prior to the event, at the initial time of the simulation, the pattern matches the composite with an upper level trough located over western United States with weak vorticity aloft and southerly flow at the surface (Fig. 3.9). Twenty four hours into the run, the upper level low pressure system and trough have progressed eastwards, consistent with the Maddox synoptic type flooding event, and the vorticity has become organized and stronger (Fig. 3.10). The trough has dug further to the south and the southerly winds at the surface are pumping even more moisture into the Gulf States than was seen in the previous twenty-four hours. Hour 48 of the simulation, on the day of the composited extreme precipitation event,

the trough has progressed to the central United States located within the latitude and longitude bounds that was part of the criteria for the extreme precipitation events selected (Fig. 3.11). A weak surface high pressure system has moved southeastward and is located over the southwestern portion of the United States and a low is centered over southern Indiana. The upper level vorticity has reached its maximum intensity as the trough, which is positioned over the central United States has begun to lift north. By 72 hours the upper trough has lifted to the northeast and weakened, although a concentrated vorticity center is located immediately north of New York State (Fig. 3.12). The upper level synoptic pattern is relatively zonal with a weak trough oriented from the northwest to the southeast over the eastern United States however, the trough previously located over southern Indiana has strengthened by 4mb between Figures 3.11d and 3.12d.

As the synoptic pattern is consistent with the Maddox synoptic type event leading up to and during the event, so is the precipitation, which falls under the right entrance region of the upper level jet streak, which can be seen by comparing Figure 3.13 with the 250mb plots in Figures 3.10a and 3.11a. Shown in Figure 3.13 is the cumulative 72 hour precipitation total with 12 kilometer grid spacing. Two precipitation maxima exist; one in northeastern Arkansas and one across Kentucky and West Virginia, the latter of which falls to the north of the composite boundaries. The precipitation first begins to fall over the Kentucky and West Virginia border as well as sporadic other locations across the domain, and by the 34th hour of the simulation, a line of precipitation sets up running from the northeast corner of Louisiana to West Virginia (Fig. 3.14). The most intense precipitation falls during the 34th hour of the simulation and the line of steady precipitation dissolves shortly after as the surface low

pressure system approaches. Precipitation continues to fall, with the period from the 24th hour to the 48th hour experiencing the heaviest precipitation with a twenty-four hour maximum of about 3.5 inches in certain locations (Fig. 3.15).

The pattern of the precipitation evident in Figure 3.13, is oriented from the southwest to the northeast, aligning with the low level isobars which can be seen in the 850mb maps of Figures 3.10c and 3.11c. The moisture from the Gulf of Mexico is pulled into this region, providing a sufficient amount of moisture to the area for a heavy rainfall event. One factor that contributes to this moisture transport is the low level jet. After analyzing the strongest winds at 850mb, it is apparent that a low level jet is in place for an ample amount of moisture to be transported to the region with the heavy rainfall (Fig. 3.16a,b). At the start of the time period when the most precipitation occurs, a broad low level jet is positioned from the western Gulf of Mexico reaching northward to Kentucky (Fig. 3.16a). At hour 33, the low level jet still feeds the Gulf States with moisture however, the maximum winds are moving northeast away from the Gulf of Mexico (Fig. 3.16b). By the end of the twenty-four hour heavy precipitation event, the low level jet has moved northward from the Gulf and the geostrophic winds have switched to westerly, cutting off the moisture supply in the process (Fig. 3.16c).

The low level jet supplied the area with an ample amount of moisture, but other factors contributed to an environment favorable for precipitation. The upper level jet streak at the 24th hour is positioned such that the right entrance region is located above the area where precipitation fell, creating lift (Fig. 3.10a). The convective available potential energy (CAPE) is moderate, with a twenty-four hour average from the 24th to the 48th hour, or 1200UTC of

the second day to 1200UTC on the third day, of 306.19 J/kg over the area of the heaviest precipitation, with the average computed for the area bounded by 29.5° to 39° latitude and -95° to -85° longitude. The convective inhibition (CIN) values are also fairly low for the duration of the entire simulation except during the nighttime hours, although during the twenty-four hour period when the most precipitation falls, large reflectivity values are still evident even during the nighttime hours (Fig. 3.17). These combinations of favorable factors play a role in the producing a slightly unstable environment for this heavy precipitation event.

Understanding and analyzing the present-day simulation reveals a Maddox synoptic type precipitation event where 3.5 inches of rain fall in twenty-four hours in an environment favorable for enhanced rising motions. The majority of the precipitation is stratiform however, there are a few convective cells popping up through the 72 hour simulation (Fig. 3.13). The next step is to apply climate change parameters to run the future case.

3.1.3 Application of Climate Change Parameters

Once the present-day simulation is completed, the next step is to apply the climate change parameters as described in Chapter 2. The main features of the future simulation are analyzed first, which will be discussed in the subsection below. After that, the analysis focuses on impacts caused by changing the thermodynamic properties, for example the differences in the precipitation totals, the jets, and the instability, and lastly we examine how the dynamic components respond to these thermodynamic changes and what effects the responses cause.

3.1.3.1 Main Features

As dictated by our methods, the future simulation begins with a synoptic pattern that is almost identical to the present-day simulation with the only main difference being the higher heights in the future run due to the increase in temperatures and water vapor (Figure 3.18). Despite the higher heights, the pattern itself is still the same. Because of the increase in temperatures there is also more moisture in the future simulation, as mandated by the assumption of constant relative humidity. As time goes by though, the pattern begins to diverge from that seen in the present-day simulation. Twenty-four hours into the simulation, the upper trough in the future simulation is weaker than that in the present-day simulation (Figs. 3.19 and 3.10). The trough has not dug as far south during its rapid progression to the east. The upper level jet and vorticity in the future simulation is very similar to that seen in the present-day simulation. The 500mb vorticity at this time has increased in magnitude from the values observed at the initial time, with the most positive values occurring in the axis of the trough. The winds are still from the south however, the moisture content has increased over the Gulf States (Figs. 3.19d and 3.10d). By hour 48 of the model simulation, important differences between the future and present day simulations have developed (Figs. 3.20 and 3.11). The upper jet is stronger in the future, leading to a more strongly lifting upper trough (Figs. 3.20a and 3.11a). Consistent with this, the vorticity structure in the future upper trough is much weaker than that in the present-day simulation (Figs, 3.20b and 3.11b). The surface low pressure system has shifted eastward and although the moisture content is still greater than that seen in the present-day run, it has decreased slightly (Figs. 3.20d and 3.11d). Finally, at hour 72 in the future simulation, the upper level flow is much more zonal than in

the present-day run at this time and the 500mb vorticity is much weaker (Figs. 3.21 and 3.12). The moisture has decreased and the surface low pressure system has weakened.

Because the synoptic pattern in the future simulation evolves differently from the present-day run, the precipitation changes as well. A maximum of precipitation falls over southwestern Arkansas and another maximum is located over eastern Tennessee (Fig. 3.22). In the present-day simulation the precipitation is oriented from the southwest to the northeast however, in this run the precipitation bullseye in southwestern Arkansas is oriented from the northwest to the southeast (Fig. 3.15). The majority of the precipitation in the future simulation falls between the 24th and the 48th hour period (Fig. 3.23). Unlike the present-day simulation, the low level jet is very weak in the future run, its spatial extent is not nearly as large, and no precipitation falls near the jet (Fig. 3.24). A more detailed analysis will be presented in the section below, but this decrease in intensity of the low level jet for the future run can be seen in Figure 3.24. The upper level jet however, which can be seen in the four panel plots of Figures 3.19 and 3.21, does and the location of the right entrance region corresponds to where the majority of the precipitation falls. The precipitation in the future simulation begins falling over Arkansas and Tennessee and by the 27th hour a plume of moisture from the Gulf of Mexico is moving into the area similar to that seen in the present-day run (Fig. 3.25). During the 27th hour the plume of moisture is very well-defined however, it dissipates soon after. Comparisons between the precipitation in the future and present-day simulations are analyzed in the section below with respect to this time period.

The vorticity also produces conditions favorable for heavy precipitation as there were small maxima of positive vorticity over Arkansas and Tennessee between the 24th and 48th

hours enhancing the rising motion. The CAPE is also larger in the future simulation, as shown in Figure 3.25. The time area averages for CAPE were taken with the bounds of 29.5° to 37° latitude and -95° to -85° longitude and during the period from the 24th through the 48th hour. The time area averaged for the present-day simulation was 306.19 J/kg, which is much lower than the time area average for the future simulation which was 969.46 J/kg. This will be discussed more below. This can also been seen in Figure 3.26, where the convective precipitation is larger in the future run, however, the stratiform precipitation is larger in the present-day run.

All in all, the future run exhibits a similar pattern compared to the present-day run at the very beginning, but as time passes the synoptic pattern and associated upper-level trough evolution diverges. This section described the general features of the future simulation but a more in depth analysis of the reasons behind these differences between the future and present-day runs is presented in the section below.

3.1.3.2 Thermodynamic Impacts and the Dynamic Response

The section above detailed the general features of the case associated with the future simulation and made a few comparisons of similarities and differences with respect to the present-day simulation, but more than that we want to address and answer the main questions that were introduced in the very first chapter. First of all, how did changing the thermodynamic properties affect the precipitation and secondly, how did the dynamic properties respond to these thermodynamic changes?

The future simulation contains more moisture and warmer temperatures however, the

overall precipitation is less than the present-day run on the two innermost domains. A difference field plot (Fig. 3.27) indicates that different areas received more or less precipitation in the two model simulations, and so an area average using the domain grid sizes for the total 72 hour precipitation is calculated and still, over all three domains the present-day run shows more precipitation. These differences in the area-averaged total precipitation of the present-day and future runs can be seen in Table 3.1. With more moisture and warmer temperatures, we expected to see an increase in the total precipitation but the opposite occurred for the inner domains, so now the question is, why?

We start by looking back at the synoptic system. The future version of this system is weaker than in the present-day run and the low level jet that is prevalent in the present-day run, as mentioned above, is also weaker in the future simulation, which can be seen in the four panel plots. The low level jet pumps a good amount of moisture into the Gulf States during the present-day run, but even though the jet in the future is not strong there is still more moisture in the atmosphere during the entire duration of the run than seen in the present-day simulation. The low level jet is one of the dynamic components of interest in this study and since it weakens instead of intensifies in the warmer climate, the amount of convection is examined, which is the other dynamic forcing of interest along with the synoptic lift.

Since the total precipitation is what we are interested in, it is suitable to perform an area average to understand how much it changes. For CAPE and omega however, a time average is performed which is then used for the area average. The time period selected for the time average is the twenty-four hour period between the 24^{th} and 48^{th} hours. The reason

for this is because, as in the present-day simulation, this is the twenty-four hour period that experiences the heaviest rainfall. Once the areal time averages are computed, the resulting twenty-four hour averaged CAPE for the present-day run on the 12 kilometer domain within the bounds of 29.5° to 37° latitude and -95 to -85° longitude is 306.19 J/kg and 969.46 J/kg for the future run, so the future shows a much more unstable atmosphere during this time period. Domain 2 is used for these averages in order to see the bigger picture and the third domain values are consistent with these (not shown). The twenty-four hour time averaged CAPE for the present-day and future simulations is shown in Figure 3.28. What this, as well as the areal time averages, show us is the future run had more moisture, warmer temperatures, more instability than the present-day simulation, but less total precipitation.

At the beginning of the time period of heaviest precipitation, the surface low pressure system progresses eastward at the same rate as in the present-day run, but toward the end of the twenty-four hours the surface low pressure system in the present-day simulation speeds up and intensifies while the one in the future simulation lingers in the same located and moves slowly northeastward while slightly intensifying (Fig. 3.29b). During these same times, the upper level systems behave very differently as well. Around hour 24 both troughs are in similar locations. The present-day simulation intensifies between the 24^{th} and 42^{nd} hours while in the future run the trough is already lifting (Fig. 3.30). A short wave trough develops in both and can be seen in the 42^{nd} hour of Figure 3.30 but while the present-day simulation maintains the shortwave trough through the 54^{th} hour, the future simulation does not. The future simulation trough begins lifting around the 54^{th} hour (Fig. 3.30b), twelve hours before it does so in the present-day run.

Using this in conjunction with hourly CAPE values, the CAPE is very large at the beginning of the twenty-four hour period when the rain is the heaviest, but as the surface low pressure system approaches and nighttime falls, the CAPE values drop. By the time the sun is back up the low pressure system in the future simulation has reached the area, bringing a few convective cells around its center and stratiform rain elsewhere, and the CAPE values do not return to their previous larger values (Fig. 3.31). The atmosphere after the heaviest precipitation has fallen is slightly stabilized over this region as reflected in the CAPE values.

Because we are interested in the most extreme precipitation, the next analysis is directed toward the state where the maximum precipitation occurs in both the future and current runs: Arkansas. Figures 3.13 and 3.18 show the 72 hour precipitation values for the present-day and future runs, respectively, and as seen there, in our area of interest two main maxima occur within this state. Both the future and present-day runs saw heavy amounts of precipitation occurring on the 24^{th} hour as mentioned above, and since the following eighteen hours experience the heaviest amount of rain, the 24^{th} through the 42^{nd} hour period is used again. Using this time period, the difference between the precipitation total on the 42^{nd} hour and the precipitation total on the 24^{th} is computed for the present-day and future simulations (Fig. 3.32a). Although the 72 hour total precipitation for the future simulation decreases, during this time period the amount of precipitation was actually greater in the future simulation. Creating an area average using the latitude and longitude bounds roughly corresponding to the state of Arkansas, the present-day run has 8.56 mm of precipitation during this time period and the future run shows 10.80 mm of precipitation (Fig. 3.32b). The total precipitation in the present-day run does not reach the amount that is seen in the future

run until three hours later. Although the total precipitation decreases in the present-day run, there is heavier precipitation falling in a shorter amount of time early on in the event which has implications both in terms of flash flooding, and for the upper-level dynamics of the system.

The heavier rain earlier in the event for the future simulation is consistent with stronger latent heating, and this could explain why the upper trough exhibited a stronger downstream jet and lifting behavior as seen in Fig. 3.30. The lifting behavior seen in the trough could be due to this early shot of latent heating or the application of warmer temperatures, and to test this the 200mb difference in east-west horizontal winds between the future and present-day at the 24^{th} and 48^{th} hours are plotted (Fig. 3.33). If it is due to the applied warming, the difference in the east-west horizontal winds should stay the same during both time periods. The plots suggest otherwise though, and show difference fields that are not constant as they should be. This points to the early shot of latent heating as being a more probable cause for the stronger downstream jet and lifting behavior of the trough in the future simulation. Although subtle, this explanation is consistent with the subsequent dissipation of the surface low, and overall weakened forcing for ascent in the future simulation after this early period of precipitation. Although the shot of early precipitation in the future simulation appears to have played a role in the weakening of the trough, it could also be due to the addition of larger heights to the south (Fig. 3.34). The larger heights added to the south could shift the trough to the north and cause it to weaken.

In order to determine if the increase seen in the eighteen hours of the heaviest rainfall is sub, super, or scales with the Clausius-Clapeyron relation, it is first necessary to identify

how much the lower-tropospheric moisture increased. Using the same time and area averaging techniques for hours 24 through 42 for Arkansas, the specific humidity at 850mb in the present-day simulation is 8.68 g/kg and the future contains 11.05 g/kg. These values calculated together give the percentage increase in the moisture from the present-day to the future, which is about a 27% increase. In order for this increase in moisture to be consistent with the 7% vapor increase per degree Celsius of the Clausius-Clapeyron relation, the areal averaged temperature increase would have to be around 3.85°C. After averaging the temperature, the average is a warming of 3.8°C between the future and present-day simulations, so the time averaged moisture increase is indeed consistent. For the precipitation to have a super Clausius-Clapeyron relation it would have to increase at a rate faster than 27%. The precipitation percentage increase is calculated in the same manner with a resulting increase of 26%. This shows that during this time period of the most intense precipitation, the scaling is approximately consistent with the Clausius-Clapeyron relation.

All in all, the results are surprising to see at first glance. At the beginning of the run, the dynamics, including the vertical velocities, are largely set by the initial conditions, so one expects a Clausius-Clapeyron increase in precipitation. The results reveal though that the future simulation displays less total precipitation and also a weaker low level jet. Although the 72 hour total precipitation, and even the heaviest 24 hour total precipitation, do have less precipitation than the present-day simulation, there is a shorter time period early in the future simulation that exhibits heavier precipitation showing that more precipitation fell earlier in the future run in a shorter time period. This precipitation however, does not increase at a super Clausius-Clapeyron rate but rather scales approximately with the Clausius-Clapeyron

vapor increase. This initial precipitation appears to have had the effect of weakening the upper-level trough, resulting in weakened forcing for ascent during the middle and later stages of the future model simulation. The upper trough was of modest intensity in the present-day simulation, but in the future run, the trough weakened more in response to heavier rain earlier in the event. Thus, the dynamical response to the warming in this case resulted in weakened ascent and less overall precipitation in the future simulation, despite more CAPE and moisture. Note that it is also possible that the upper-trough changes seen between these two simulations were due to the addition of larger heights to the south. Lackmann (2012) found faster upper-tropospheric winds, and a more progressive upper trough in current and future simulations of a flooding event in Tennessee. The bottom line for this weakly forced event is that the overall precipitation decreased in a warmer climate due to a weakened and more progressive upper trough. These trough changes could be due to the large-scale warming, to greater latent heating early in the model simulation, or both.

3.1.4 Summary

The composite, which was created from thirteen extreme precipitation events, was used as the initial and boundary conditions for the present-day run using the WRF model. Both the composite and present-day simulation are characteristic of a Maddox synoptic-type flooding event. Once the present-day simulation was completed, the thermodynamic changes were applied to the composite and the future run was conducted. By observing the synoptic and mesoscale structures of the present-day and future simulations and then comparing them to each other, similarities and differences were noted that required additional detailed

analysis.

The future simulation showed less 72 hour precipitation than in the present-day run by about 6.7%, however, during the most intense precipitation (24-42 hours over Arkansas) the future simulation showed more precipitation earlier in the run, although it scaled only approximately with the Clausius-Clapeyron increase. The total 72 hour precipitation did not increase apparently due to a weakened and more progressive upper trough. After the initial period of heavy rain the present-day precipitation continued to fall and reached the highest totals of the future simulation. The intensity and paths taken by the surface low pressure systems are related to changes in upper-level forcings. In the future run the low pressure system moved very slowly eastward between the 24th and 42nd hours and was weaker, when the precipitation was the strongest, whereas the present-day low pressure system moved rapidly northeastward and intensified. Large amounts of rain in both simulations fell during this time period (more in the future run for this 18 hour period) however, after 42 hours in the future run the precipitation dwindled as the low pressure did not intensify but in the present-day simulation the strong surface low pressure system contributed to heavier rainfall in the later hours of the run (Fig. 3.35).

This thirteen event composite was a weakly-forced event because the synoptic and mesoscale forcings, as well as the amount of precipitation that fell, were modest. Our findings showed that in a warmer climate, this weakly-forced event had an overall decrease in precipitation compared to the present-day run due to changes in the upper-level dynamics. Figure 3.36 shows that the future simulation experienced more light precipitation however, the present-day simulation contained more heavy precipitation. Previous studies have found

that weaker events are expected to decrease in a warmer climate, so these results of less precipitation in the future when there are weaker forcings and not much precipitation support those findings (Allen and Ingram 2002; Chou and Neelin 2004).

3.2 The Stronger Event

Due to the nature of the compositing process, the thirteen event composite had fairly weak atmospheric forcings. The upper level and surface systems were not strong and weakened in the future simulation. In order to contrast this with a simulation event with stronger forcing, the nine-case composite is analyzed. Both the weakly and strongly-forced event have large amounts of precipitation that are consistent with the three or more inches in twenty-four hours or less, however, this stronger forced event has a larger spatial extent of heavy precipitation, and larger amounts. While this composite suffers from the same issues as the 13-case composite, the events were all selected with a strong trough over the southwestern U.S., so that there was less of a tendency for cancellation, and resulting increases in upper forcing relative to the 13-case composite.

Section 3.2.1 discusses the nine event composite, which is then followed by the analysis of the present-day simulation, and then finally the impacts of a warmer climate are examined with a future simulation.

3.2.1 The 9-Event Composite

This strongly-forced event consists of nine Maddox synoptic type events that occurred in Texas, Louisiana, Mississippi and Alabama during the months of March, April

and May. As the thirteen event composite was described as a weakly forced precipitation event, this one is a stronger event with stronger synoptic and mesoscale forcings. The troughs from the individual events that created this composite aligned more with each other than those that created the thirteen event composite, resulting in less smearing of the synoptic pattern and stronger forcings.

The synoptic pattern two days prior to the strongly-forced precipitation event shows a trough located over the western United States, however, it is already much deeper and farther south than the one in the weaker thirteen event composite (Fig. 3.37). An upper level low pressure system is located over western Canada, and an elongated upper level jet is over western and central United States. In addition to a southwesterly jet, a strong northwesterly jet is also seen along the west coast to the west of the trough axis, which is consistent with maintenance of the amplitude of this trough as it advances eastward. The vorticity is widespread with values maxing out at $16\text{x}10^{-5}s^{-1}$ in the axis of the trough, however, a positive vorticity maximum is upstream of the trough at this time, poised to reinforce the trough as it progresses eastward. The surface low pressure system is identifiable, unlike the weaker event, and the implied geostrophic surface winds are blowing from the south bringing moisture to the Gulf States from the Gulf of Mexico. As the time steps forward twenty-four hours, the low pressure system has strengthened (Fig. 3.38). The upper trough at this time has dug even further to the south and has moved slightly to the east, with a stronger and more elongated upper level jet associated with it and with a strong jet also to the west of the trough axis (Fig. 3.38a). The implied surface winds are still from the south and moisture is still over the Gulf States (Fig. 3.38d). On the day of the composite precipitation event, the composite

low pressure system has reached its maximum intensity while the trough has reached its southernmost location (Fig. 3.39). The upper level jet has intensified and the jet streak has moved eastward through the trough. With stronger winds now to the east of the trough axis, a lifting configuration has developed. The vorticity at 500mb has also reached its highest values of about $20\text{x}10^{-5}s^{-1}$, and the surface winds are still from the south. At the very end of the seventy-two hours, the low pressure system has weakened and the trough has lifted to the north (Fig. 3.40). The upper level jet has decreased in magnitude, as well as the 500mb vorticity and the surface flow from the south.

During this composite evolution, the upper and low level jets are prominent features. The upper level jet is a large, elongated swath with a broad right entrance region, and the low level jet is strong and pumping an abundant amount of moisture into the Gulf States. The 500mb vorticity is fairly strong with maximum values on the day of the precipitation event of about $20\text{x}10^{-5}s^{-1}$, with the largest values occurring when the low pressure system and trough have reached their peaks in strength, again on the day of the event, which is also the time period when the low pressure system at the surface has reached its maximum intensity during its eastward progression. This composite, as does the thirteen event composite, resembles the Maddox synoptic type system, however, in this composite the upper-level forcing responsible for the precipitation event is much more pronounced, and is located at a more southerly latitude.

The total precipitation for the strongly-forced composite is shown in Figure 3.41. The heaviest precipitation falls in the Gulf and Central United States, maxing out just below three inches. The precipitation is widespread and a good amount of precipitation falls over the

northern states. These values of precipitation are on a coarse grid scale so it is important to initialize the model simulation in order to use smaller grid spacings and see a better representation of the total precipitation from this strongly-forced composite, on top of using the model to apply the climate parameters and observe how the dynamic components respond.

3.2.2 Present-day Simulation: Composite Comparison and Main Features

Again, there are expected differences between the composite and the simulation since the simulation is initialized with the first time from the composite and is free to evolve as an actual dynamical event rather than as a composite derived from analyses. This comparison of the composite and the simulation is not to be a verification of the simulation, but rather just a note of the differences between the two.

The simulation based on the 9-case composite shows stronger upper air synoptic forcing than the composite, although they are very similar to each other (Figs. 3.42, 3.43, 3.44, 3.45). The main differences aside from the upper air strength, is that the present-day simulation shows a stronger surface system than the composite, with a stronger low level jet and more moisture over the Gulf States. The 500mb vorticity is also stronger in the simulation than the composite. The upper level jets in both the composite and simulation are in favorable locations for upward motion, considering the region of focus is the Gulf States.

The precipitation for the present-day simulation is very scattered spatially (Fig. 3.46). The precipitation is oriented from the southwest to the northeast and consists of several bands of heavy precipitation in this orientation. There are many precipitation maxima across the

entire central United States with the largest maximum in northern Tennessee of 10.97 inches over the seventy-two hour period.

The precipitation begins falling very early in the simulation, but it is not until the 35th hour that the moisture feed from the Gulf is seen directly influencing the precipitation (Fig. 3.47b). The majority of the precipitation before this point is associated with what appears to be a warm frontal boundary (Fig. 3.47a) and the surface low pressure system, as well as the upper level low pressure system, both of which are moving eastward. The instability in the atmosphere during this present-day simulation is somewhat unstable however, the highest CAPE values fall where the low pressure system is located, unlike the weakly-forced event where the instability was high before the low pressure system even arrived (Fig. 3.40a).

The majority of the precipitation falls between the 24th and 48th hours in the central United States (Fig. 3.49a), however, from the 48th hour to the 72nd hour, the precipitation falls in the central United States as well as in the northern states (Fig. 3.49b). The CAPE values are not very high during this first time period over the area over precipitation, but the low level jet is playing an active role (Fig. 3.50). Even at the very beginning over the 24th hour, the low level jet is already in place. Not only this, but it intensified throughout the 24 hour period, with help from the low pressure system. This pumped moisture over the central and eastern United States, which can be seen in the four panel plots (Figs. 3.43, 3.44, and 3.45). This location of this jet at 850mb can be compared with the precipitation between the 24th and 48th hours in Figure 3.49a and the majority of the precipitation does indeed fall in the same path where the low level jet occurs. The other precipitation further north is associated with the low pressure system. The precipitation in the latter 24 hours of the

simulation occurs mainly in the northern states where the low pressure system is, but there is also another swath of precipitation in the central states and looking again at Figure 3.48, the reflectivity shows the presence of strong southerly flow from the Gulf.

This present-day simulation showed a very strong and widespread precipitation event. The low level jet played a large role, as did the surface low pressure system with maintaining the intensity of the jet as it progressed eastward. Larger than that though was the role of the strong upper trough, since it dictated where and how strong the surface low became, and provided lift for precipitation. The precipitation fell parallel to the plume of moisture brought in from the low level jet as well as around the low pressure system. The question now is how will this strongly-forced precipitation event with strong forcings change in a warmed climate?

3.2.3 Application of Climate Change

The thermodynamic changes are applied using the same method as was used for the thirteen event weak case. The changes are applied to the present-day composites and simulated using the WRF model with the same settings.

Since only the thermodynamic components are changed, the synoptic pattern is the same but the temperatures are warmer which causes the heights to be higher. The surface and upper level low pressure systems in the future simulation propagate eastward much more quickly than in the present-day simulation, which is consistent with the 13-event composite based simulation findings (Figs. 3.45 and 3.36). At the very first hour, the pattern is the same as the present-day simulation with, as mentioned before, higher heights and also more

moisture (Fig. 3.51). At hour 24 of the future simulation, the low pressure system and upper level trough have progressed eastward (Fig. 3.52). The trough has not dug further to the south however, it has not weakened either. The 500mb vorticity at this time is stronger with maximum values around $20\text{x}10^{-5}s^{-1}$ in the trough and the moisture has increased from the previous twenty-four hour plot. The low pressure system at this time is also more organized and pronounced than at the very end of the simulation. Forty-eight hours into the run, the upper level trough is beginning to lift northeastward as the upper level and surface lows move eastward (Fig. 3.53). The moisture, which is being pulled northward by the strong surface low pressure system, is reaching from the Gulf of Mexico all the way to the Great Lakes. The 500mb vorticity values have reached their highest values yet of about $28\text{x}10^{-5}s^{-1}$ in the trough axis and the upper level jet is still strong and elongated. On the 72nd hour, the upper level low pressure system has progressed further east and the trough is now oriented from the northwest to the southeast and has lifted northward (Fig. 3.54). The vorticity at 500mb is still large and the upper level jet is positioned with a right entrance region of the jet streak over the Gulf States. The surface low pressure system has propagated to the northeast and continued to intensify, reaching its maximum intensity with a low pressure center of 992mb at this time.

The precipitation is still very spatially spread out however, the bulleyes are larger in value and more concentrated (Fig. 3.55). Also, compared to the present-day simulation more precipitation fell in the northern states. The surface low pressure system is stronger in the future simulation for this strongly-forced event, and wraps more moisture up to these northern states. This can be seen in the four panel plots, as well as when separating the

precipitation into convective and stratiform-type (Fig. 3.56). The future simulation shows more convective and stratiform precipitation when compared to the present-day simulation, with greater amounts of both types over the northern states. The precipitation begins to fall, as in the present-day simulation, early compared to the weakly-forced event, and the majority of the precipitation at the beginning falls along the warm front and parallel to the 850mb and surface flow as the moisture is pumped in from the Gulf and pulled northward from the approaching surface low pressure system (Fig. 3.57a). By the 35th hour the moisture plume in place and the low pressure system is slightly more intense than that in the present-day simulation, although the locations of the lows are similar (Fig. 3.57b, 3.39b).

Breaking down the precipitation into two twenty-four hour totals as done previously, Figure 3.58 shows the plots for the total between the 24th and 48th hours, as well as between the 48th and 72nd hours. The location of the precipitation swaths in the two 24 hour periods is very different. From the 24th hour to the 48th hour, the precipitation is located mainly in the central United States with some falling in the northern states around the low pressure system, but during the last 24 hour period the precipitation is almost completely isolated to the northern states. To understand this fully, we look at the low level jet, the surface low pressure system, and the CAPE values.

As a comparison to the present-day simulation, the CAPE for this future simulation is shown in Figure 3.48 for hours 24, 42, and 54. It is clear that the system is more convective in the future, with higher CAPE values existing further north. The CAPE values are also larger in the very last plot (Fig. 3.40) as the low pressure system has moved over the central United States. The low pressure system is the same intensity in the future simulation as that

seen in the present-day simulation but with more tightly packed isobars, and it pulls about 3 g/kg of moisture more than the present-day system into the central and northern states throughout the duration of the run. Because of the strong low pressure system at the surface and aloft, the low level jet is much stronger than in the present-day simulation (Fig. 3.59). The 850mb isotachs show that at the beginning of the 24 hour period between the 24th and 48th hours, the low level jet is strong but not yet wrapped around the low pressure system. At the very end of this time period though, the jet has wrapped around the system pulling an abundant amount of moisture with it. From the 24th to the 48th hours, the precipitation was focused mainly in the central United States where the low level jet is pumping moisture in and in the process of wrapping around the low while the low is intensifying. During the last 24 hour period between hours 48 and 72 however, the precipitation is located in the northern states, where the intensified low pressure system is located, still supplied with the moisture from the Gulf. This moisture stayed with the system all the way until the end of the simulation, so the low level jet played a very large role in where the precipitation fell.

When spatially averaging the precipitation over the entire 12km grid spacing domain of precipitation, the future precipitation averages 2.21 mm whereas the present-day precipitation averages 1.70 mm. So, unlike the 13 event simulations, this event does indeed show an increase of precipitation in the future. Since we are interested in the most extreme precipitation, a smaller area is used to hone in on the maximum amounts of precipitation for both the present-day and future total precipitation amounts. The same sized latitude-longitude areas are used for both, however, since the precipitation maxima differed in the present-day and future simulations, the areas are in different locations. For the present-day precipitation,

the area averaged is 36° to 38° latitude and -89° to -81° longitude, while for the future precipitation the area averaged is bound by 42° to 50° latitude and -95° to -93° longitude (Fig. 3.60). So, the areas are the same size however, reason for having different latitude longitude boundaries is because of the different locations of the precipitation maxima between the present-day and future simulations. When averaging these heavy precipitation areas, the present-day areal averaged precipitation is 35.23 mm, and the future areal averaged precipitation is 47.09.

Looking even further into this increase in precipitation, we analyze the area averaged vapor increase to determine if the increase in precipitation was constrained by the Clausius-Clapeyron relation or if it exhibited a super Clausius-Clapeyron relation. The area averaged water vapor across the entire domain of precipitation shows an increase of about ~20%, and the precipitation increases by ~30%. This shows a super Clausius-Clapeyron relation. When looking at the areas though with the maximum precipitation values, the area average for the moisture at 850mb is taken with respect to those same boundaries increases in the future by about 23.6%. This increase in moisture is consistent with the 7% per degree Celsius relation because the areal averaged temperature needs to show a warming of about 3.4°C, and it when averaged it shows a 3.19°C increase. When the area averaged precipitation from the present-day simulation is subtracted from the future simulation and then that total divided by the present-day, a super Clausius-Clapeyron relationship is revealed showing an increase in precipitation of about 34%, which is larger than the ~22% increase expected by the Clausius-Clapeyron relation. A large reason behind this super Clausius-Clapeyron relationship is the low level jet, which upon being analyzed shows a strengthening and elongating in the future,

thereby providing evidence of nonlinear factors (Fig. 3.61). This enhanced low level flow was an additional forcing that causes the additional precipitation in the future simulation to scale at a rate larger than the expected 7% per degree Celsius. The surface low pressure system also played a role, as it was more intense in the future simulation and wrapped more moisture to the northern states (Fig. 3.62). It could also be due to more CAPE, as Lackmann (2012) found, and can be seen through the more convective precipitation in the future simulation.

3.2.4 Summary

The simulations from the strongly-forced event showed much different results than from the weakly-forced event. The main difference between the two was that the weakly-forced event had much weaker synoptic and mesoscale forcings, which ultimately resulted in a decrease of precipitation in the future, whereas the strongly-forced event had very strong synoptic and mesoscale forcings that lead to a super Clausius-Clapeyron precipitation increase. The low level jet in the weakly-forced event future simulation was minimal at best, but the low level jet in the strongly-forced event future simulation increased in strength and southward extent, creating a positive feedback loop as it pumped even more moisture into the southern and central United States, creating more condensation and more precipitation, which in turn strengthened the low level jet and so on and so forth. This type of increase was not observed in the weakly-forced event because there was very little precipitation falling in the vicinity of the low-level jet in that case.

In the weakly-forced event, the already-modest upper forcing was even weaker in the

future event due to either more precipitation early in the simulation, or to the general acceleration of the upper-level trough due to the imposed large-scale warming. In the strong case simulations, the trough also lifted more and dropped heavier precipitation at more northerly locations, but the forcing was strong enough to still result in heavy rain.

Our focus on one weakly and one strongly-forced precipitation event allowed for clear comparisons between both types to determine what differences and similarities occur when altering the thermodynamic components for both and how the overall precipitation is affected by the changes. These results are consistent with previous studies, because our results show that the weaker precipitation case saw a decrease in precipitation in the future and the stronger event saw an increase in precipitation in the future (Allen and Ingram 2002; Chou and Neelin 2004). However, the dynamical and synoptic evolutions indicate that the causes for these changes were complex.

4. Discussion, Conclusions, and Future Work

4.1 Discussion

4.1.1 Overview

Understanding the impacts of a warmer climate on extreme and light precipitation events is necessary as the impacts could affect many facets of our society, ranging from the integrity of the infrastructure under the threat of flooding or agriculture to human life. The first question to be answered was what are the atmospheric patterns prior to and during these extreme precipitation events, and secondly and most importantly, how would these events change in a warmer climate? Studies have delved into the impacts of climate change on precipitation, however, this study is unique in that it uses the approach of employing composites to initialize model simulations in order to identify the dynamical impacts from changing the thermodynamic properties for extreme and light precipitation events. Emori and Brown (2005) examined the thermodynamic and dynamic components in their study to determine how influential each were, and the composite approach has been used before by Mahoney et al. (2012) and Zhao et al. (2012) however, for extreme and light precipitation events in the southern United States, this combination of using the composite approach to study the impacts of a thermodynamically altered climate is novel.

Aside from understanding how these extreme and light precipitation events could change in a warmer climate, part of the motivation is to determine possible feedback loops that influence the extreme precipitation, such as a feedback from the low level jet or convective updraft strength. The feedback loops could create a super Clausius-Clapeyron relationship, meaning that the precipitation increases at a rate faster than the 7% per degree

Celsius vapor increase. In this situation there is an additional forcing that is favorable for heavier precipitation. As discussed in Chapter 1, some studies show that the extreme precipitation will be constrained by the Clausius-Clapeyron relation (Frei et al. 1998; Hennessey et al. 1998; Pall et al. 2007) whereas other studies have found that a super Clausius-Clapeyron relation will develop (Allen and Ingram 2002; Held and Soden 2006; Allen and Soden 2008; Lenderink and van Meijgaard 2008, 2010). Lenderink and van Meijgaard (2008) analyzed the relation even further by looking into not only the daily extreme precipitation values, but also the hourly values, and found that the daily values are generally constrained by the Clausius-Clapeyron relation while extreme hourly precipitation rainfall rates increase at about two times the relation.

Whether or not the extreme precipitation scales with or above the Clausius-Clapeyron relation has important implications. For example, Chou and Neelin (2004) found that where the extreme precipitation events increase in intensity, other areas that have dry conditions become drier. The intensification of extreme events has implications not only for potentially larger floods in the areas of more intense precipitation. On the other hand, the light precipitation decreasing in frequency has implications for more intense droughts in the drier areas.

4.1.2 Experimental Design

The purpose of the present study was to determine the potential impacts of a warmer climate on extreme and light precipitation events, as well as to understand how the dynamic components respond to thermodynamic changes. The events were obtained from the

Dartmouth Flood Observatory and the daily precipitation data for the events were collected from NCDC. A classification process was used to select the most extreme events. Those events between years 1985 and 2011 where at least three inches of rain fell in twenty-four hours or less at two or more rain gauge sites, which were separated by at least ten miles, were identified. After the extreme events were selected, every event was individually categorized based on the region, season, and flooding type.

Once the events were sorted and combined with others that were most similar to them, two composites were made. The first composite, which is the strongly-forced precipitation event, consisted of nine events that occurred over the southern states of Texas, Louisiana, Mississippi and Alabama during March, April and May. The second composite, which is the weakly-forced event due to less pre-event alignment, consisted of thirteen events that fell in the latitude longitude bounds of 28° to 37°N and 85° to 94°W and occurred during the months of September through May. For this second composite, one last qualification required that the final events that created the composite to have a 500mb trough or closed low pressure system over the western United States between 115° and 90°W with vorticity values in the axis of the trough of $20\text{x}10^{-5}s^{-1}$ or more.

Using the fields at all levels from the individual events, the variables were combined together to create one composite event. The two composite datasets were then used as the initial and boundary conditions for the present-day simulations using the WRF model with three domains of 36, 12, and 4 kilometer grid spacings. For the future simulations, a complicated but necessary approach was used to change the thermodynamics properties of the present-day simulations and warm the temperatures while keeping the relative humidity

values constant. By changing the thermodynamic properties and keeping the synoptic-scale pattern the same, changes in the smaller dynamical components are revealed and can be further analyzed in terms of possible feedback mechanisms.

4.1.3 Hypothesis

In review, there was one main hypothesis for this study that was built off of three points brought to light in previous literature. First of all, there was expected to be a decrease in precipitation for the light precipitation events. Secondly, by changing the thermodynamic properties in the future run and keeping the synoptic pattern the same, the moisture increased and there was expected to be with this increase in moisture more extreme precipitation in the future. Along with this expected increase in extreme precipitation was the question of whether the precipitation will scale with, below, or above the Clausius-Clapeyron relation. If the precipitation were to show a super Clausius-Clapeyron relation, the next question would be what factors are influencing the precipitation resulting in larger amounts than the 7% per degree Celsius. So for our hypothesis, with increased water vapor content, we expected there to be an increase in the strength of condensationally-driven dynamical factors which serve to amplify precipitation increases beyond the Clausius-Clapeyron implied vapor increase. This hypothesis was tested by analyzing the WRF present-day and future runs.

4.2 Conclusions

4.2.1 WRF Simulations

4.2.1.1 The Weakly-Forced Event

Due to the nature of the events in the 13-case composite, the present-day simulation for the weakly-forced event showed fairly weak synoptic forcing for ascent. A modest trough propagated eastward throughout the simulation, reaching its maximum intensity 48 hours into the present-day run, and weak southerly flow at the surface brought moisture to the Gulf States throughout the run, however, neither forcing was strong. The upper level jet right entrance region was in a favorable location for rising motion and the CAPE was moderate. The precipitation had two main bulleyes, one in northeastern Arkansas and the other over Kentucky. The swath was oriented from the southwest to the northeast, and the hours from 24 to 48 saw the heaviest rainfall.

The future simulation for the weakly-forced event showed weak forcings as well, with an even weaker low level jet, and the synoptic system propagated eastward much more quickly than in the present-day simulation. Additionally, the upper trough exhibited a more strongly lifting structure in the future simulation, which may have been due to heavier precipitation early on in this simulation. The faster eastward movement of the upper trough was also perhaps due to the large-scale temperature and moisture changes, which provide a stronger height increase to the south over much of the domain, and yield faster westerlies aloft. This is consistent with the findings of Lackmann (2012) in an analysis of the south-central US flood of May, 2010.

For this weakly-forced precipitation event, a decrease in precipitation in the future

occurred but the reasons were not clear before undertaking the analysis- here, the precipitation was lighter due to enhanced weakening and a more rapid eastward progression of the upper-level trough. After an initial burst of heavy rain, the precipitation in the warmer climate decreased, as did the synoptic and mesoscale forcings. The heaviest precipitation fell between the 24th and 42nd hours, after which the atmosphere began stabilizing, the low pressure system passed over and the CAPE values did not return to their large values, leaving very little precipitation falling in the last 24 hours. This result is consistent with previous studies mentioned in Chapters 2 and 3.

4.2.1.2 The Strongly-Forced Event

In the present-day simulation of the strongly-forced precipitation event, the forcing for ascent was much stronger due to a composite case selection that isolated events with pronounced upper-level troughs prior to the event over the southwestern United States, in addition to rain in the south-central United States at a later time. A deep trough pressed eastward across the United States and a strong low pressure system intensified throughout the simulation, as well as the low level jet which pumped a good amount of moisture over the central United States. A strong elongated upper level jet was present with the right entrance region in a favorable position for rising motion. The precipitation was much more widespread than in the weakly-forced event and was oriented from the southwest to the northeast with many bands of very heavy precipitation totals. Great amounts of rain fell between hours 24 and 48, as seen in the weakly-forced event, but during the latter 24 hours a lot of rain fell as well, however, it fell over the northern United States.

The future simulation showed a stronger synoptic and mesoscale system and, as in the weakly-forced event, the synoptic system in the future moved to the east much more quickly than in the present-day simulation. The surface low pressure system was very strong and was wrapped with moisture that was transported from the Gulf. The low level jet was also much stronger in this future simulation than in the present-day simulation, and in the strongly-forced event simulation, precipitation was falling near the low-level jet, allowing for possible feedbacks and intensification. The precipitation was still just as widespread with more precipitation falling in the north, which was due to the more intense surface low pressure system and its track further to the north.

For this strongly-forced precipitation event, we expected to see more extreme precipitation in a warmer climate and the results show just that. The precipitation in the future simulation not only increased, but it increased at the super Clausius-Clapeyron rate. The moisture over the areas of heaviest precipitation increased ~23.6% in the future simulation, and the precipitation increased by 34%. The temperature increased in the future over these heaviest precipitation areas by 3.19°C so the expected increase in precipitation had it scaled with the Clausius-Clapeyron relation would have been about 22%, but the 34% that occurred is much higher than this. The precipitation increased across the entire domain at a super Clausius-Clapeyron relation as well with the average moisture increasing by ~20% and the precipitation increasing by ~30%. This super Clausius-Clapeyron relationship was influenced by the intensification of the low level jet as well as the stronger low pressure system. Increased ascent in convective cells due to larger CAPE may also have contributed to the increase.

All in all, our results show that for the weakly-forced precipitation event during the cool season over the southern states, the precipitation decreased in a warmer climate for this case. For the strongly-forced precipitation event in the southern states during March, April, and May though, the precipitation increases. These results are supported by previous studies that are mentioned and discussed in Chapters 2 and 3. This increase scales as a super Clausius-Clapeyron relation. On top of this, the low level jet intensified and elongated in the warmer climate for this stronger event, suggesting a possible positive feedback mechanism.

One of the main findings in this study is that the precipitation response to warming is correlated to the upper-level forcing. The composites and simulations showed two separate systems, one with weak and one with strong forcings, and the precipitation responded differently in both cases. This demands more work, especially into the impact of the initial shot of precipitation in the future simulation of the weakly-forced event that could have weakened the upper-level trough, and the impact of adding higher heights to the south.

Finally, the northward shift in the region of precipitation and the faster trough progression, have additional potential societal impacts. Although additional work is needed, if shifts of this type proved to be common, there could be implications for agriculture, among other things.

4.3 Future Work

This research opens up several additional avenues of future work. First of all, it would be interesting to apply this method to a different area of the United States, such as the southeast or west. Every single event recorded from the Dartmouth Flood Observatory is

categorized based on region, season, and flooding type, and is ready to be used, so applying this method is highly advised in order to understand how a warmer climate can impact extreme precipitation events in other regions of the United States. Also, studying different types of flooding events would be helpful as well to compare the similarities and differences between the different types.

As the present study applies thermodynamic changes based on the SRES A2 scenario, future work can also examine the other scenarios as well, such as A1B, or, more importantly, using the new CMIP5 GCM data. By analyzing a few scenarios for the same season and region, the degree to which the scenarios impact the extreme precipitation relative to each other could be determined.

The composite approach used here has limitations. However, one of the weaknesses, which is smearing of features at times before the central time, was used to advantage by allowing comparison of strong and weak forcing. This is an efficient method to use because instead of running numerous case studies for each of the future projects mentioned above, only one present-day and one future simulation needed to be run. Another suggestion for future work is to use the composite approach with more cases. Using the Dartmouth Flood Observatory to acquire the extreme precipitation events that caused large floods was a sturdy approach, but if another database contains this flooding information but perhaps with years prior to 1985, more cases could be obtained resulting in more cases to use to create the composite.

The last suggestions for future work is to take all of the events that created the thirteen-event composite, as well as those that created the nine-event composite, and run each

event individually and then average the results together to see how the those results for the thirteen and nine-event composites compare with those found here. These composite-based simulations were recently rerun but instead of starting two days before the composite precipitation event occurred, they were initialized one day before the precipitation event as well as the day of the precipitation event. This was done for the weakly and strongly-forced composite-based present-day and future simulations. Further analysis is needed to compare the results analyzed above when the simulations were initialized two days prior to the precipitation, to those obtained when initializing the model simulation at a later time in order to identify similarities and differences.

FIGURES

(a)

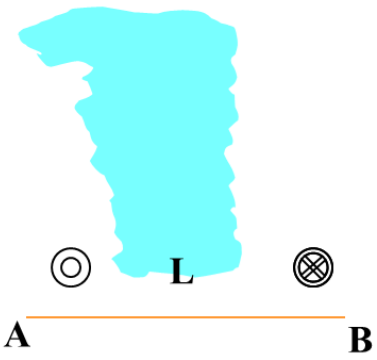

(b)

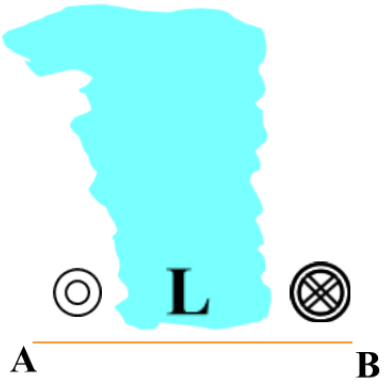

Figure 1.1: Schematic showing the intensification of the low level jet due to the increase in condensational heating: (a) earlier time with less condensational heating, (b) later time with less condensational heating. The blue area represents condensational heating and as it increases, the surface low pressure intensifies, creating stronger northerly and southerly flow, which intensifies the low level jet.

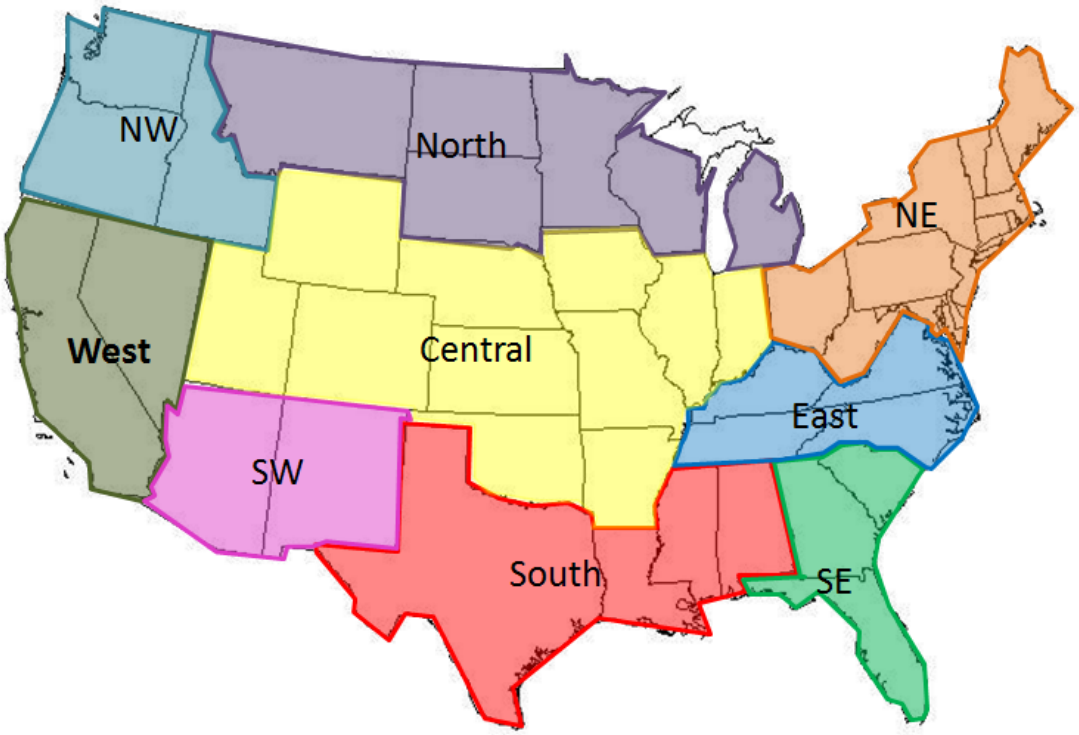

Figure 2.1: United States geographical boundaries for categorizing the individual events in the south, southeast, east, northeast, north, northwest, west, southwest, and central regions.

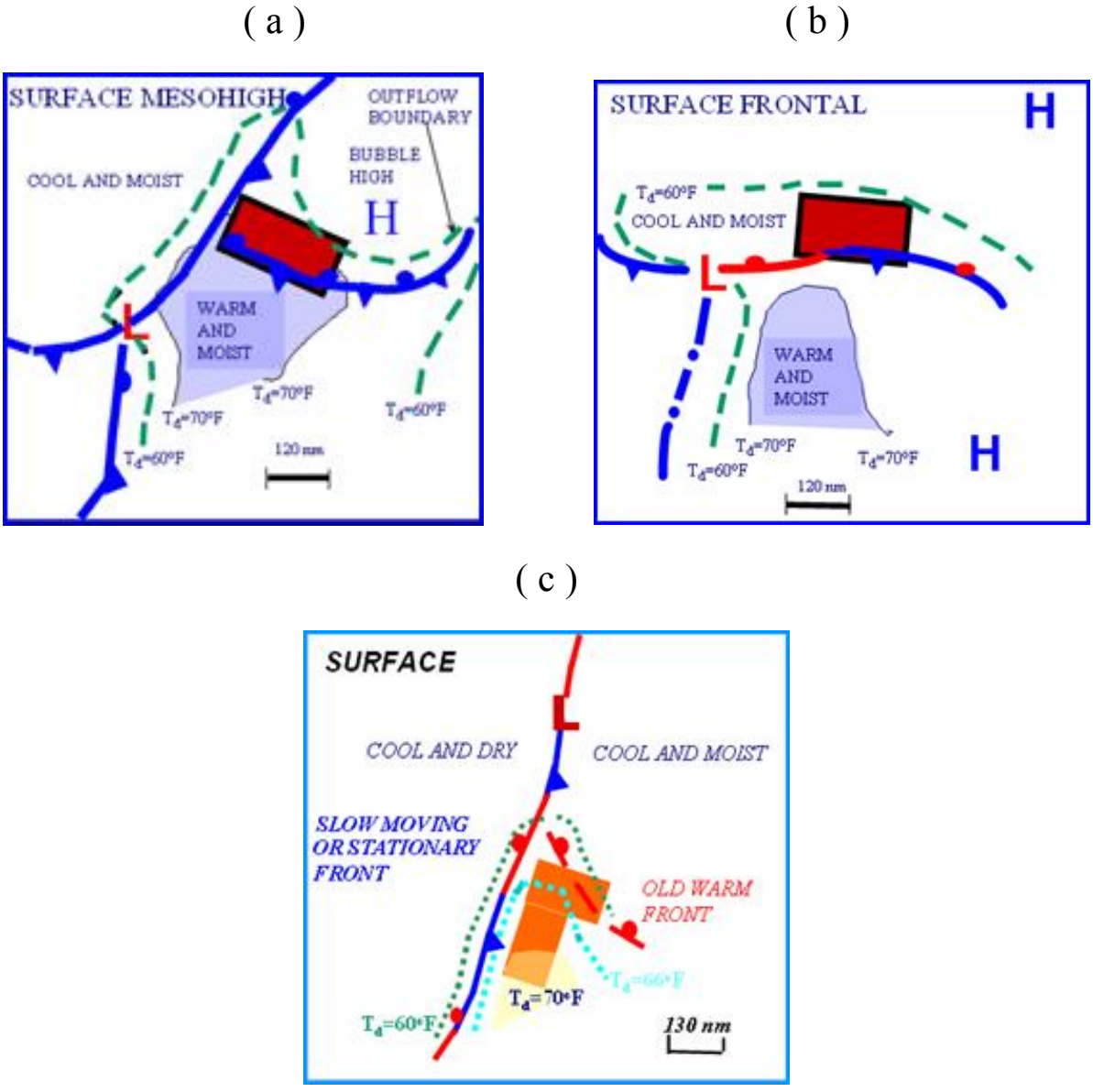

Figure 2.2: Maddox heavy precipitation type schematic of surface conditions: (a) mesohigh, (b) frontal, (c) synoptic. [Courtesy of the Hydrological Prediction Center (HPC)]

(a)

(b)

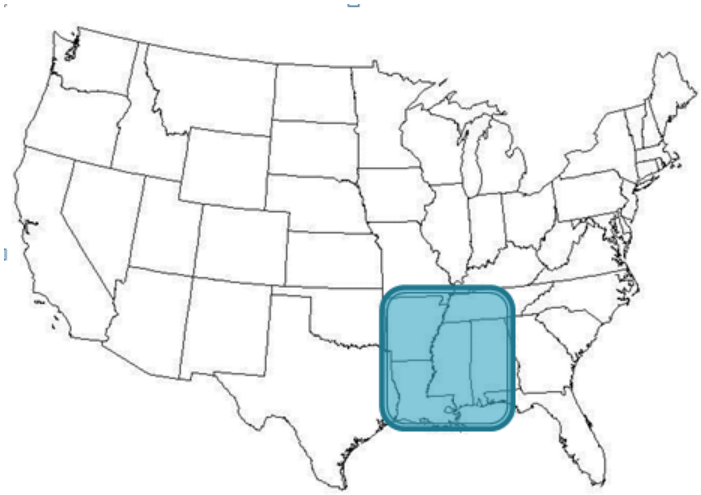

Figure 2.3: Geographic bounds for the precipitation events in the composites: (a) nine (strong) event, (b) thirteen (weak) event.

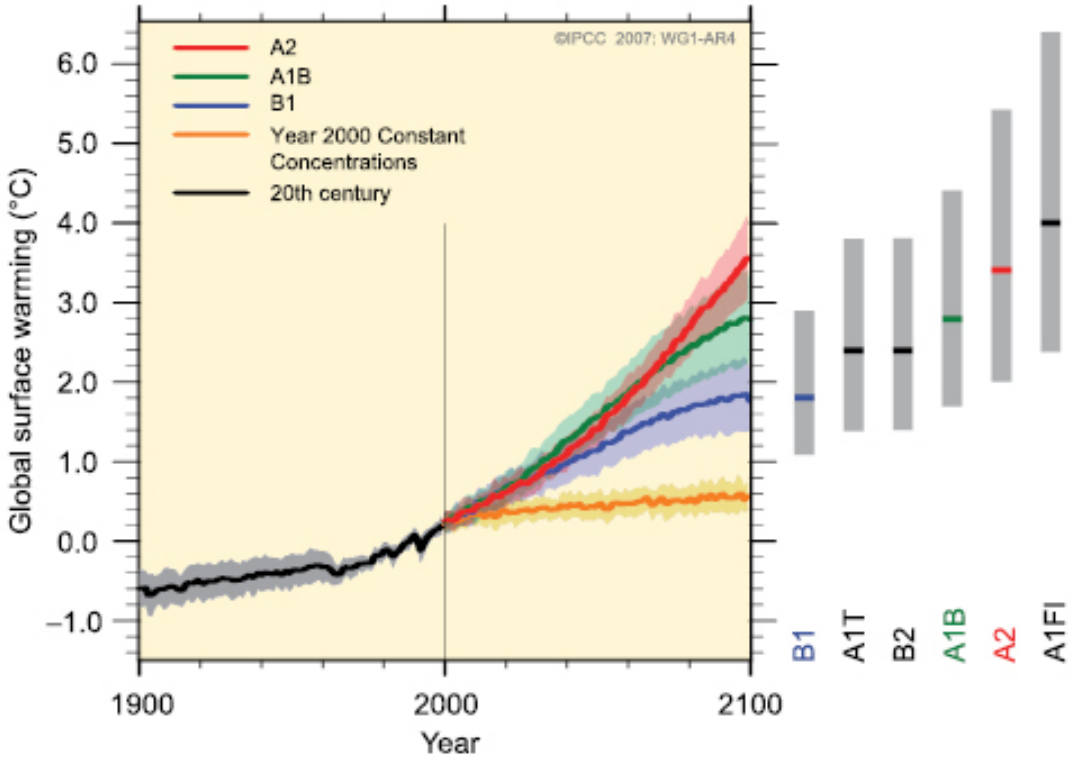

Figure 2.4: Multi-model averages and ranges of surface warming globally for the IPCC AR4 emission scenarios, B1, A1B, and A2. Grey shading shows ±1 standard deviation range and the orange line shows year 2000 values held constant. [Courtesy of IPCC AR4]

(a)

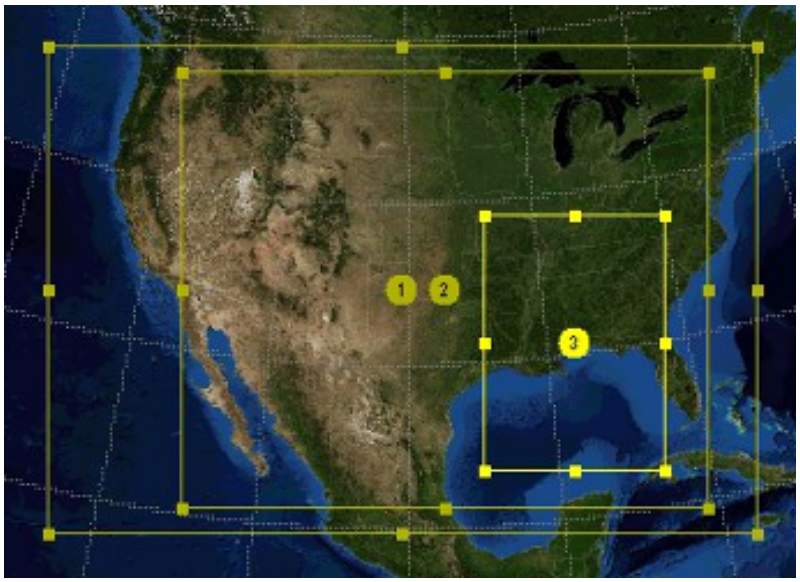

(b)

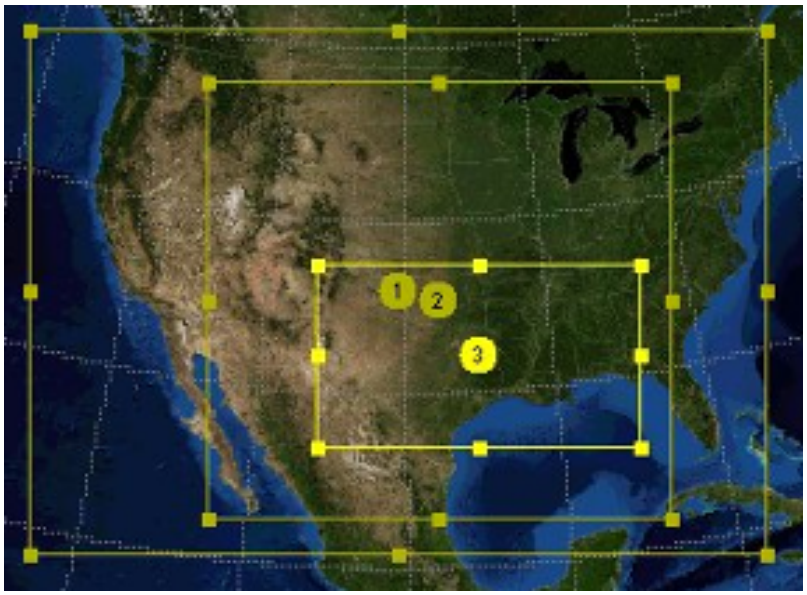

Figure 3.1: The 36, 12, and 4km grid spacing domains: (a) Weakly-forced event, (b) Strongly-forced event.

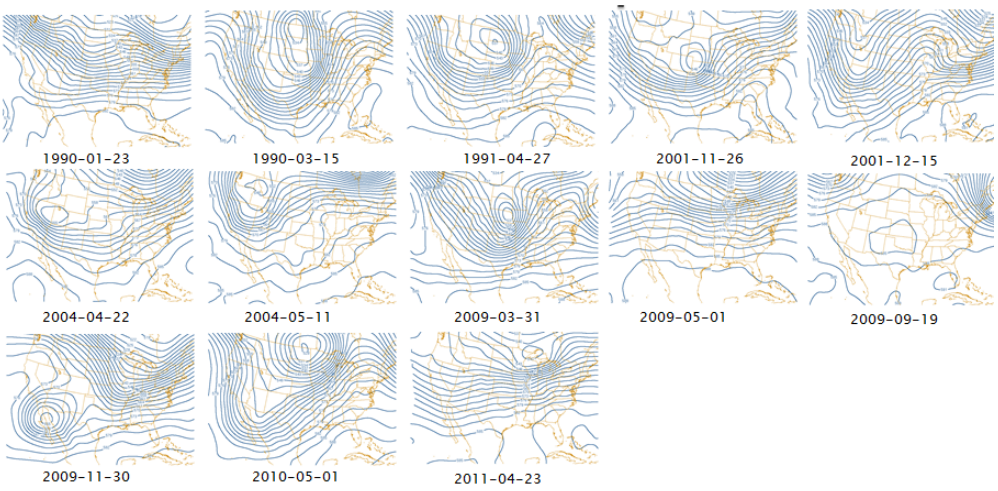

Figure 3.2: The 13 individual cases that make up the weakly-forced event two days prior to the precipitation at 1200UTC.

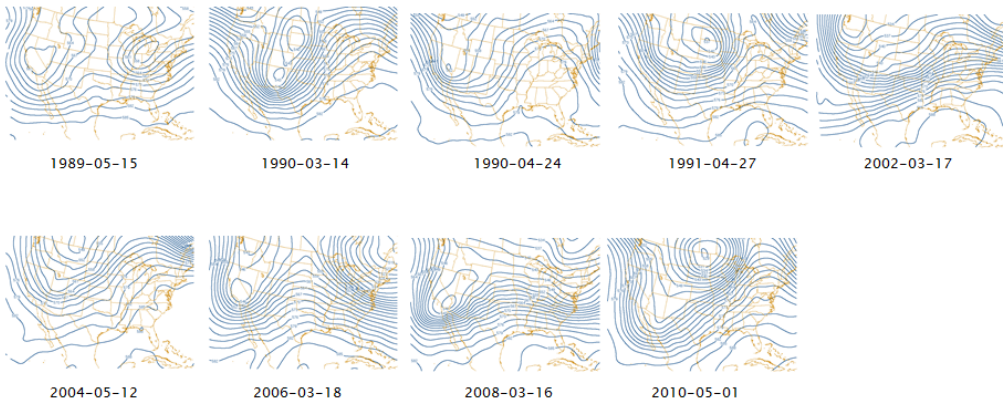

Figure 3.3: The nine individual events that make up the strongly-forced event two days prior to the precipitation at 1200UTC.

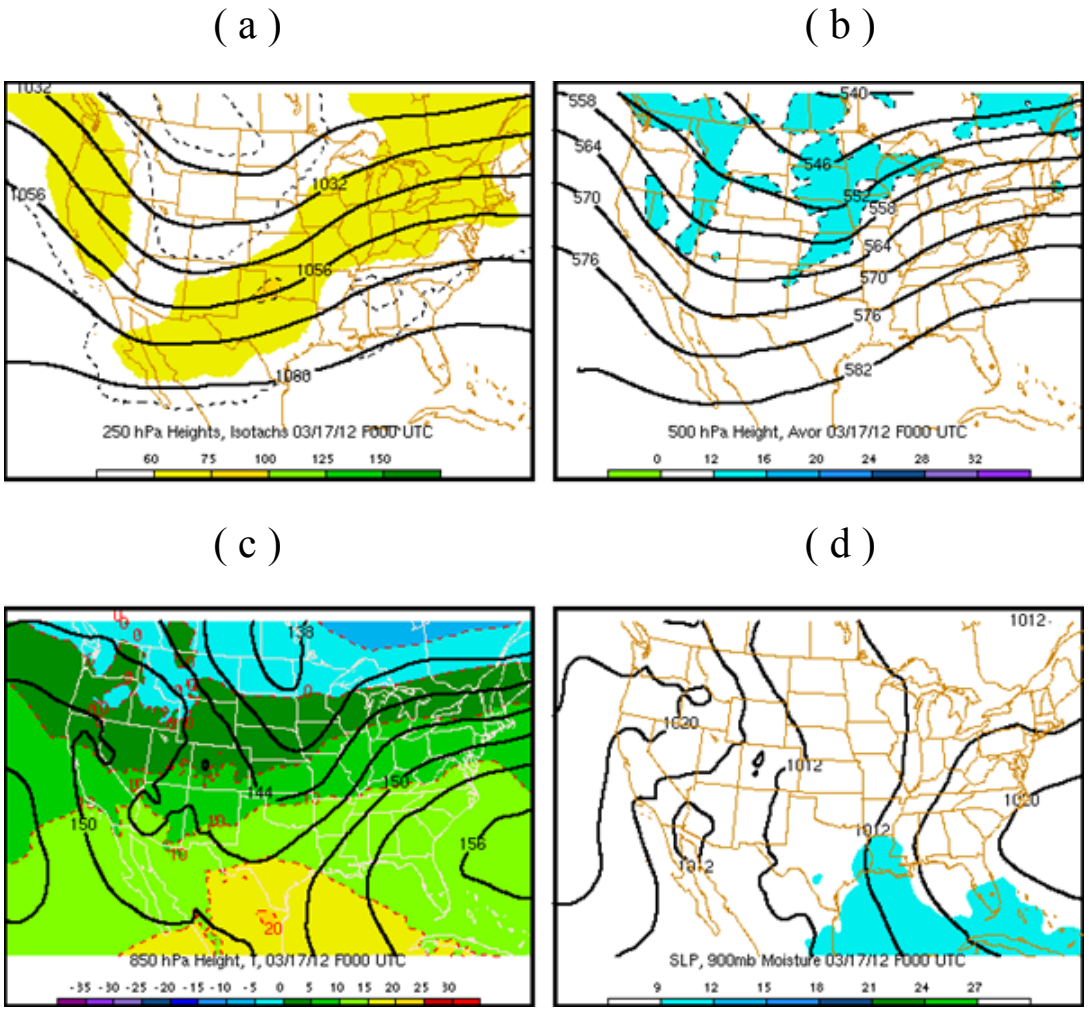

Figure 3.4: Four panel plot in the weakly-forced event composite, 2 days before precipitation event, of the atmospheric conditions: (a) 250mb isotachs (in knots) and heights (contour interval 12 dam), (b) 500mb heights (contour interval 6 dam) and vorticity (x$10^{-5}s^{-1}$), (c) 850mb heights (contour interval 3 dam) and temperatures (°C), (d) the sea level pressure (contour interval 4mb) and 900mb moisture (g/kg).

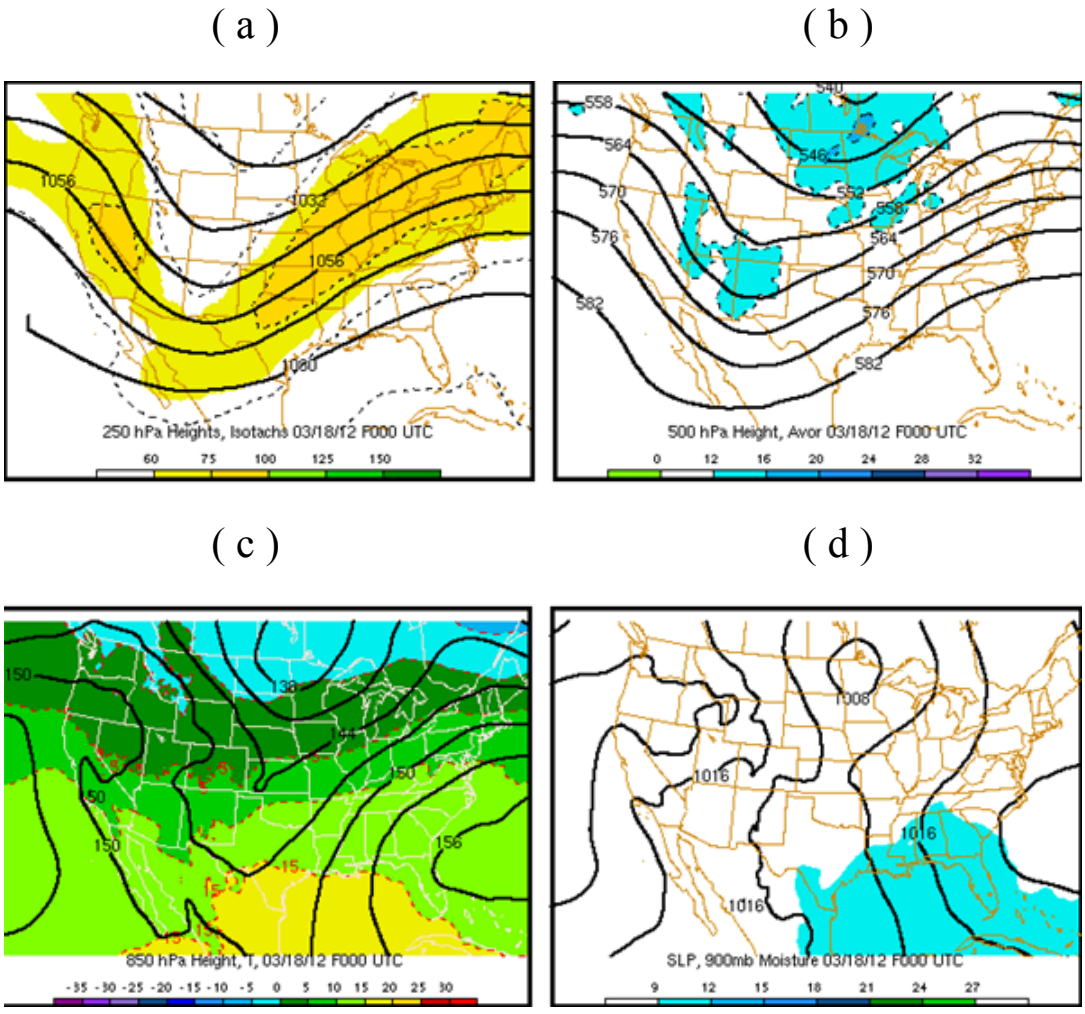

Figure 3.5: Four panel plot in the weakly-forced event composite, 1 day before precipitation event, of the atmospheric conditions.

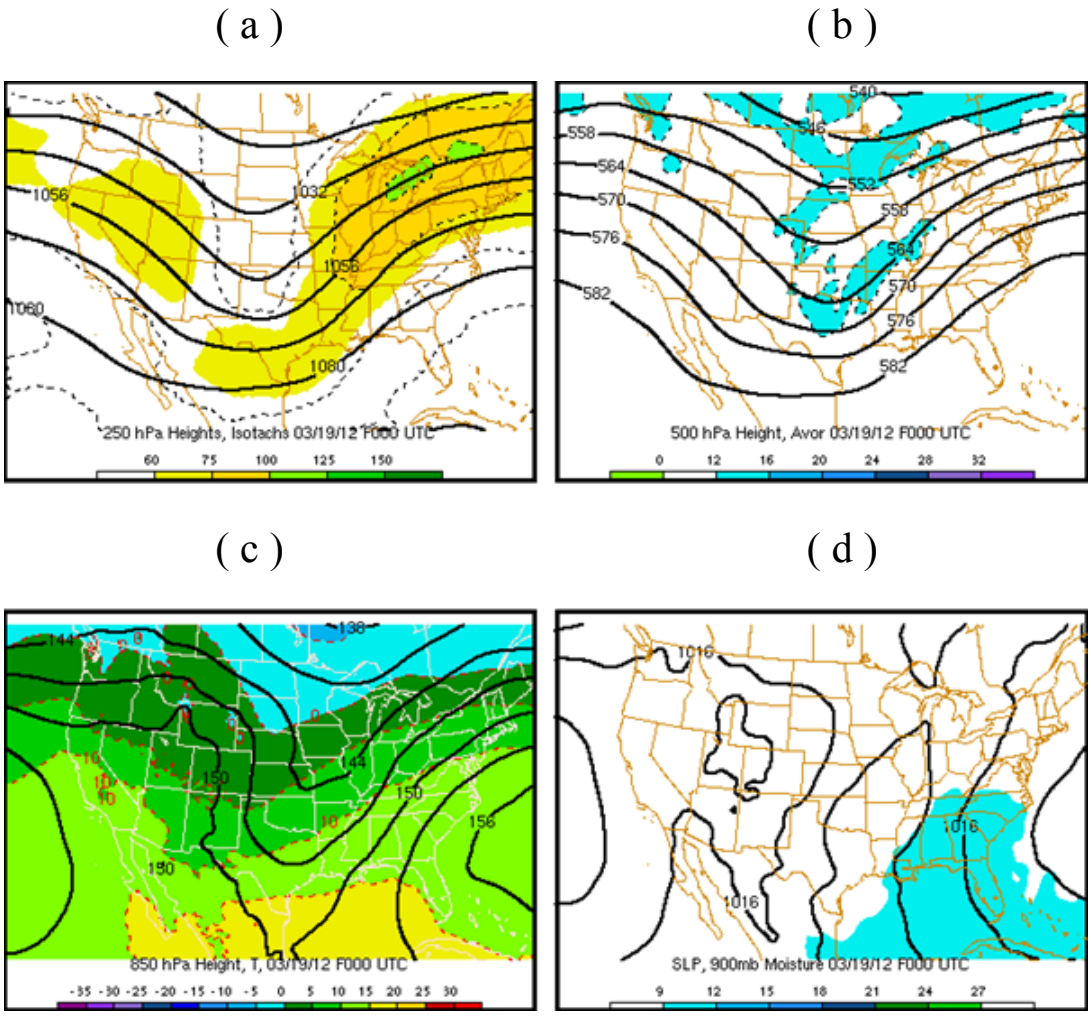

Figure 3.6: Four panel plot in the weakly-forced event composite, on the day of the precipitation event, of the atmospheric conditions.

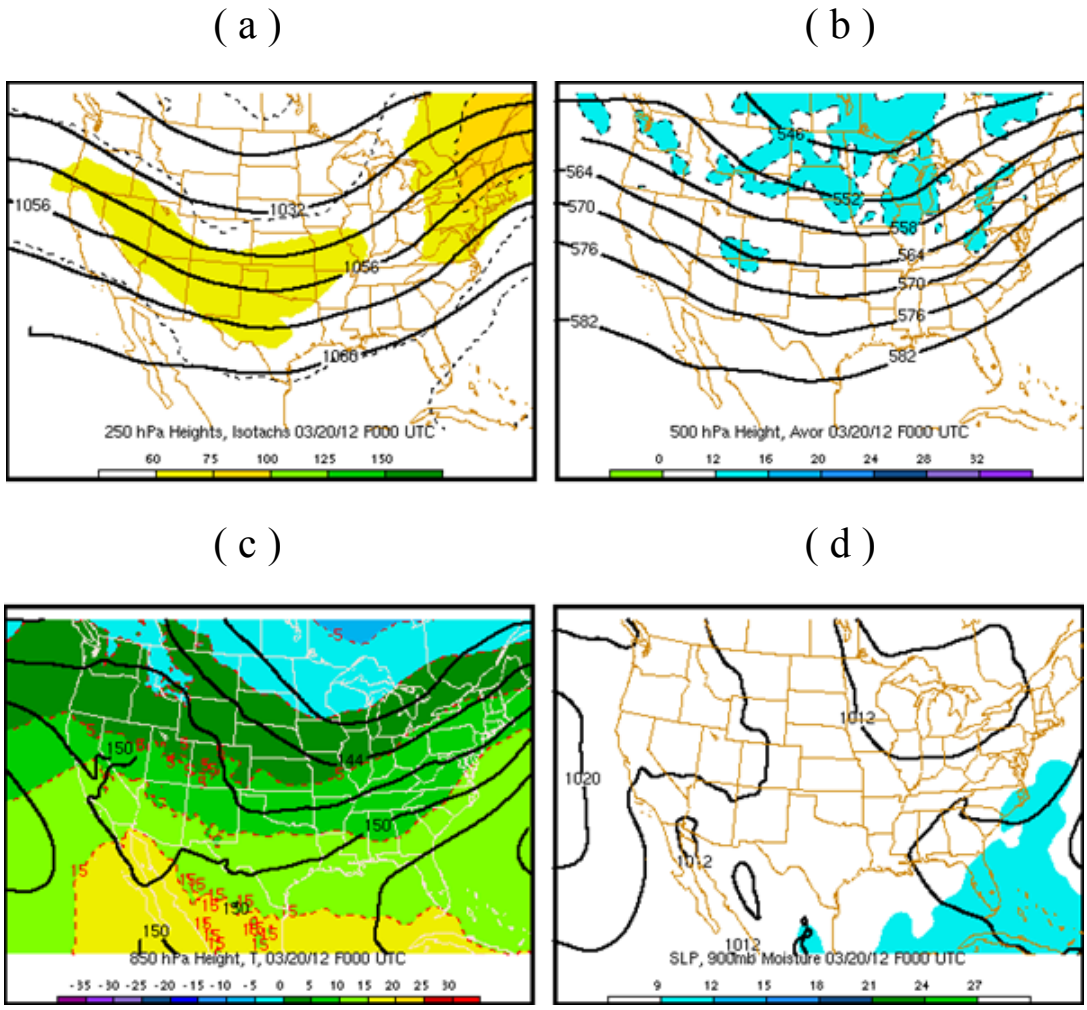

Figure 3.7: Four panel plot in the weakly-forced event composite, 1 day after the precipitation event, of the atmospheric conditions.

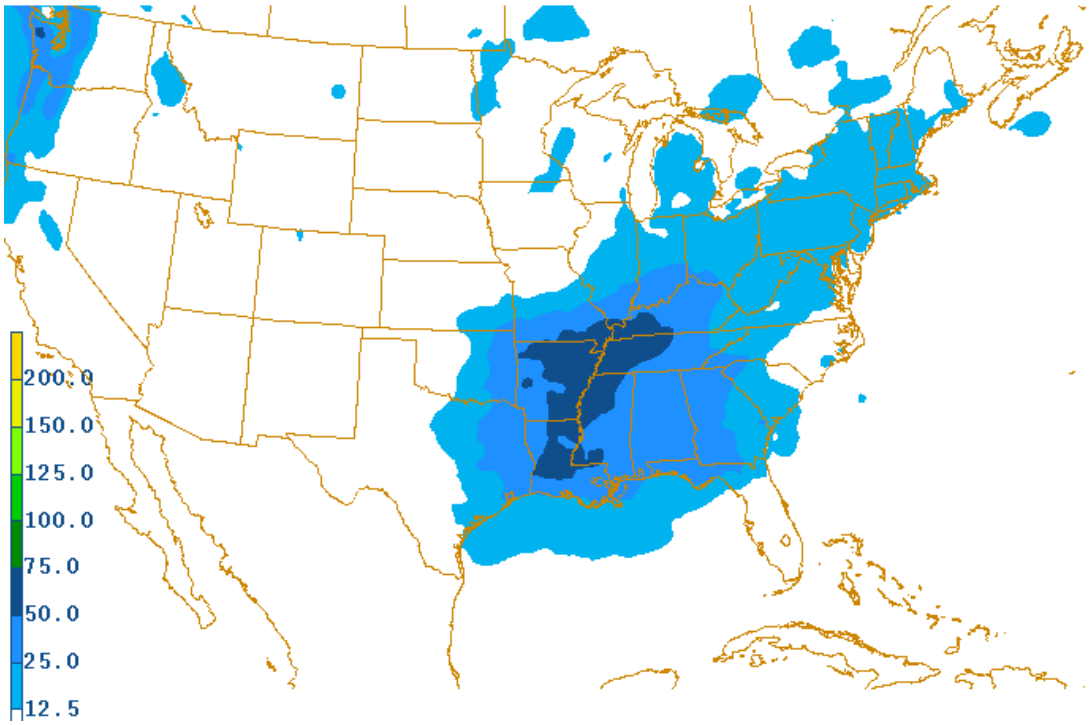

Figure 3.8: Total 72 hour precipitation (mm) for the weakly-forced composite.

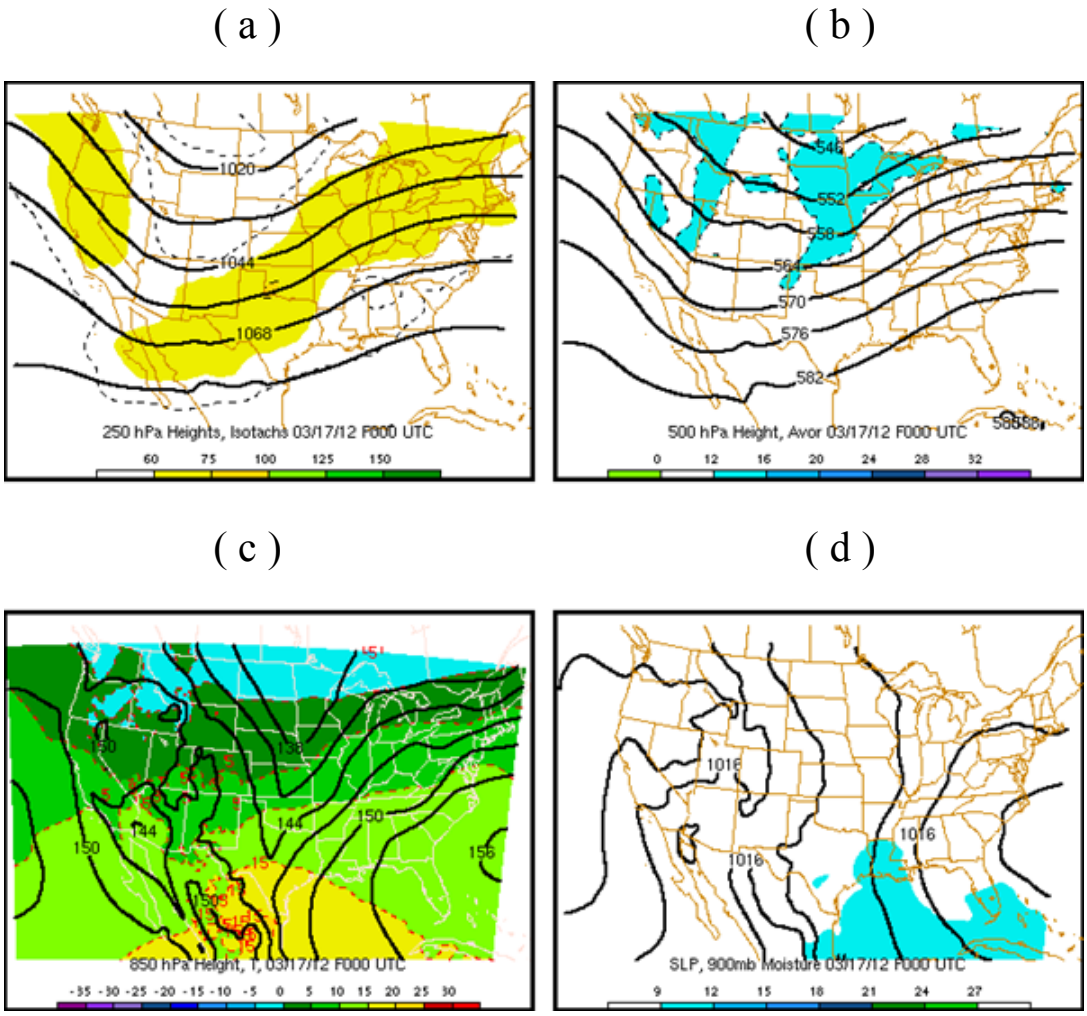

Figure 3.9: Four panel plot of atmospheric conditions for F00 (1200UTC Day 1) of the weakly-forced event present-day simulation using the WRF model at 36km grid spacing.

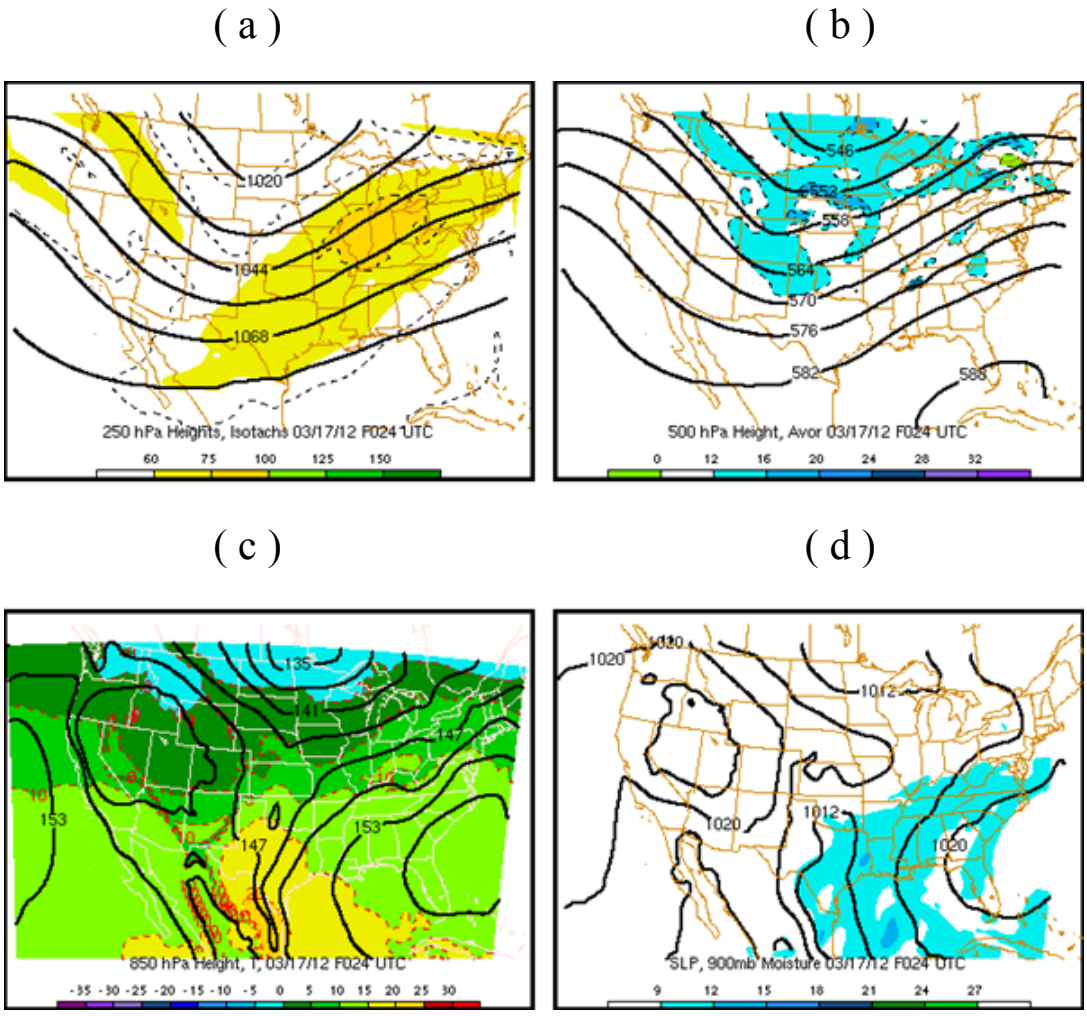

Figure 3.10: Four panel plot of atmospheric conditions for F24 (1200UTC Day 2) of the weakly-forced event present-day simulation using the WRF model at 36km grid spacing.

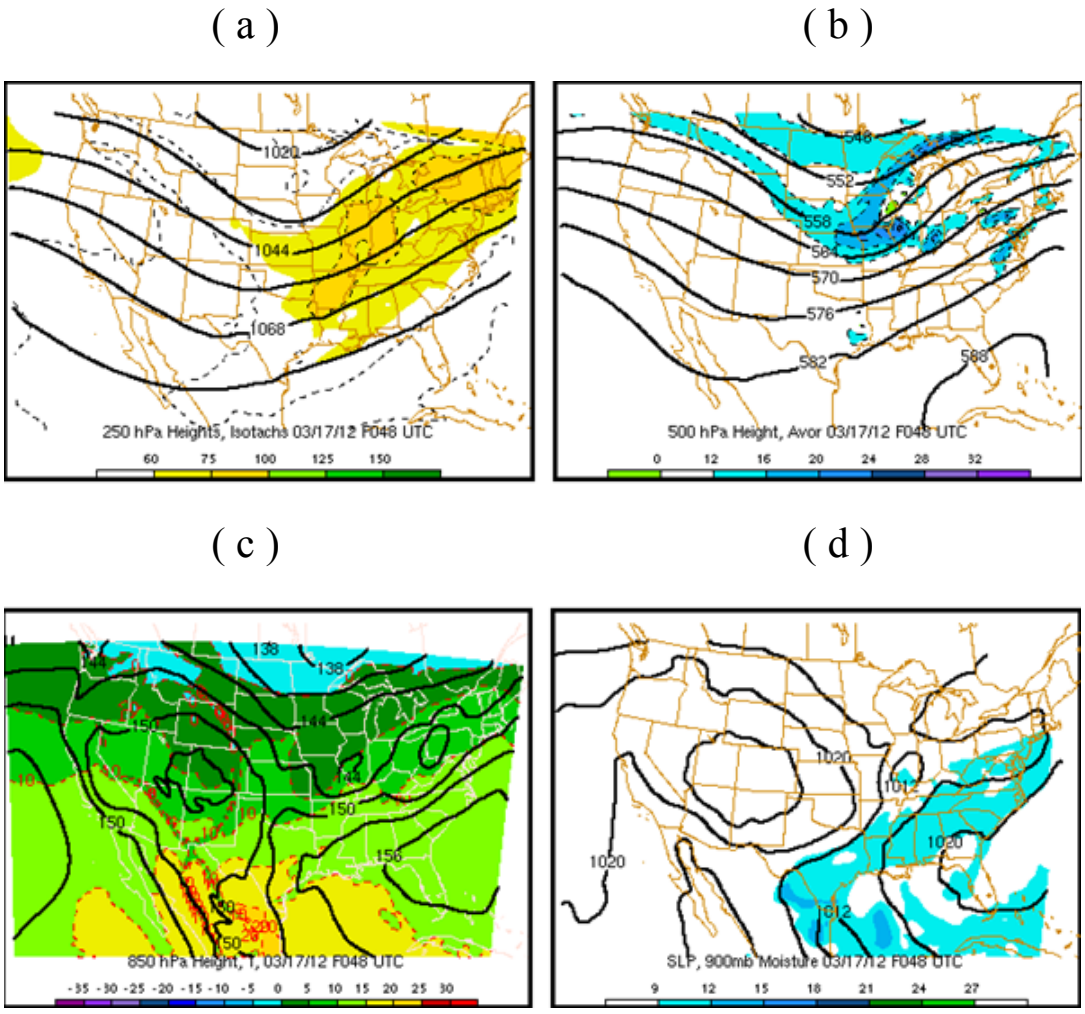

Figure 3.11: Four panel plot of atmospheric conditions for F48 (1200UTC Day 3) of the weakly-forced event present-day simulation using the WRF model at 36km grid spacing; can be compared to Figure 3.6.

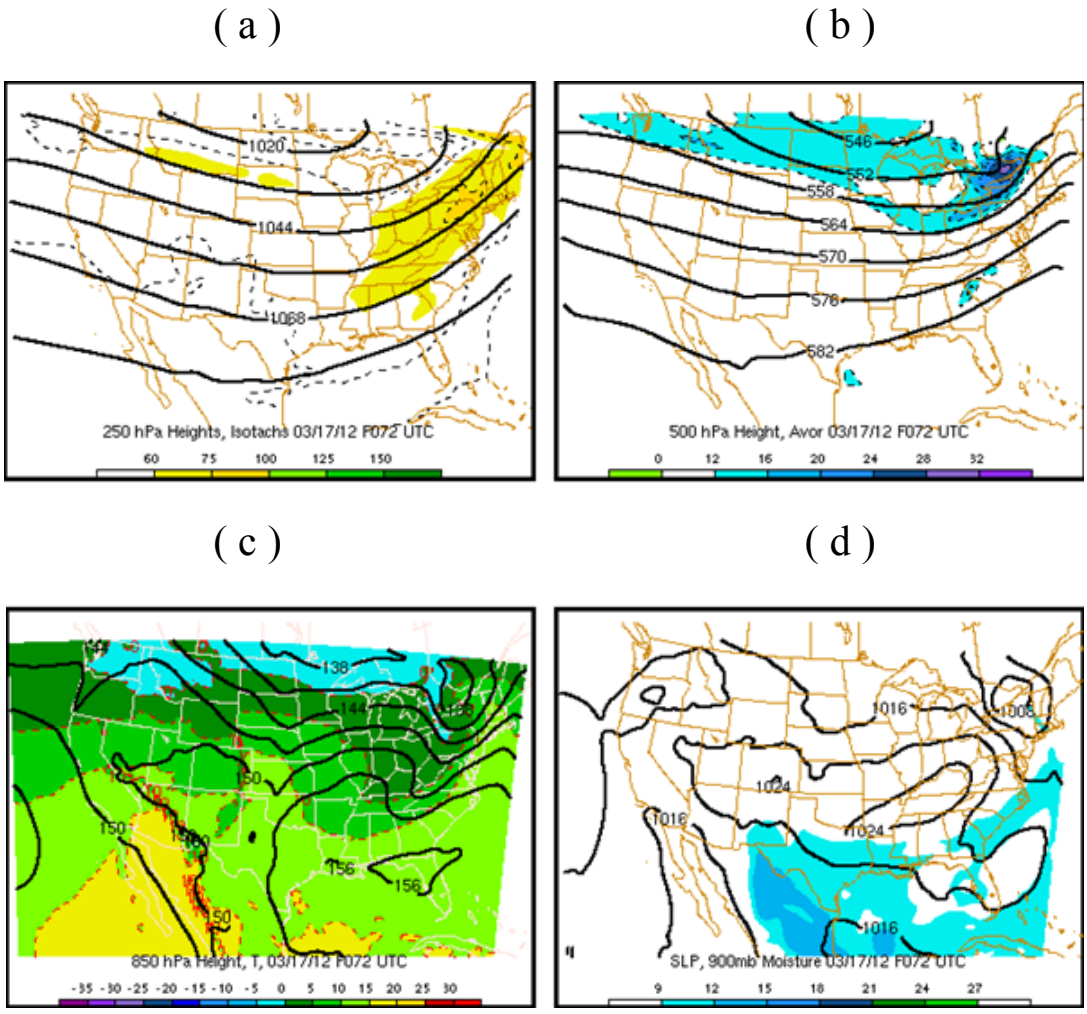

Figure 3.12: Four panel plot of atmospheric conditions for F72 (1200UTC Day 4) of the weakly-forced event present-day simulation using the WRF model at 36km grid spacing.

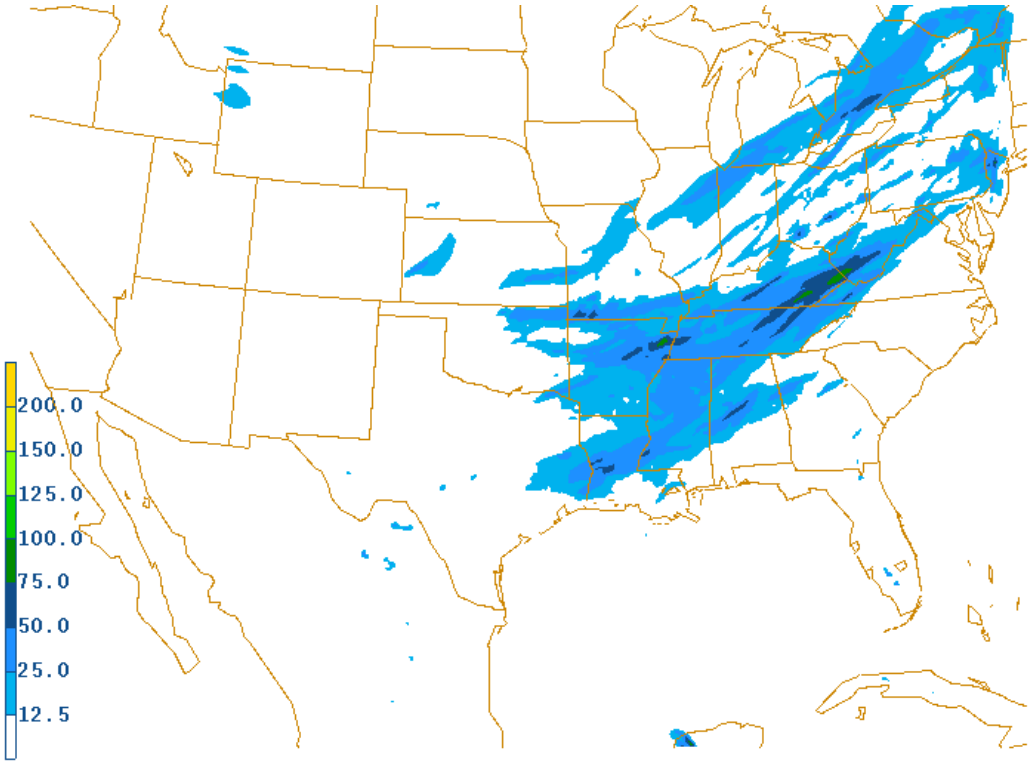

Figure 3.13: Total 72 hour precipitation for the weakly-forced event present-day simulation using 12km grid spacing. The color bar shows increments in mm.

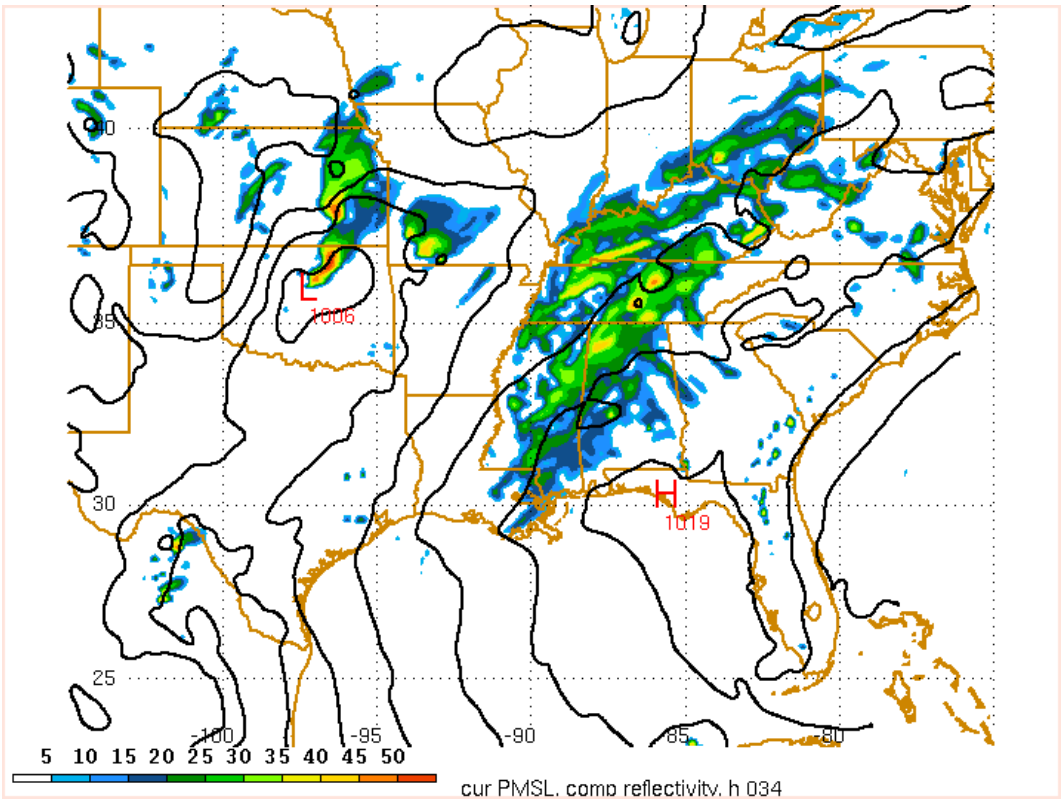

Figure 3.14: Sea level pressure is plotted with the weakly-forced event present-day simulation reflectivity for F34 (2200UTC on Day 2) using 12km grid spacing.

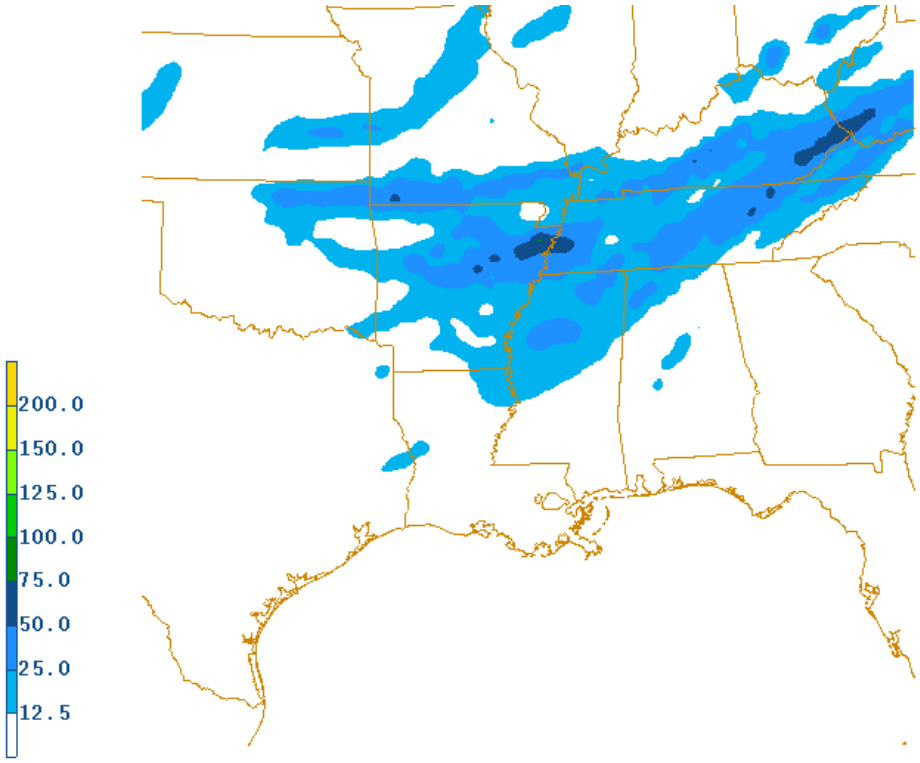

Figure 3.15: Precipitation (mm) difference between F48 (1200UTC Day 3) and F24 (1200UTC Day 2) with 12km grid spacing for the weakly-forced event present-day simulation.

(a)

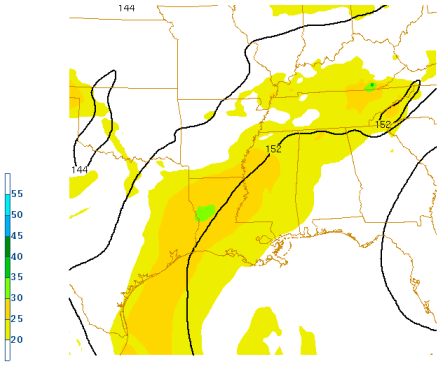

(b)

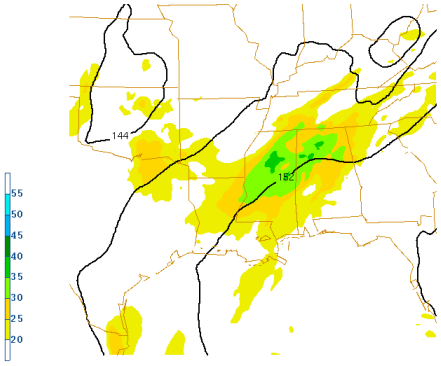

(c)

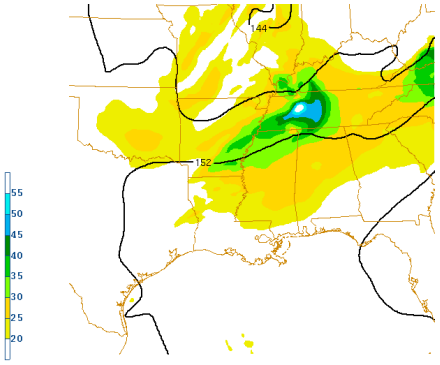

Figure 3.16: Isotachs (kt) at 850mb and 850mb heights using 12km grid spacing for the weakly-forced event present-day simulation: (a) the 24th hour (1200UTC Day 2), (b) the 33rd hour (2100 UTC Day 2), (c) the 48th hour (1200UTC Day 3).

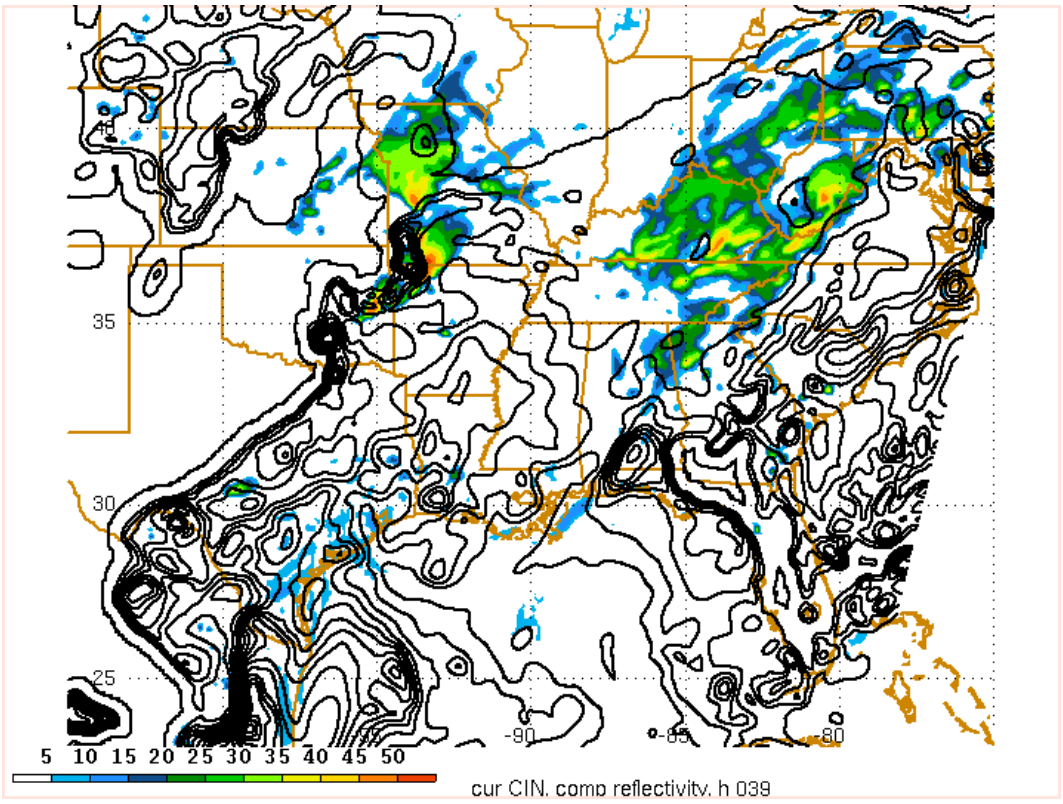

Figure 3.17: Convective inhibition (CIN) values superimposed over the reflectivity for the weakly-forced event present-day simulation during F39 (0300UTC on Day 3) with 12km grid spacing.

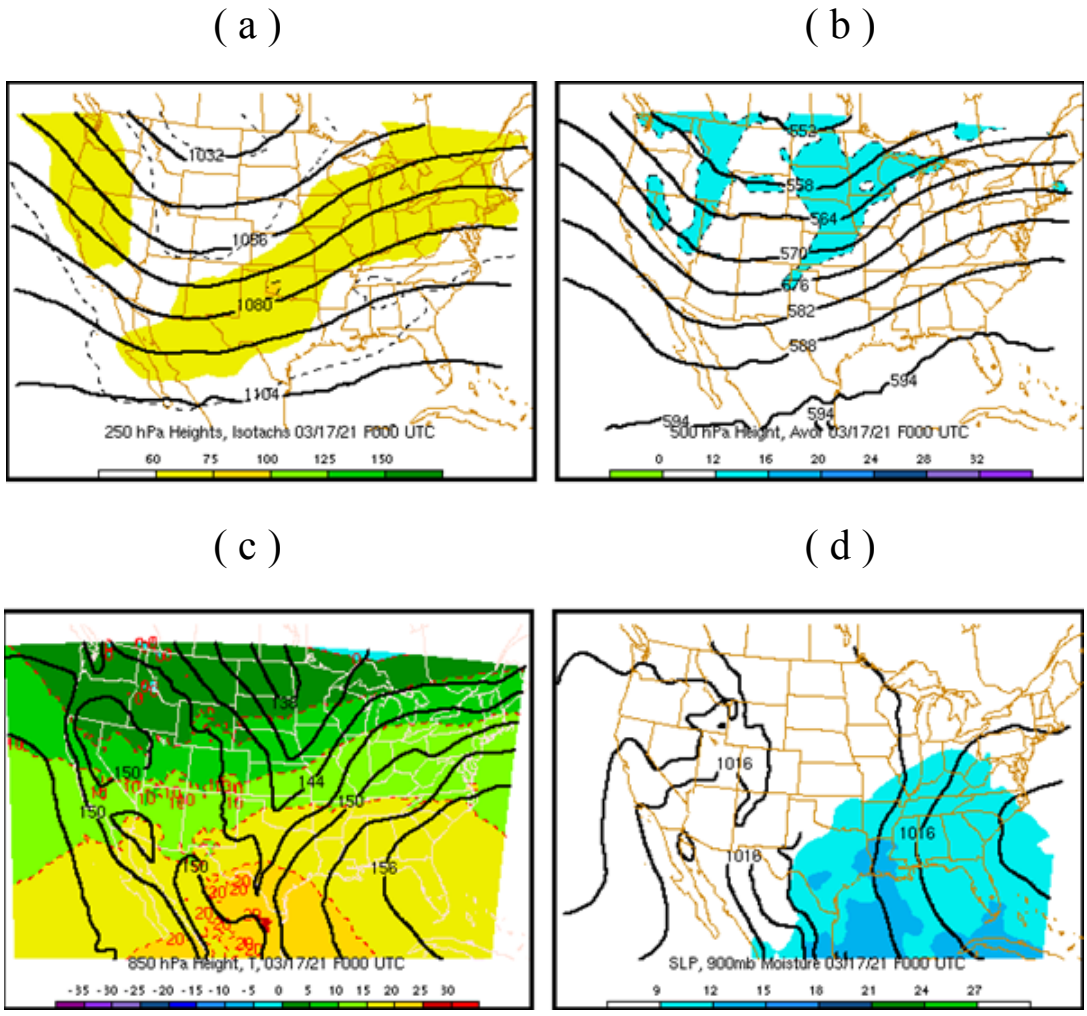

Figure 3.18: Four panel plot of atmospheric parameters at F00 (1200UTC on Day 1) for the weakly-forced event future simulation using 36km grid spacing.

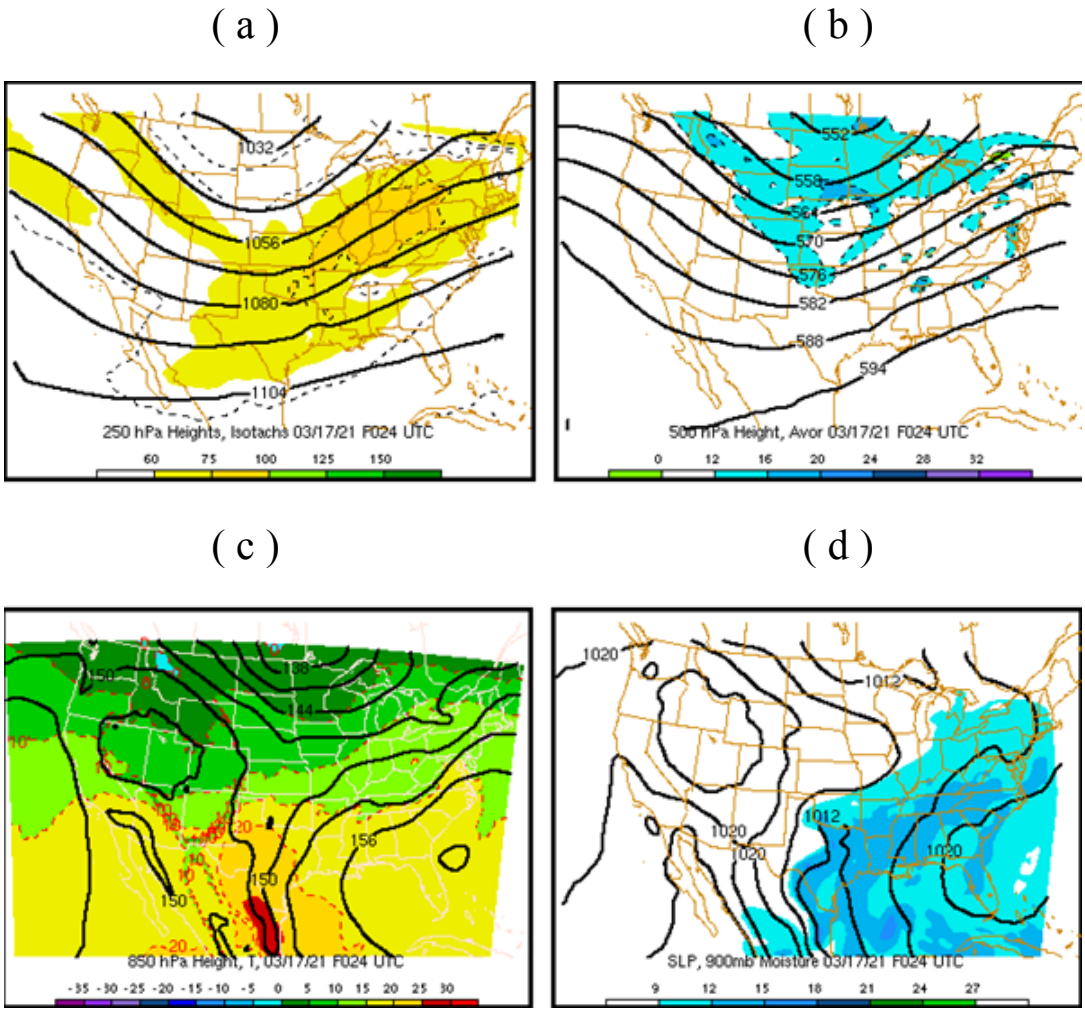

Figure 3.19: Four panel plot of atmospheric parameters at F24 (1200UTC on Day 2) for the weakly-forced event future simulation using 36km grid spacing.

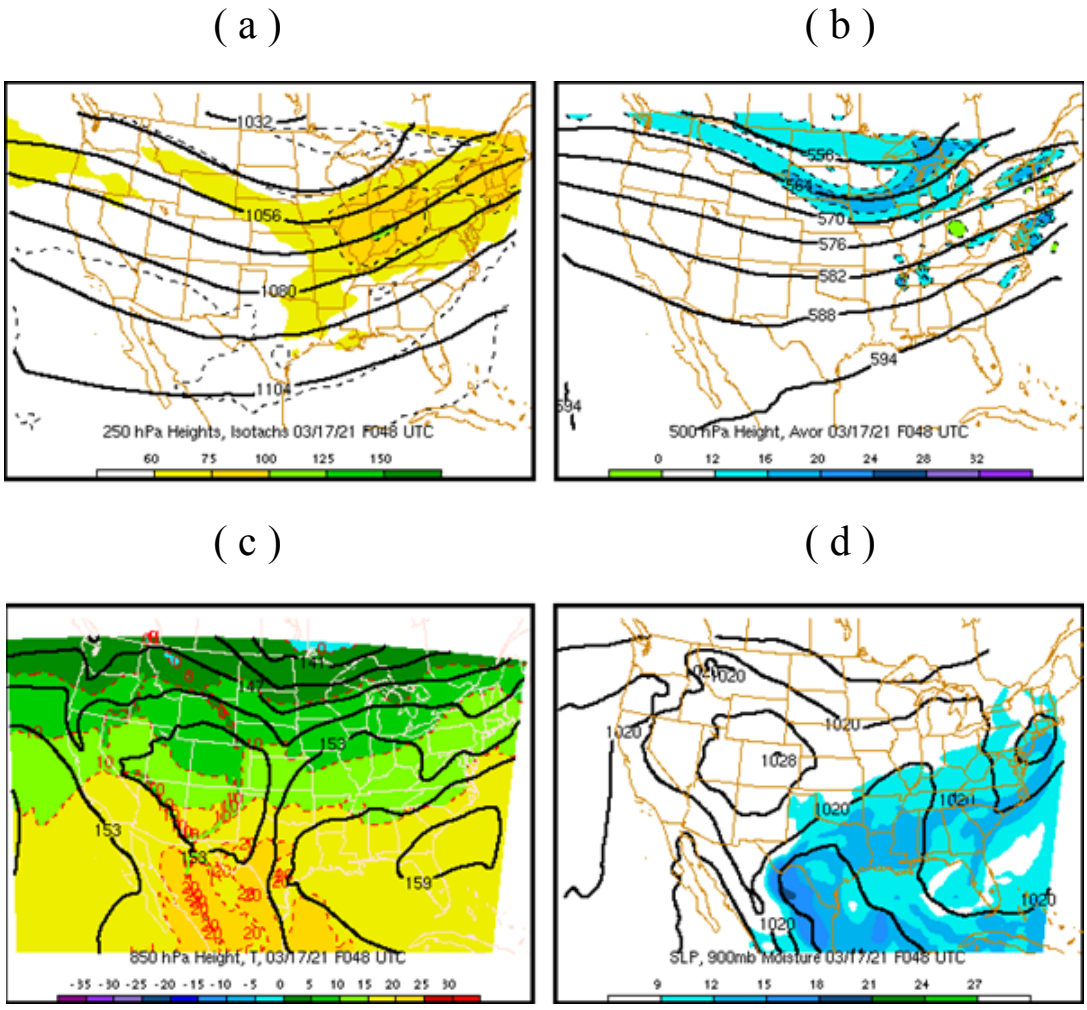

Figure 3.20: Four panel plot of atmospheric parameters at F48 (1200UTC on Day 3) for the weakly-forced event future simulation using 36km grid spacing; can be compared with Figure 3.11.

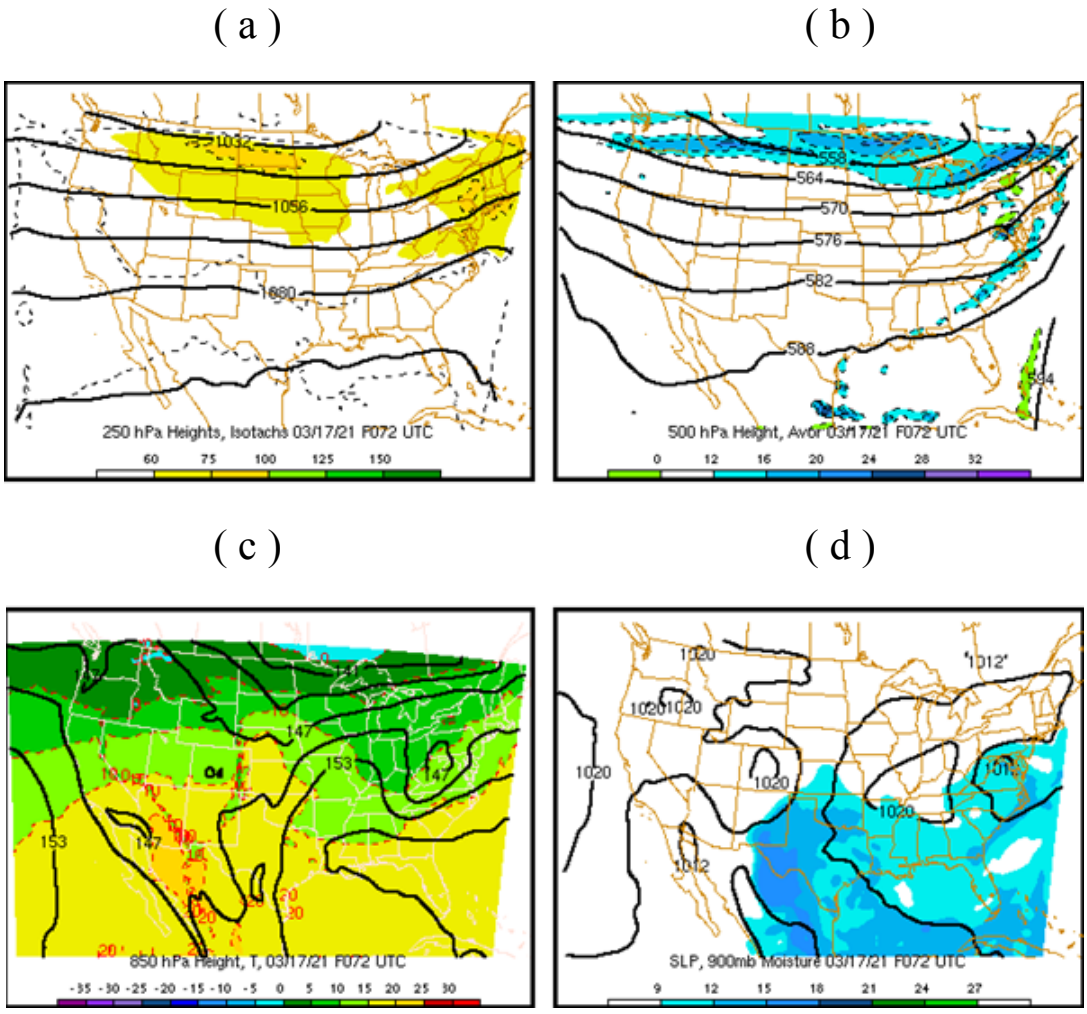

Figure 3.21: Four panel plot of atmospheric parameters at F72 (1200UTC on Day 4) for the weakly-forced event future simulation using 36km grid spacing.

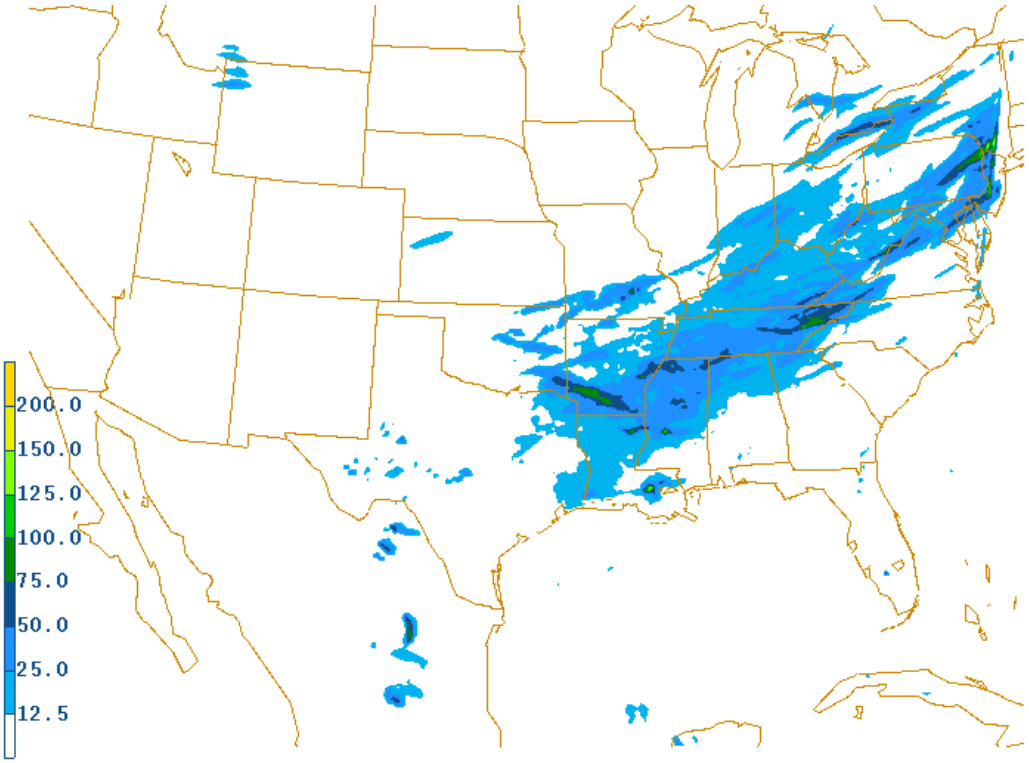

Figure 3.22: Total 72 hour precipitation (mm) for the weakly-forced event future simulation using 12km grid spacing; can be compared with Figure 3.13.

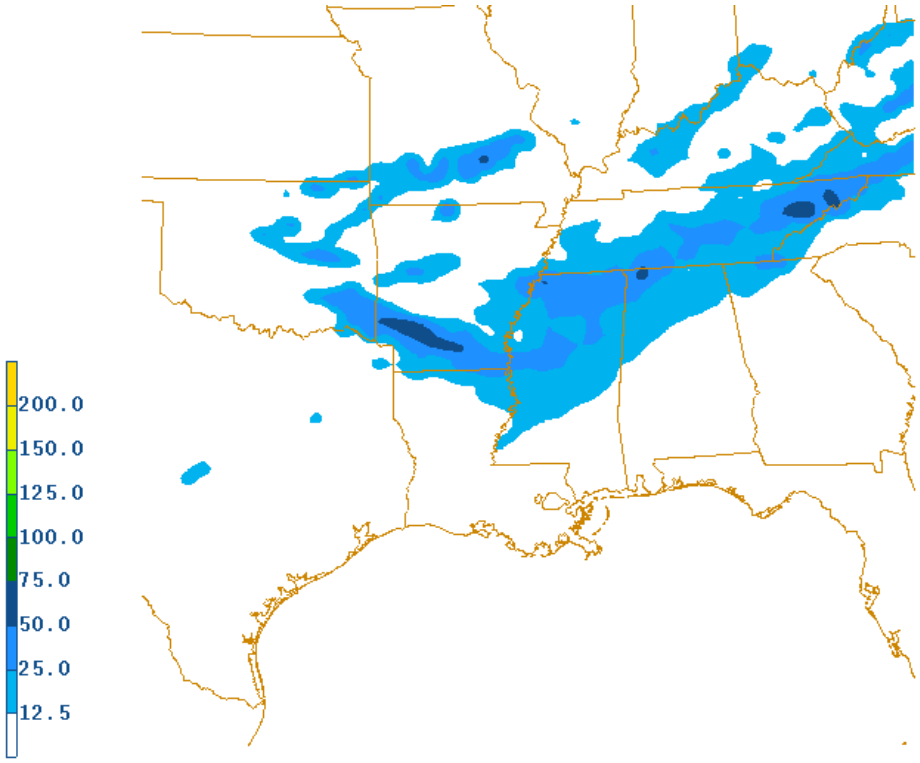

Figure 3.23: Precipitation (mm) difference between F48 (1200UTC Day 3) and F24 (1200UTC Day 2) using 12km grid spacing for the weakly-forced event future simulation.

(a)

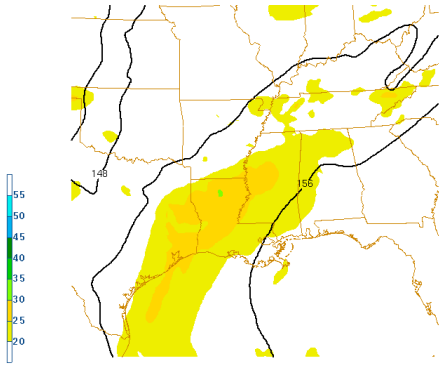

(b)

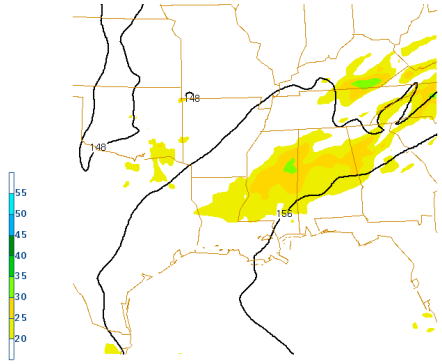

(c)

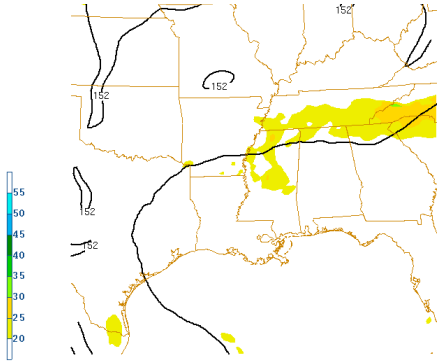

Figure 3.24: Isotachs (kt) at 850mb and 850mb heights (dam) using 12km grid spacing for the weakly-forced event future simulation: (a) F24 (1200UTC Day 2), (b) F33 (2100UTC Day 2), (c) F48 (1200UTC Day 3); can be compared with Figure 3.16.

(a)

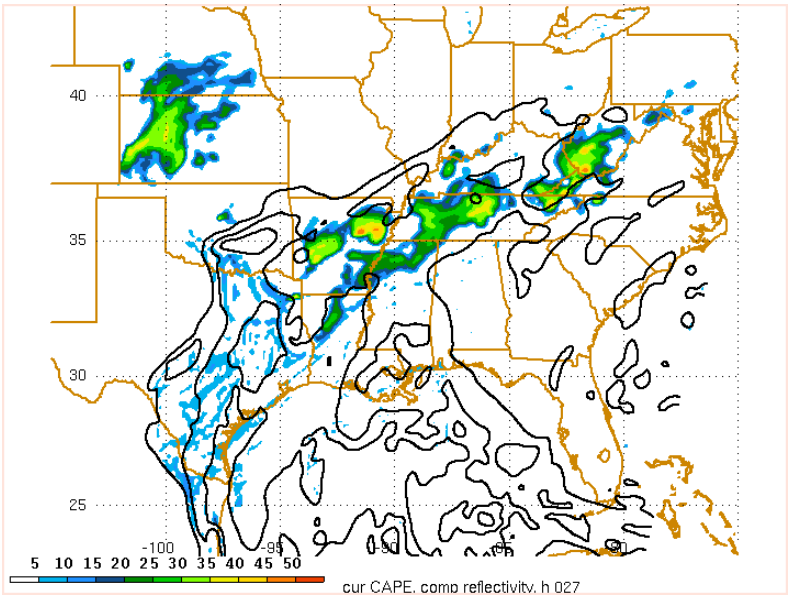

(b)

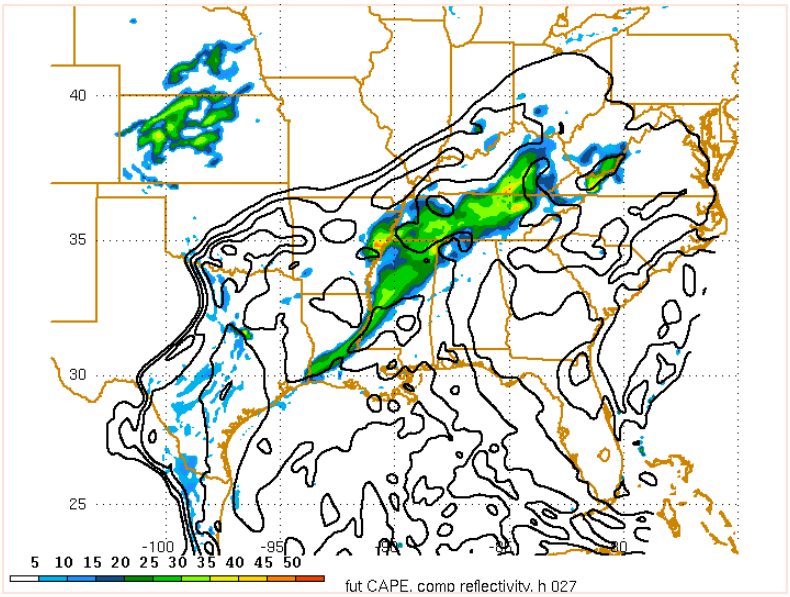

Figure 3.25: Convective available potential energy (CAPE) values, incremented every 500 J/kg, and the reflectivity during the F27 (0300 Day 2) using 12km grid spacing: (a) the weakly-forced event present-day simulation, (b) the weakly-forced event future simulation.

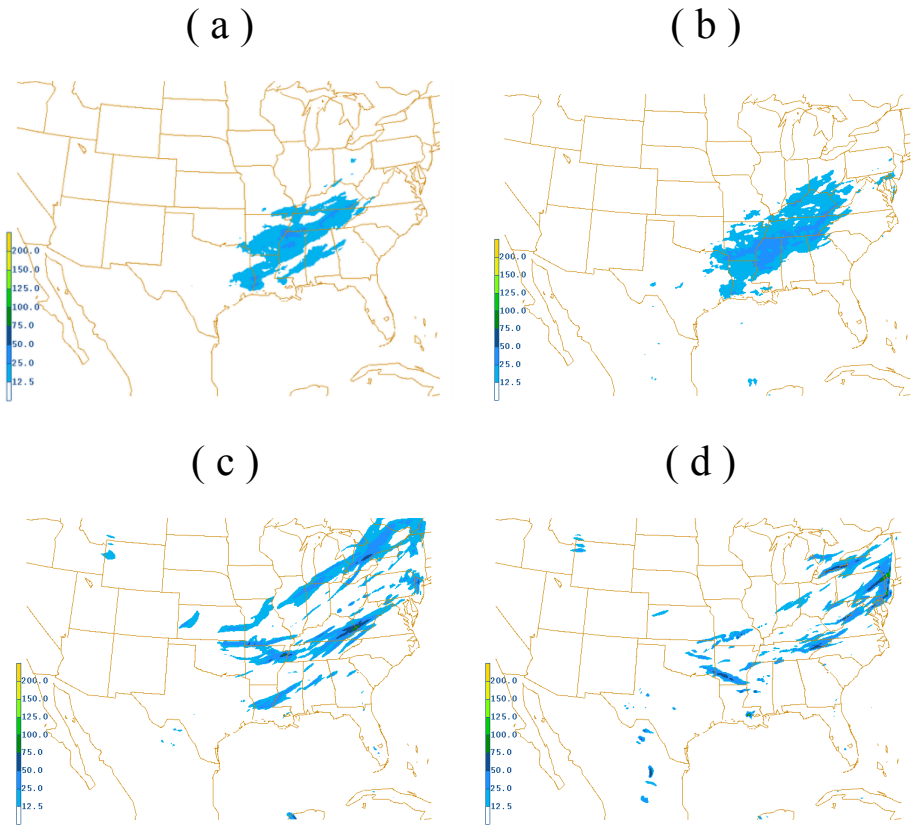

Figure 3.26: The 72 hour total precipitation values for the weakly-forced event: (a) Present-day convective precipitation, (b) Future convective precipitation, (c) Present-day stratiform precipitation, (d) Future stratiform precipitation.

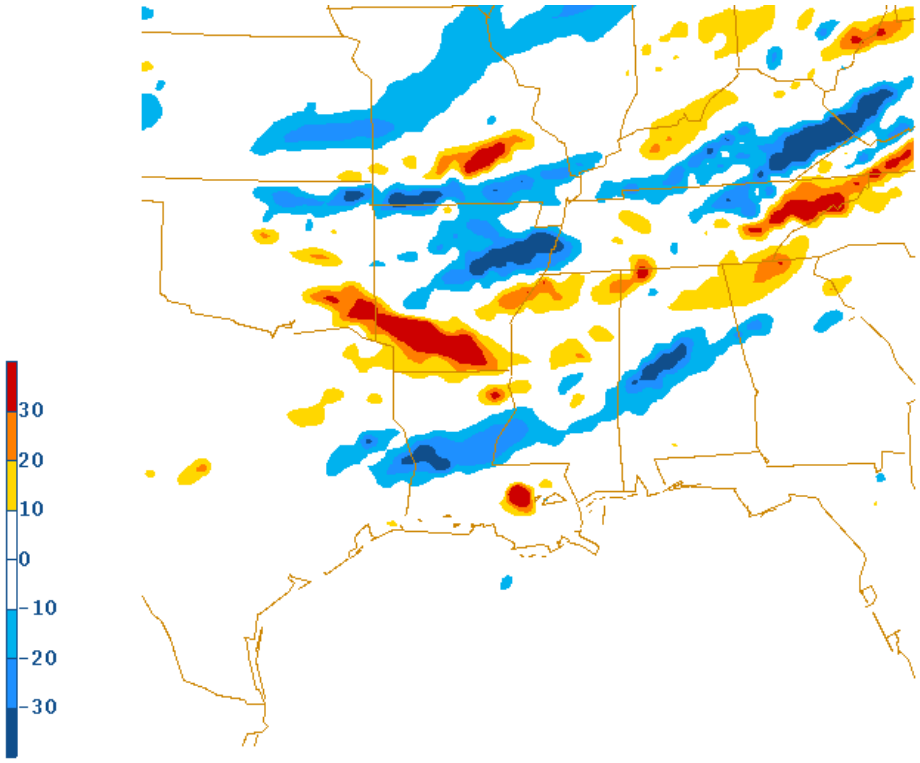

Figure 3.27: Precipitation (mm) difference using 12km grid spacing between the F72 (1200UTC Day 4) total weakly-forced event future simulation precipitation minus the F72 (1200UTC Day 4) total present-day precipitation. Red colors represent areas where the future precipitation totals are higher and blue colors represent areas where the present-day precipitation is higher.

Table 3.1: Area averages of the 72 hour precipitation for the present-day and future simulations across all three domains (36, 12, 4km). The area averages were taken within the longitude bounds from -95° to -85° and the latitude bounds of 29.5° to 37°, which encompassed the area of the heaviest precipitation.

	Present-Day Simulation	Future Simulation
Domain 1 (36 km)	9.52 mm	9.97 mm
Domain 2 (12 km)	13.24 mm	12.46 mm
Domain 3 (4 km)	19.05 mm	14.17 mm

(a)

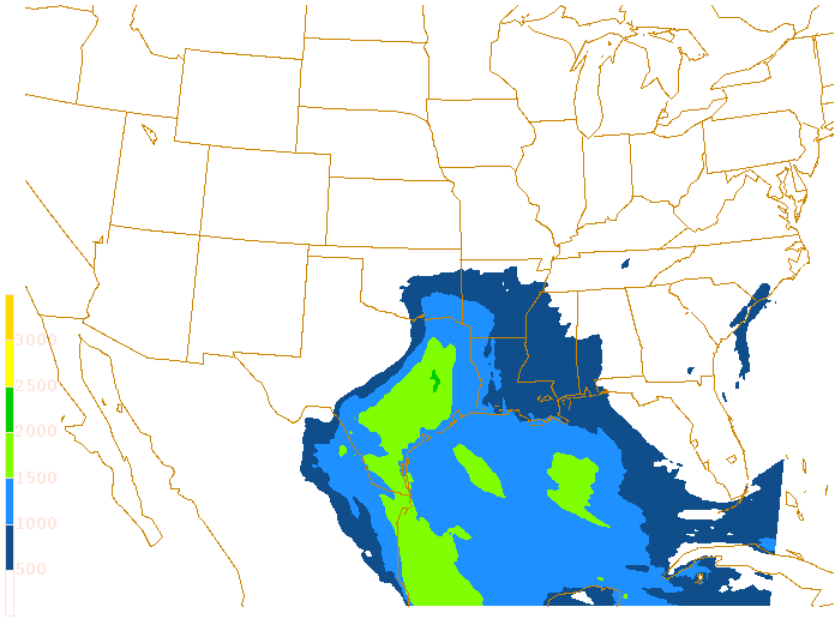

(b)

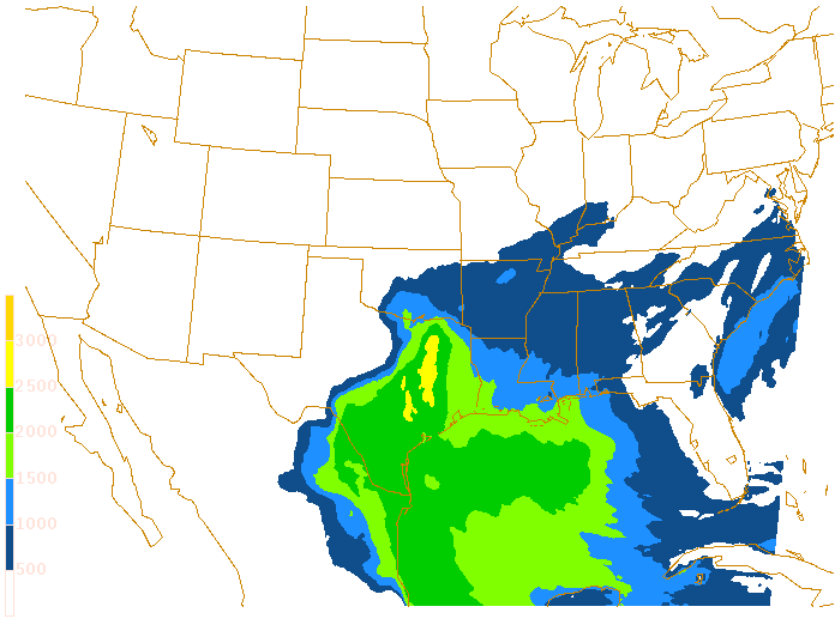

Figure 3.28: Time averaged CAPE (contour interval 500 J/kg) for the weakly-forced event from F24 through F48 using 12km grid spacing: (a) the present-day run, (b) the future run.

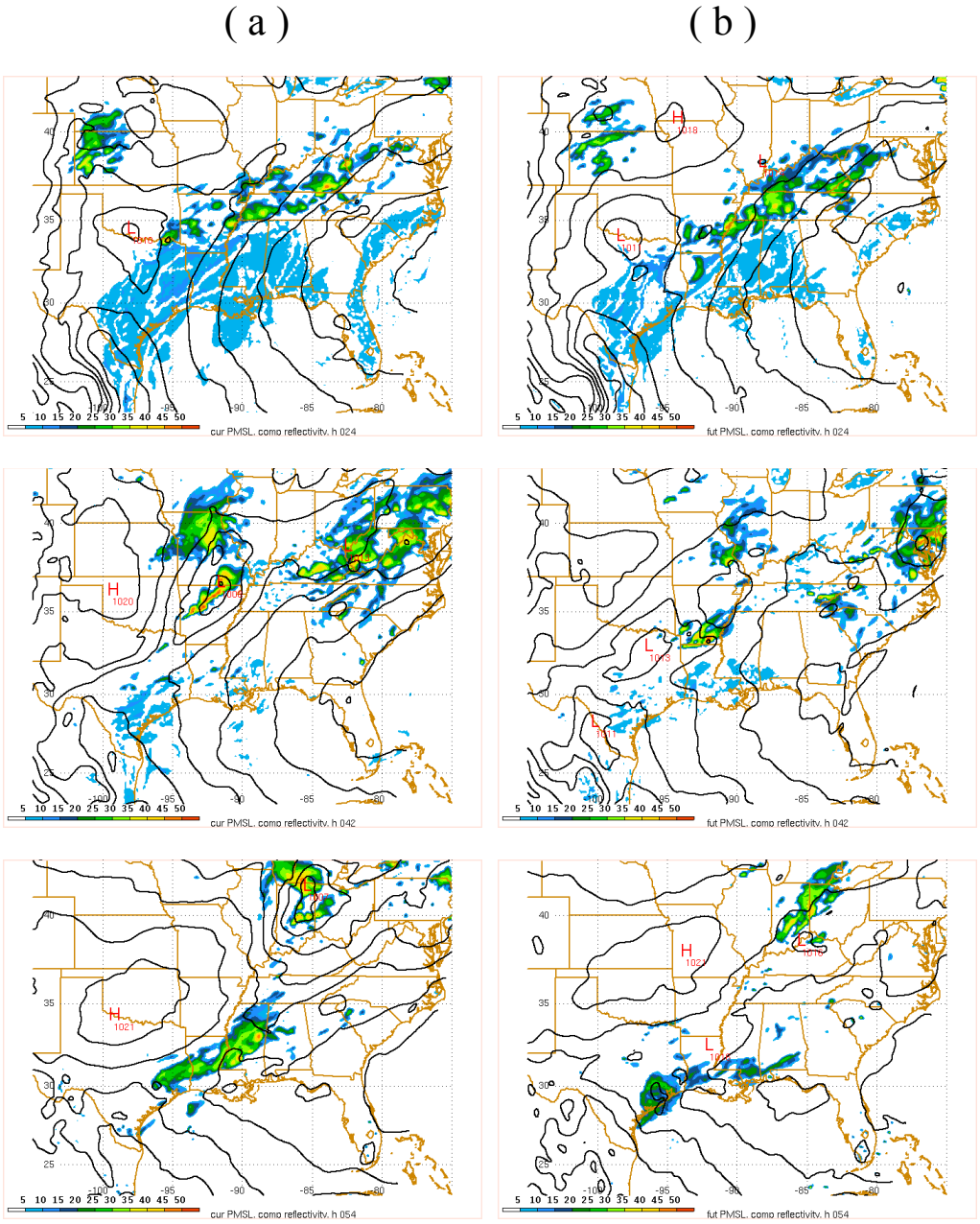

Figure 3.29: SLP and reflectivity for F24 (1200UTC on Day 2), F42 (0600 on Day 3), and F54 (1800UTC on Day 3) using a 12km grid spacing for the weakly-forced event: (a) the present-day simulation, (b) the future simulation.

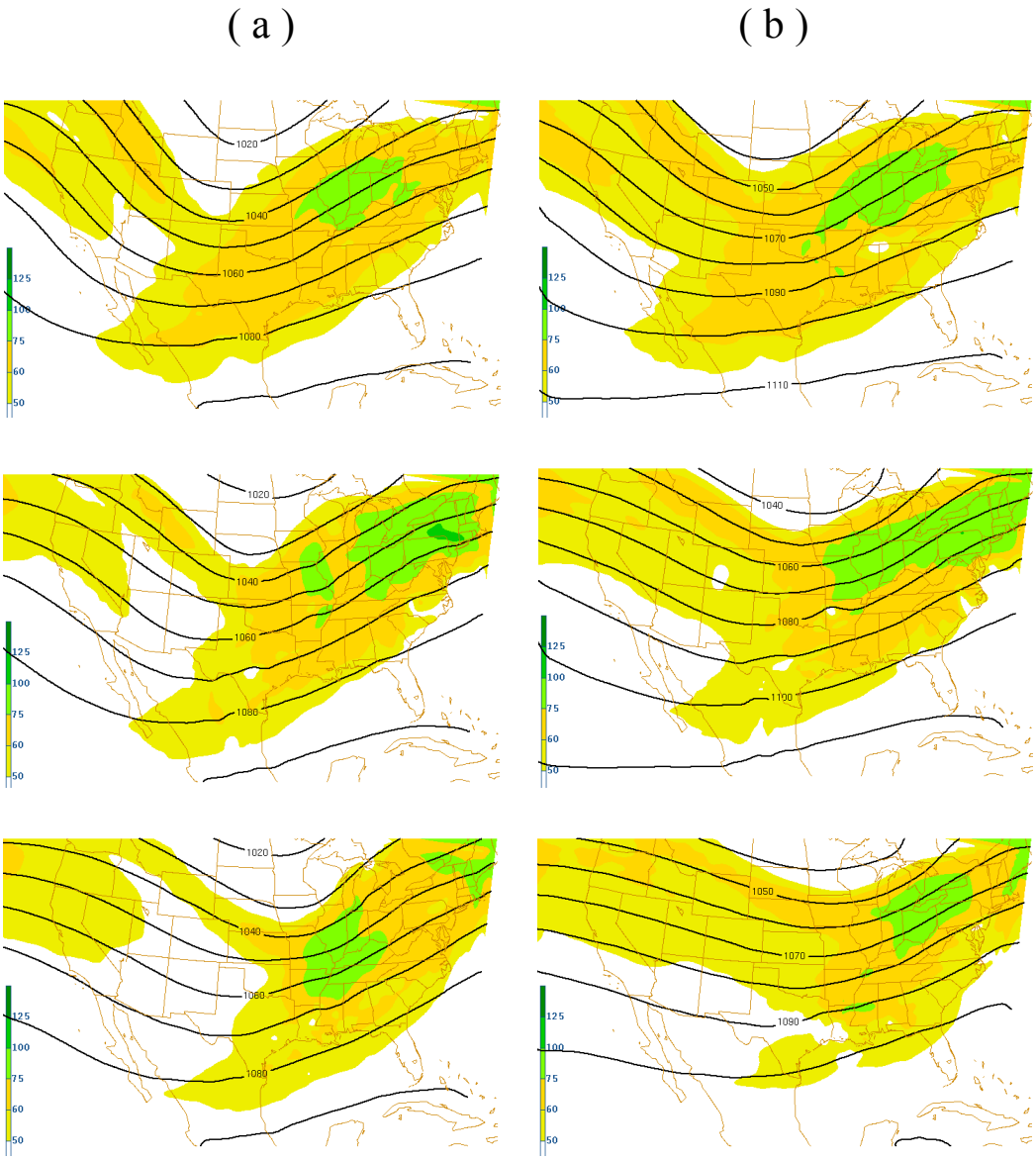

Figure 3.30: 250mb heights (contoured interval 3 dam) and isotachs (kt) for F24 (1200UTC on Day 2), F42 (0600 on Day 3), and F54 (1800UTC on Day 3) using a 36km grid spacing for the weakly-forced event: (a) the present-day simulation, (b) the future simulation. Note: the isotach contour values are different than that seen in the four panel plots.

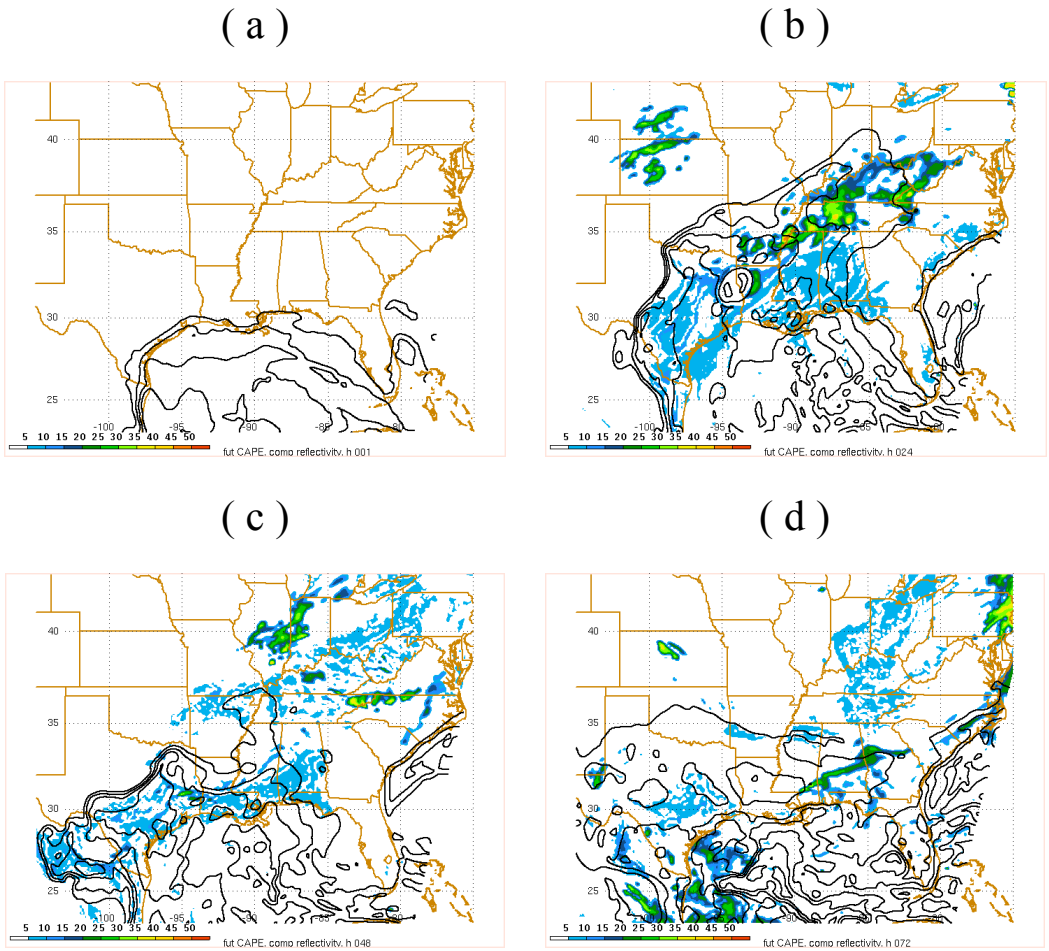

Figure 3.31: CAPE (contour interval 500 J/kg) for the weakly-forced event future simulation using 12km grid spacing: (a) F01, (b) F24, (c) F48, (d) F72.

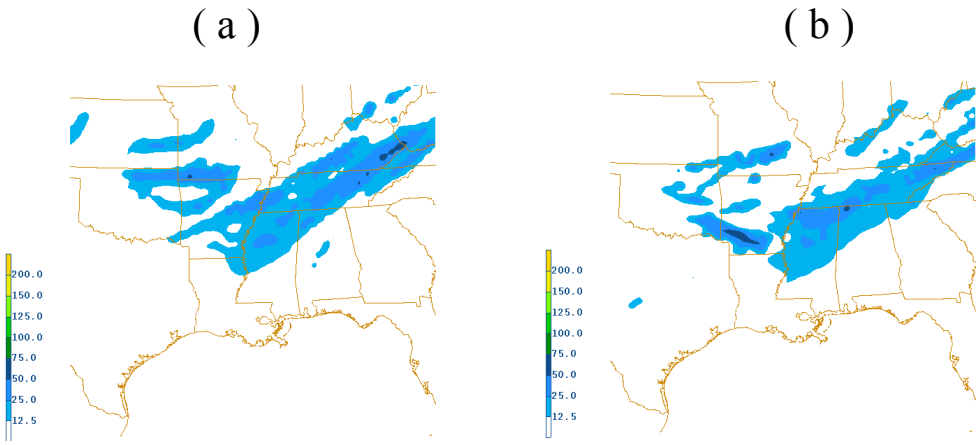

Figure 3.32: Precipitation (mm) difference between F42 total precipitation minus F24 total precipitation using a 12km grid spacing for the weakly-forced event during the: (a) present-day simulation, (b) future simulation.

(a)

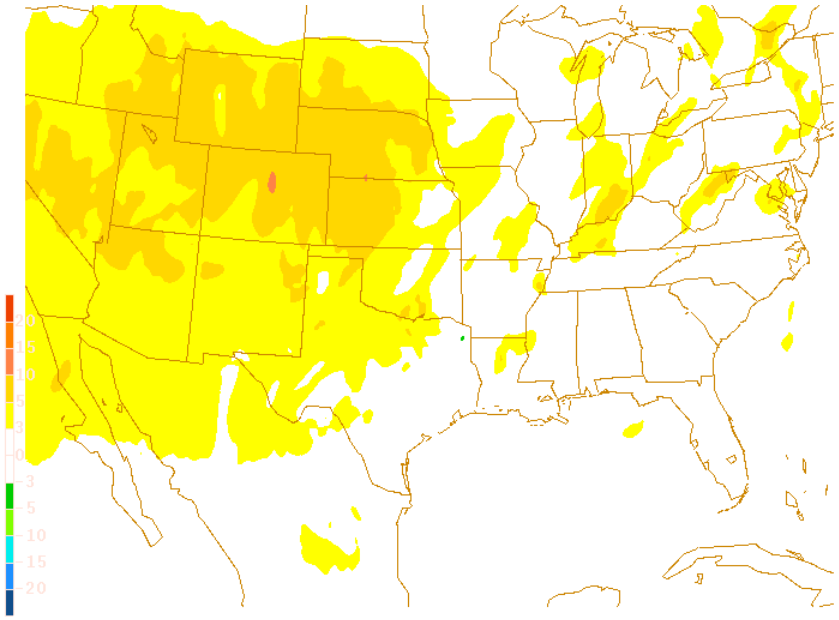

(b)

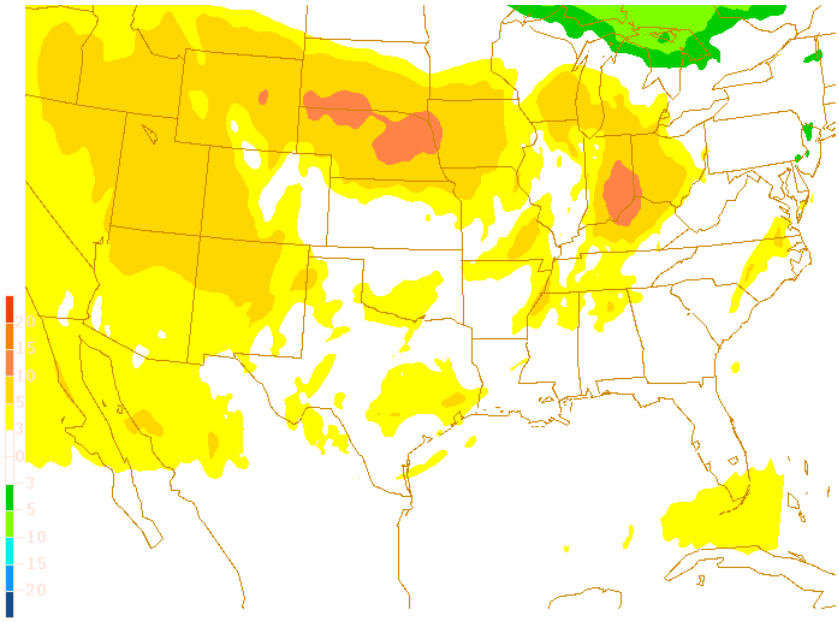

Figure 3.33: Difference between the future and present-day east-west horizontal wind values at 200mb: (a) 24th hour, (b) 48th hour.

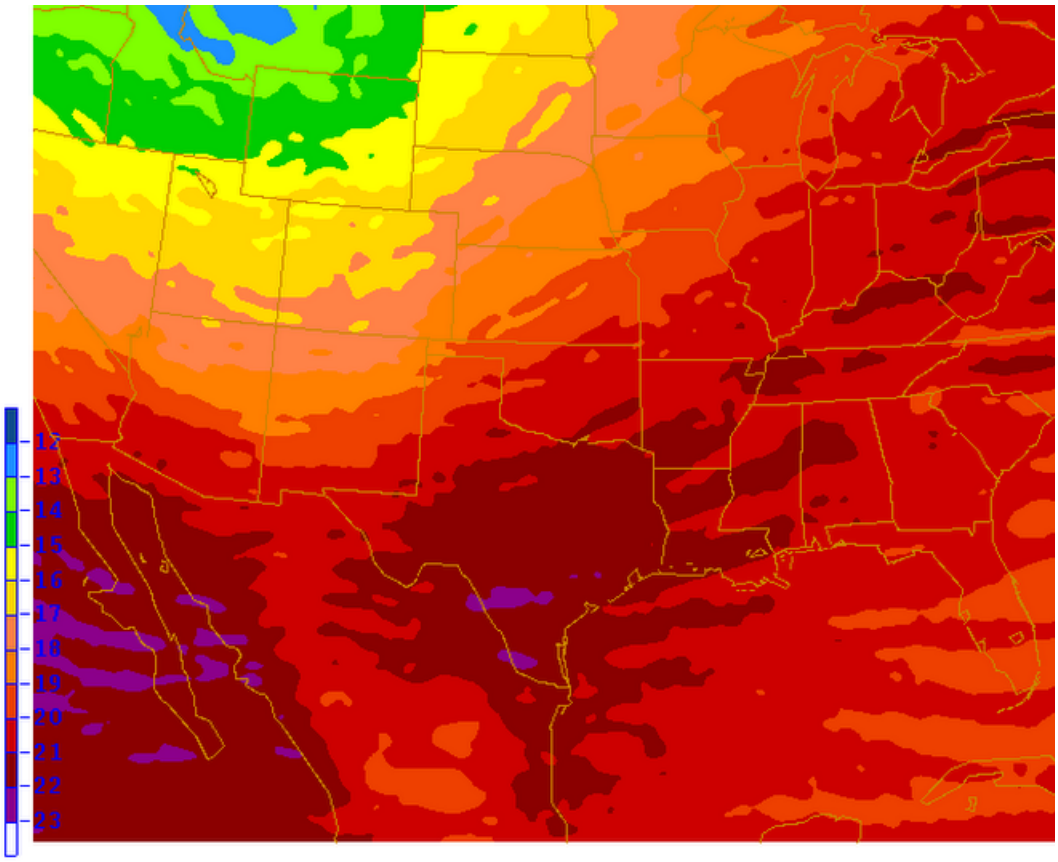

Figure 3.34: 250mb height difference at F00 between the present-day and future simulations. The reds represent larger heights and blues represent smaller heights.

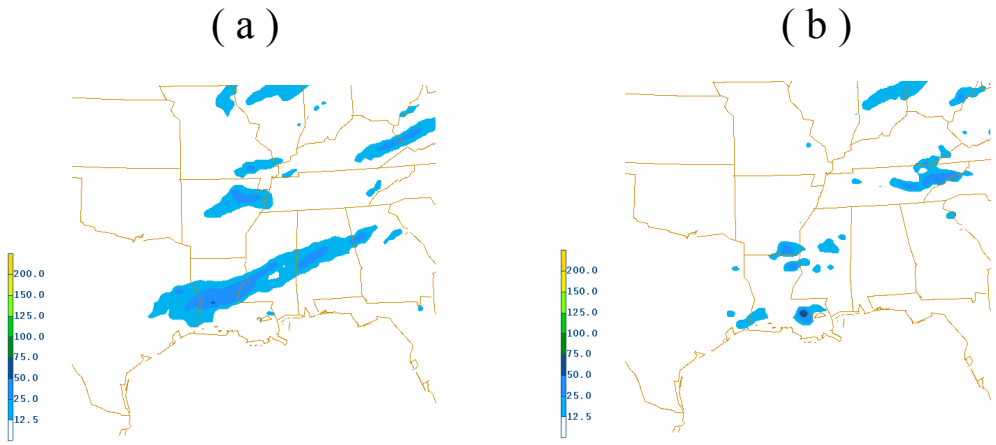

Figure 3.35: Precipitation difference between F72 total precipitation and F42 total precipitation using the 12km grid spacing for the weakly-forced event: (a) the present-day simulation, (b) the future simulation.

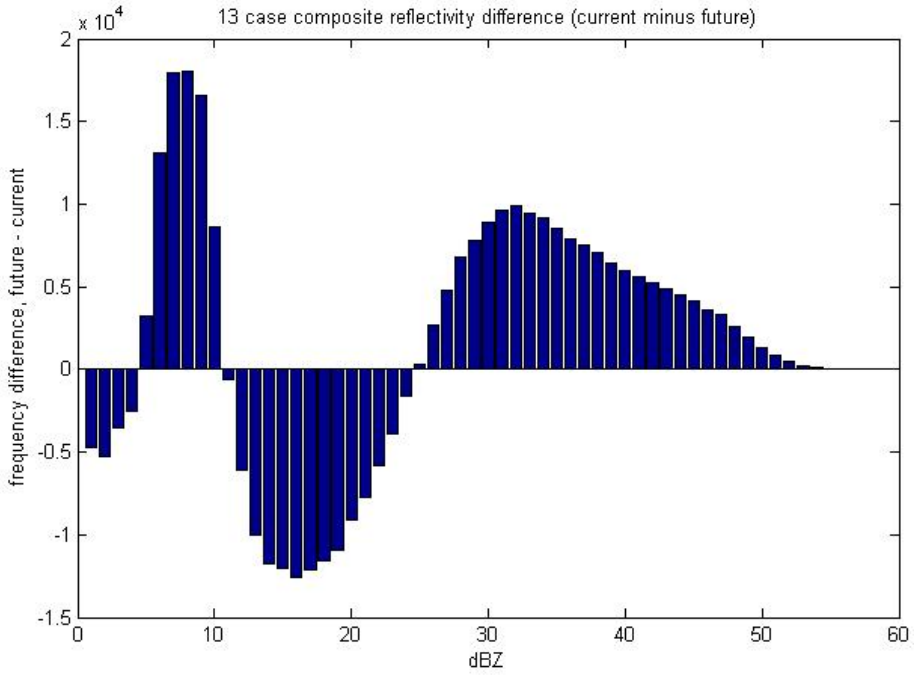

Figure 3.36: Weakly-forced event histogram showing the difference in composite reflectivity between the present-day and future simulations at 4km grid spacing.

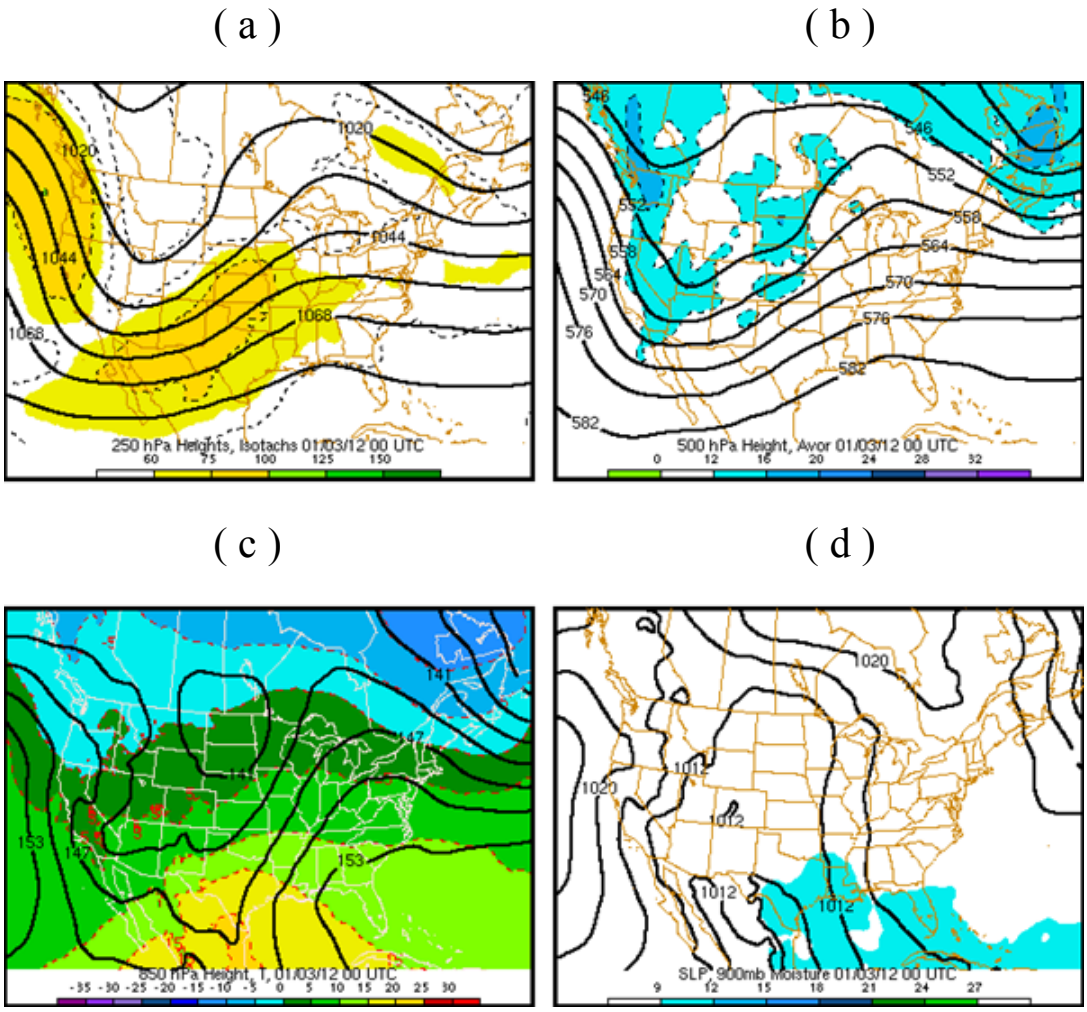

Figure 3.37: Four panel plot in the strongly-forced event composite, 2 days before precipitation event, of the atmospheric conditions: (a) 250mb isotachs (in knots) and heights (contour interval 12 dam), (b) 500mb heights (contour interval 6 dam) and vorticity ($x10^{-5}s^{-1}$), (c) 850mb heights (contour interval 3 dam) and temperatures (°C), (d) the sea level pressure (contour interval 4mb) and 900mb moisture (g/kg).

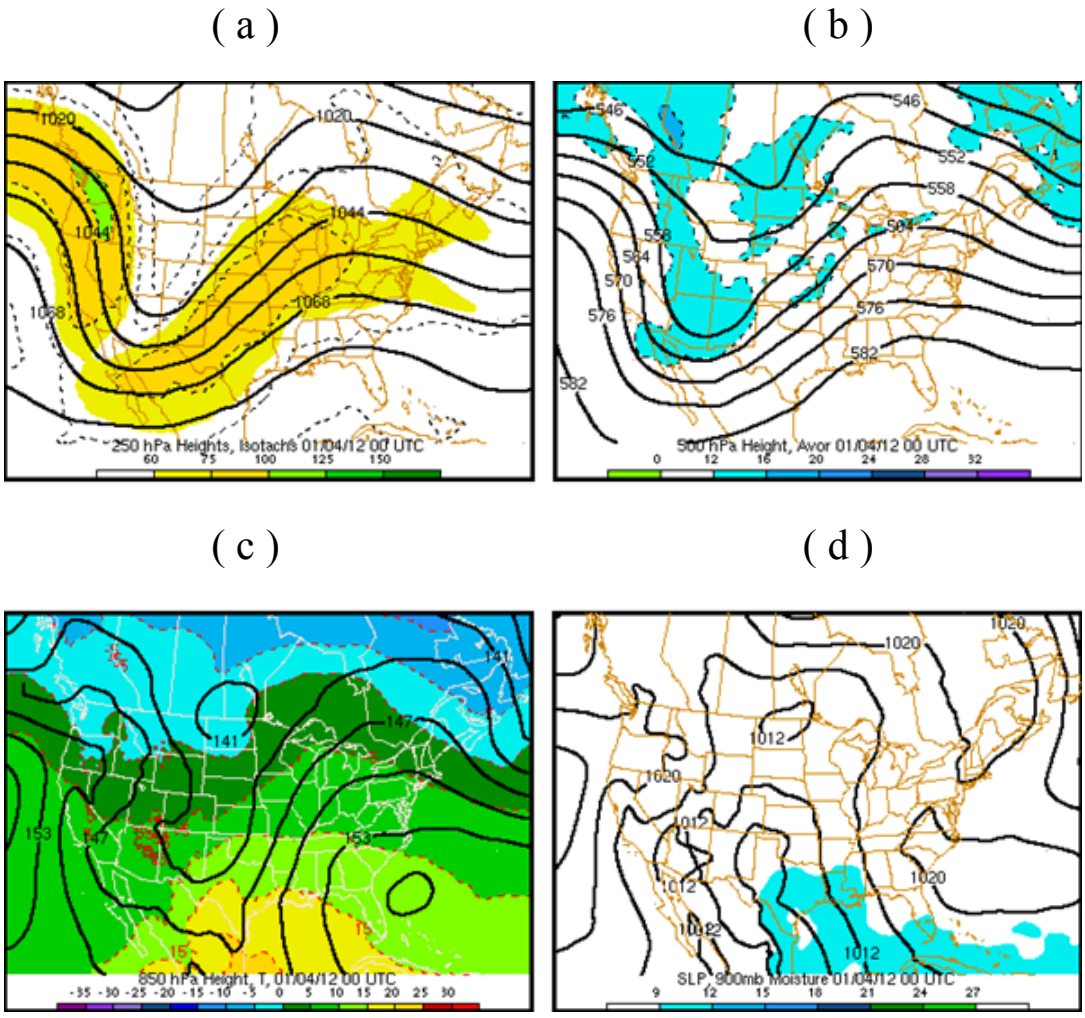

Figure 3.38: Four panel plot of atmospheric conditions, 1 day before precipitation event, for the strong composite.

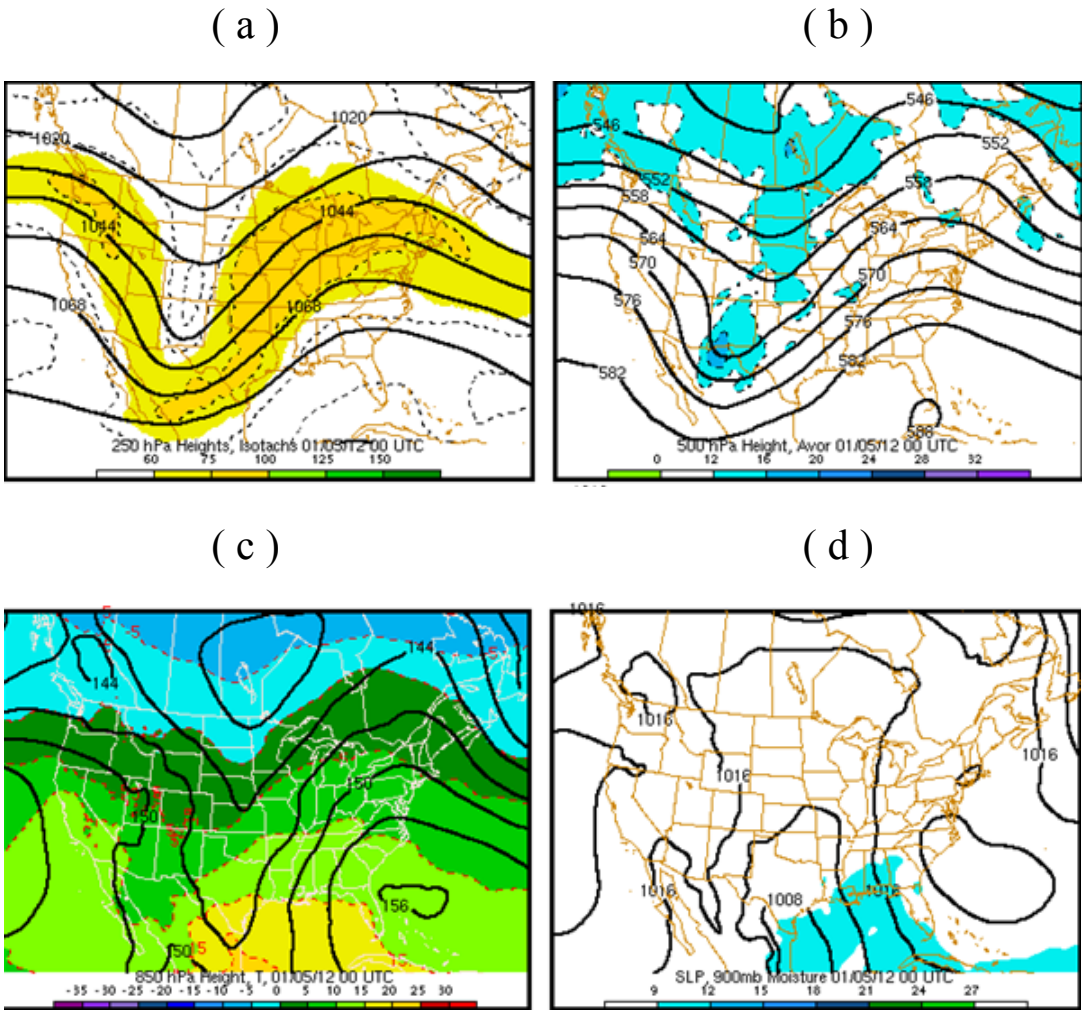

Figure 3.39: Four panel plot of atmospheric conditions, day of precipitation event, for the strong composite.

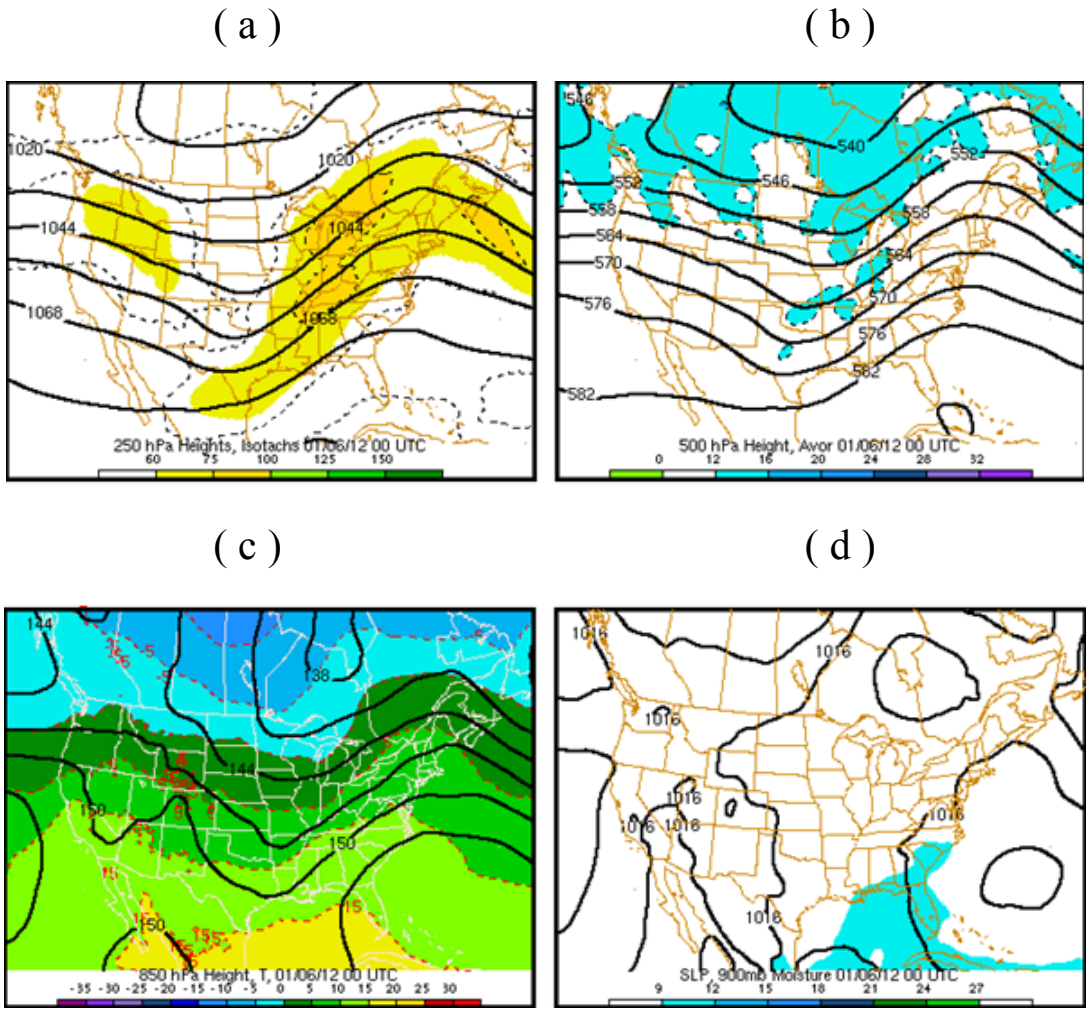

Figure 3.40: Four panel plot of atmospheric conditions, 1 day after precipitation event, for the strong composite.

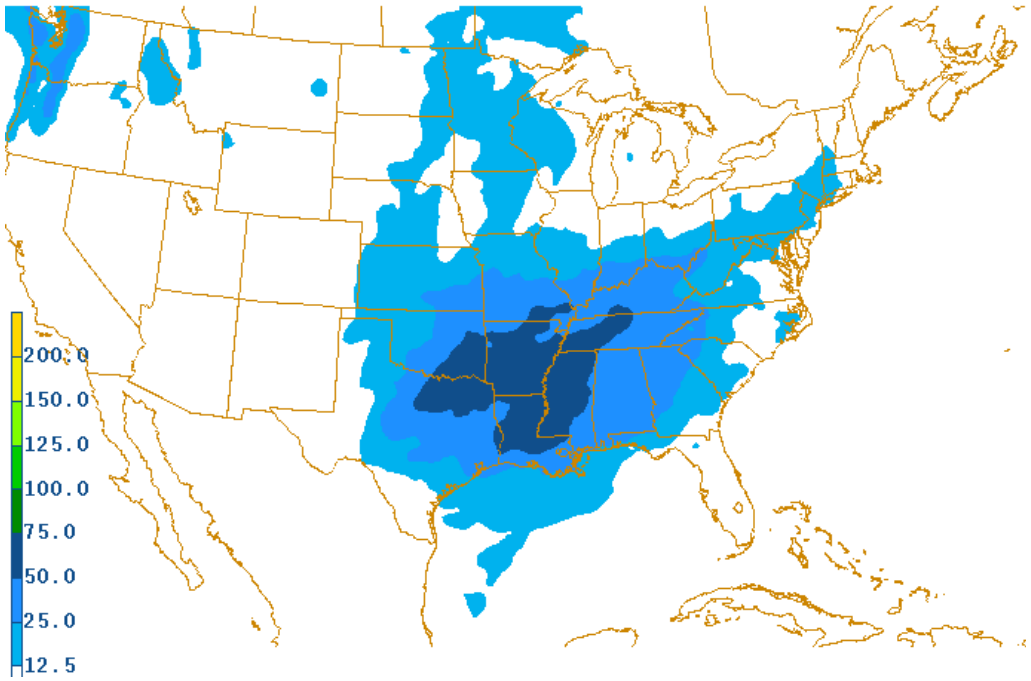

Figure 3.41: Total precipitation (mm) for the strongly-forced composite.

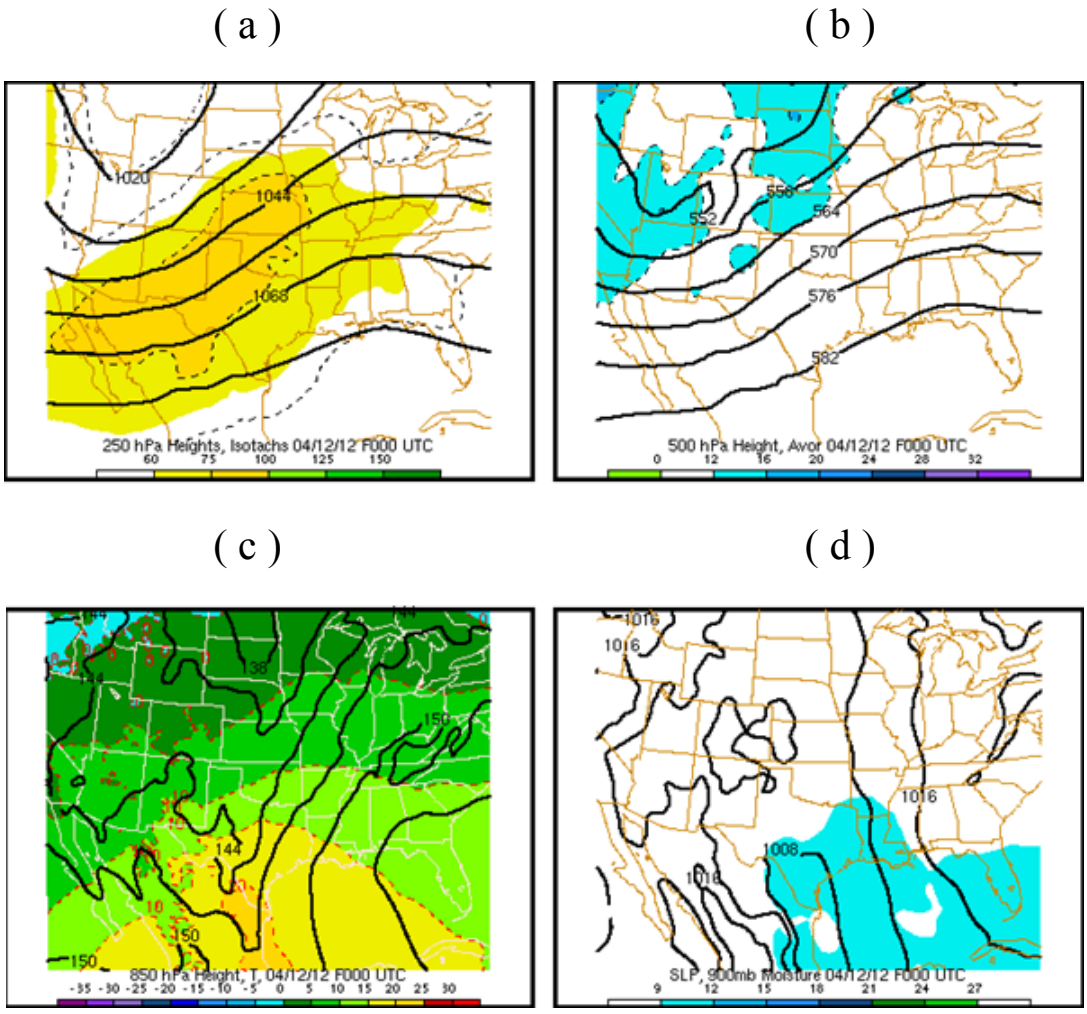

Figure 3.42: Four panel plot of atmospheric conditions for F00 (1200UTC Day 1) of the strongly-forced event present-day simulation using the WRF model at 36km grid spacing.

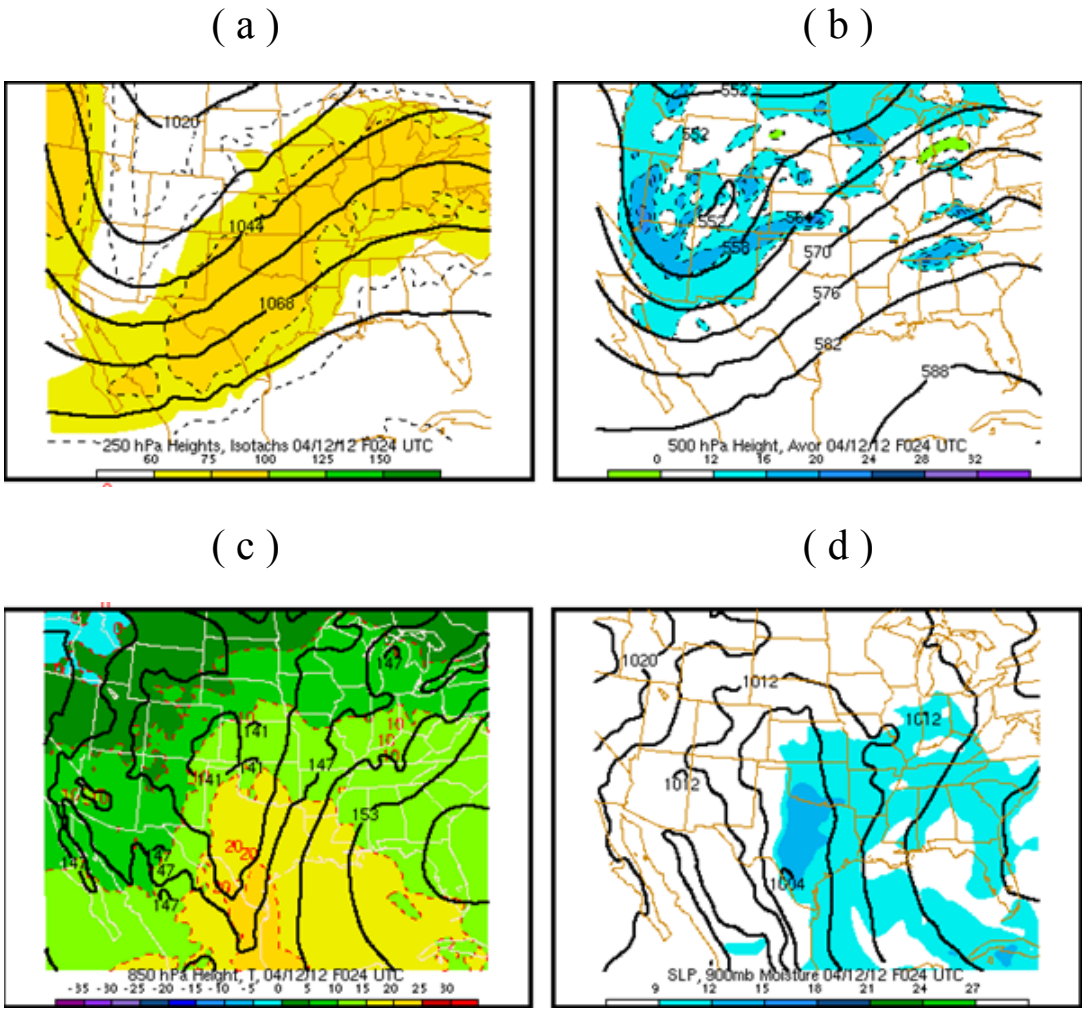

Figure 3.43: Four panel plot of atmospheric conditions for F24 (1200UTC Day 2) of the strongly-forced event present-day simulation using the WRF model at 36km grid spacing.

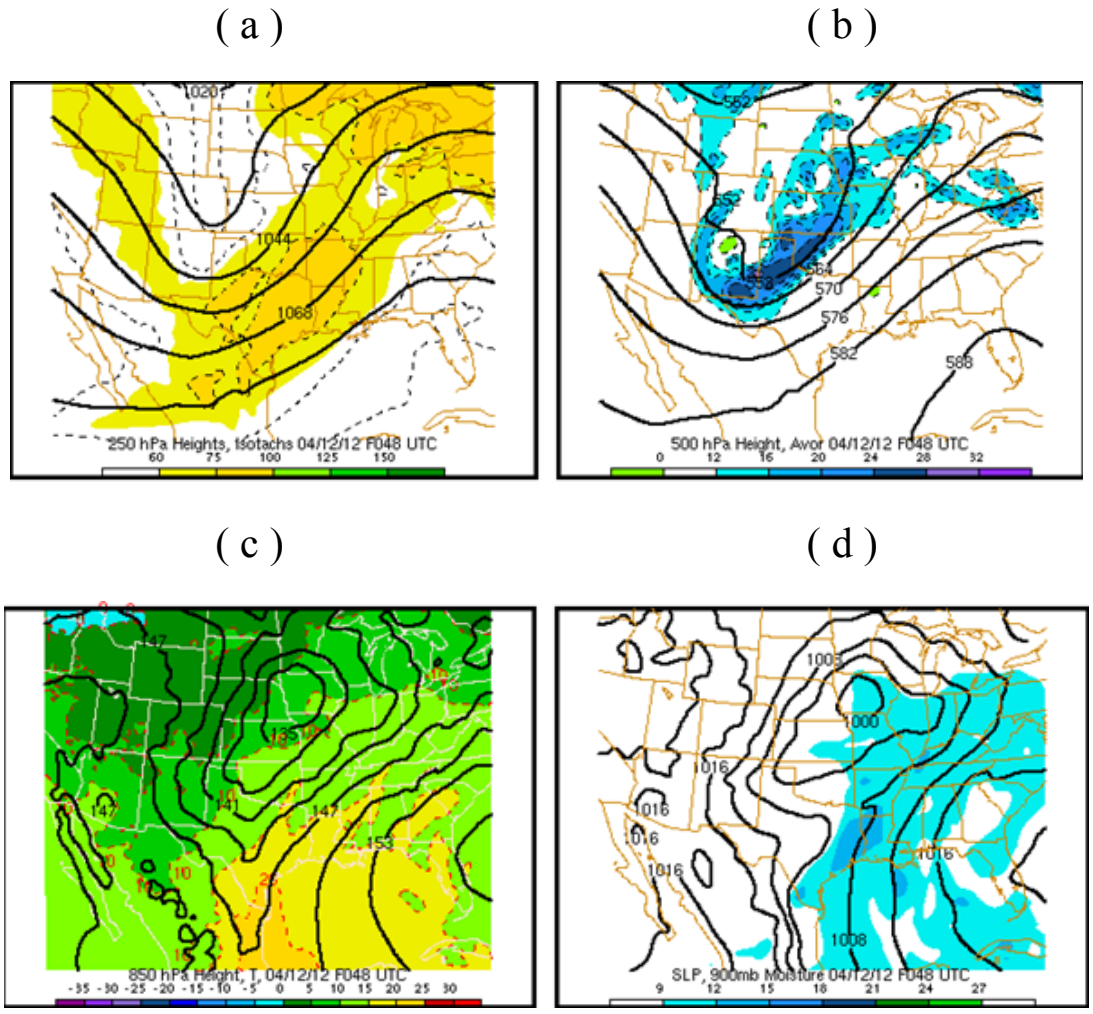

Figure 3.44: Four panel plot of atmospheric conditions for F48 (1200UTC Day 3) of the strongly-forced event present-day simulation using the WRF model at 36km grid spacing.

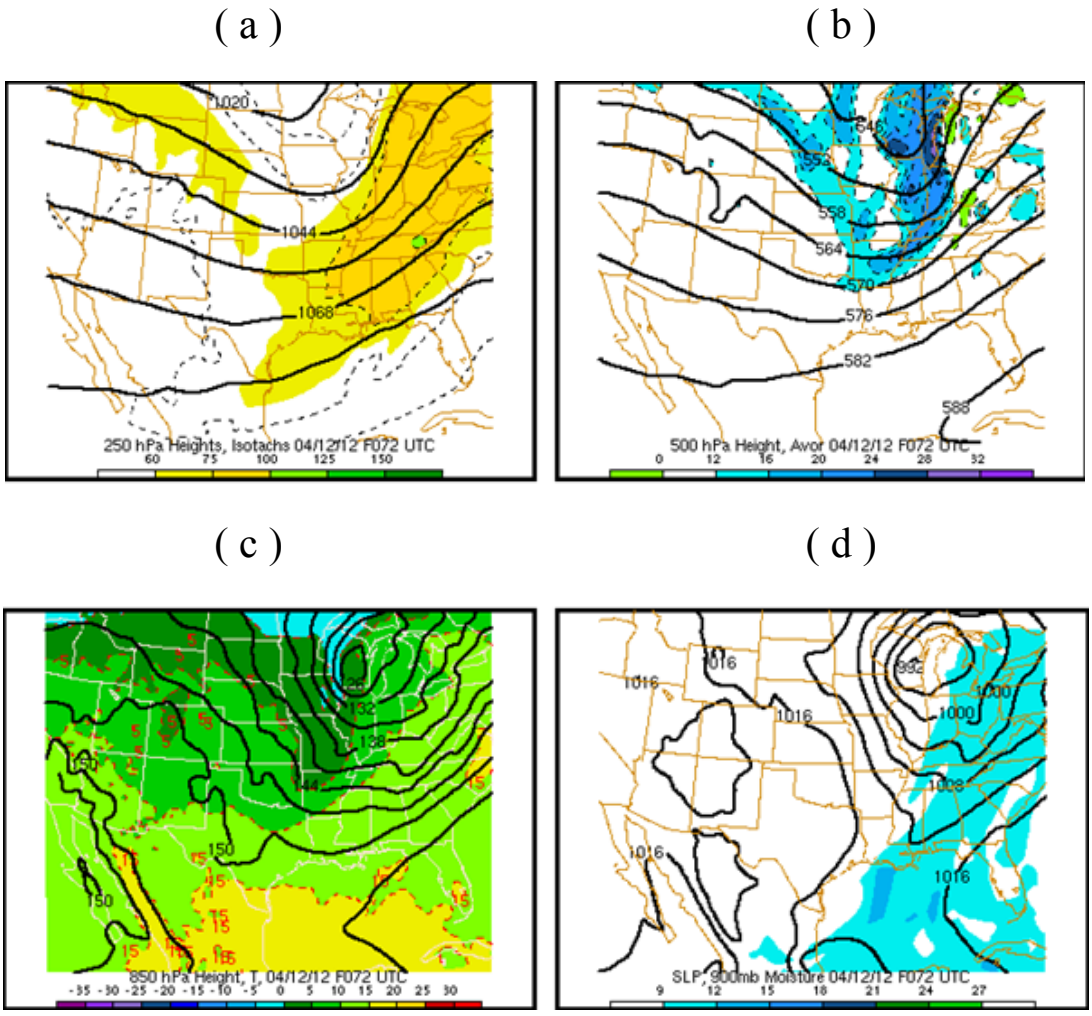

Figure 3.45: Four panel plot of atmospheric conditions for F72 (1200UTC Day 4) of the strongly-forced event present-day simulation using the WRF model at 36km grid spacing.

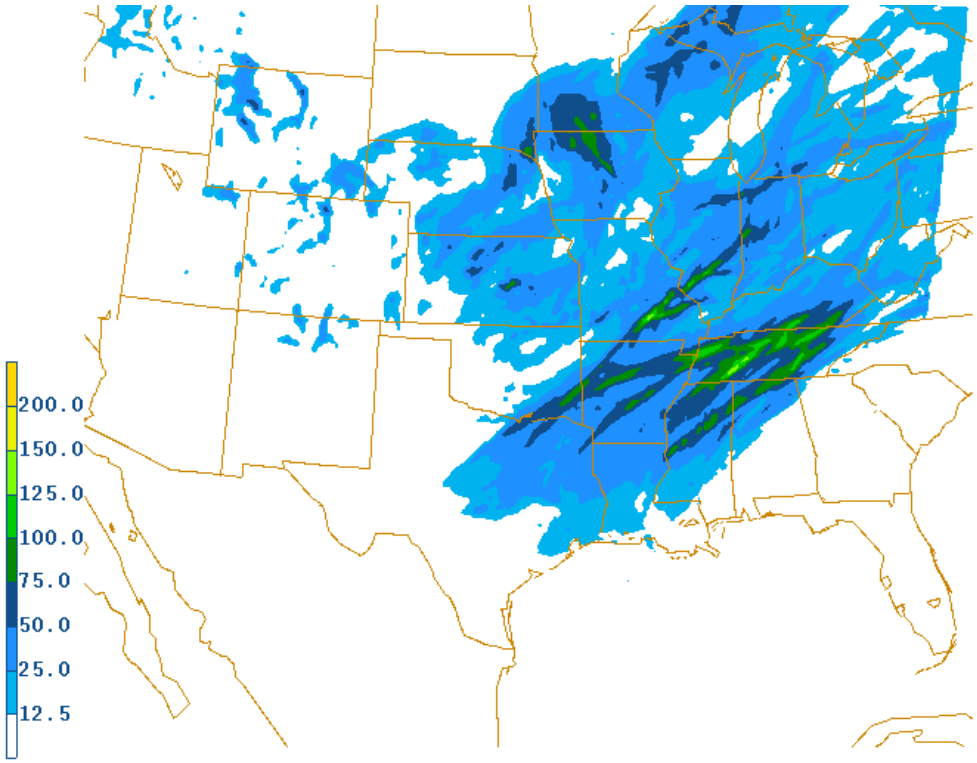

Figure 3.46: Total 72 hour precipitation for the strongly-forced event present-day simulation using 12km grid spacing. The color bar shows increments in mm.

(a)

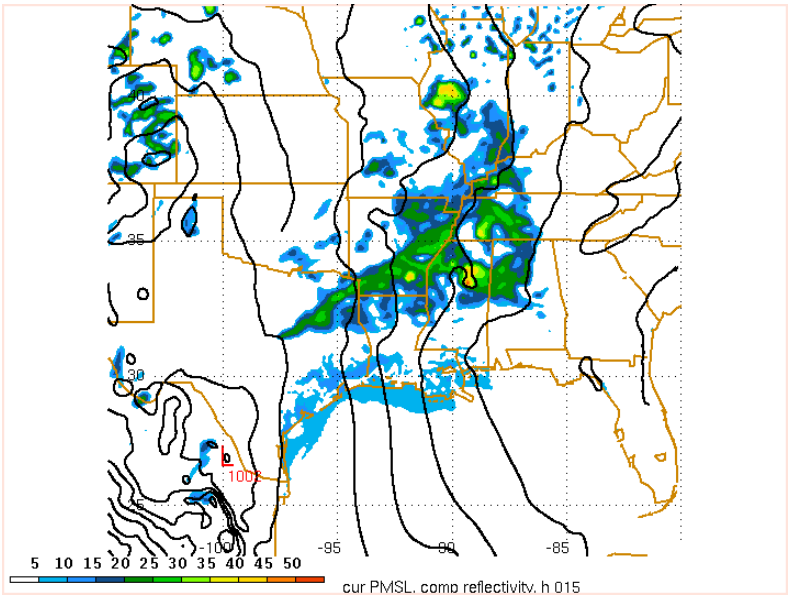

(b)

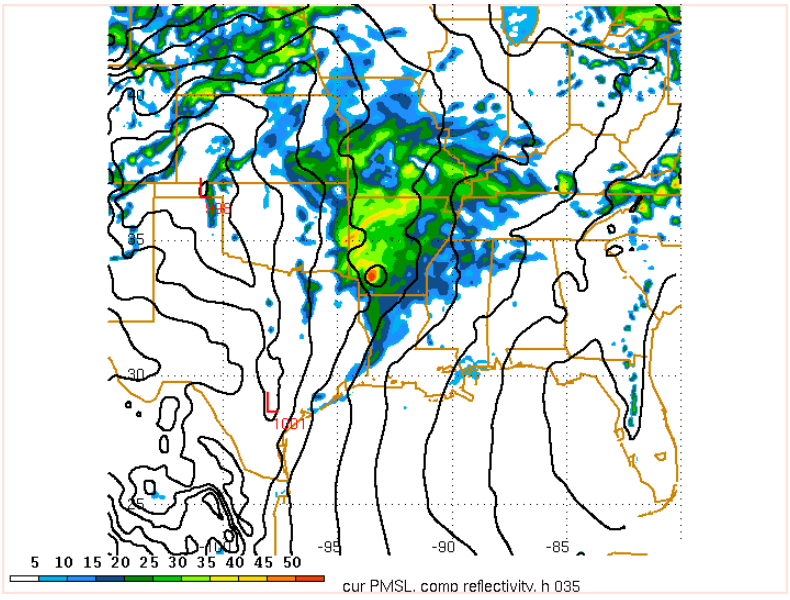

Figure 3.47: Sea level pressure and reflectivity using 12km grid spacing for the present-day simulation of the strongly-forced event: (a) F15, (b) F35.

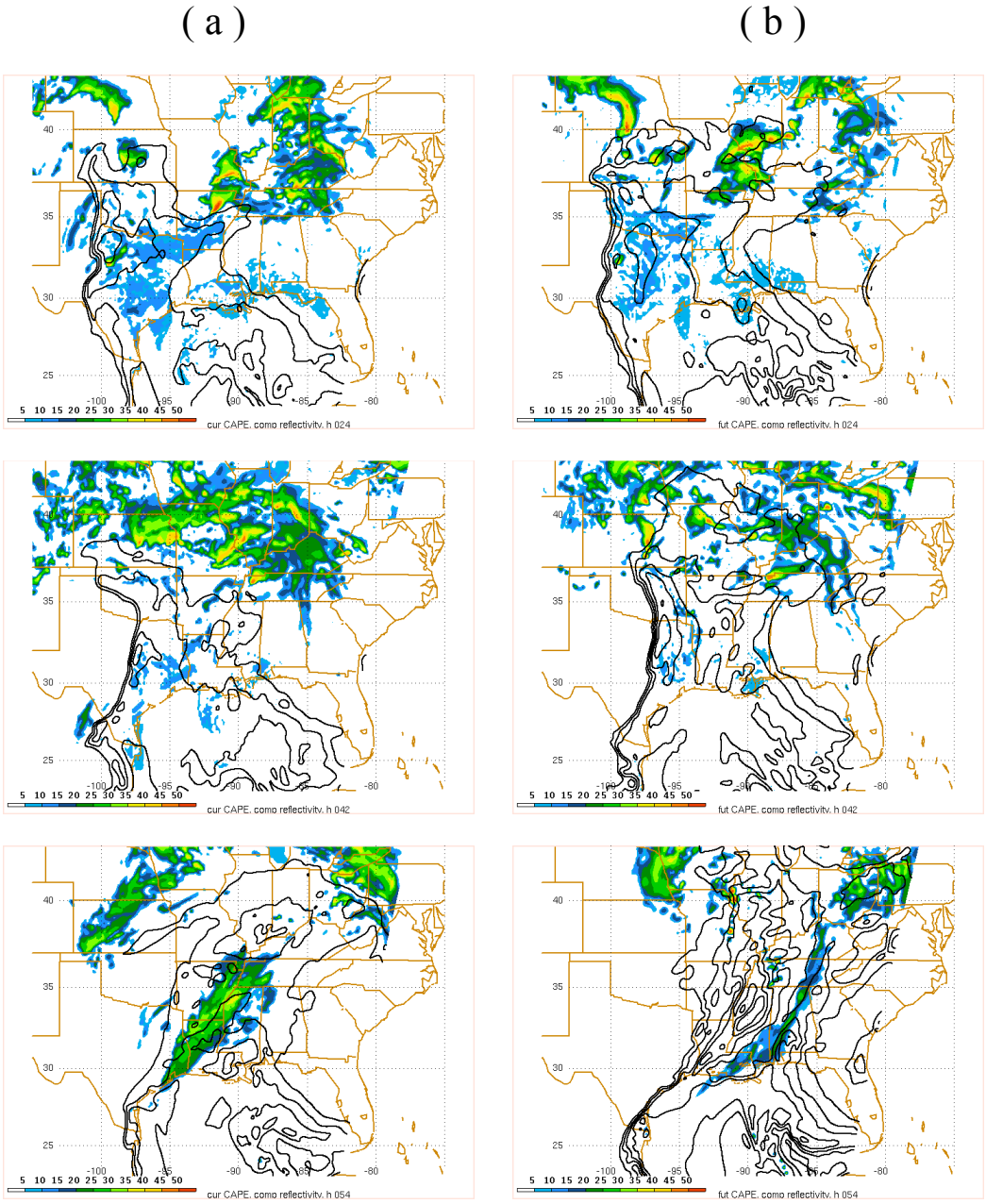

Figure 3.48: Reflectivity and CAPE values (contour interval of 500 J/kg) for F24, F42, and F54 using the 12km domain for the strongly-forced event: (a) present-day simulation (b) future simulation

(a)

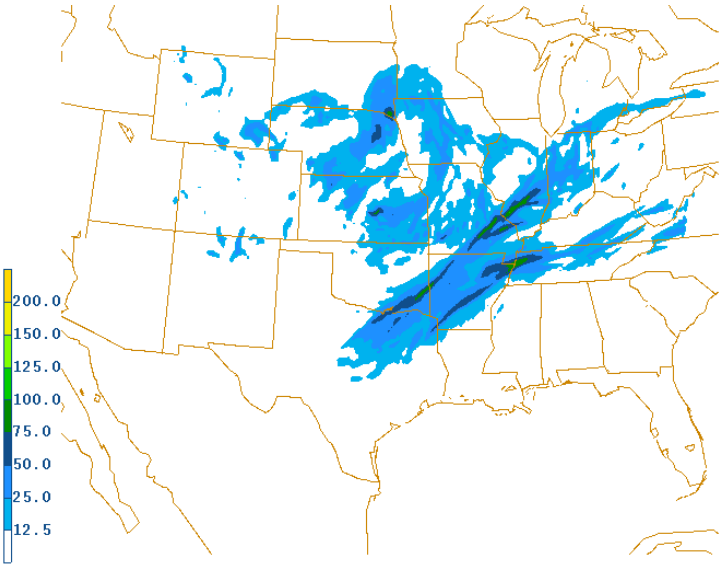

(b)

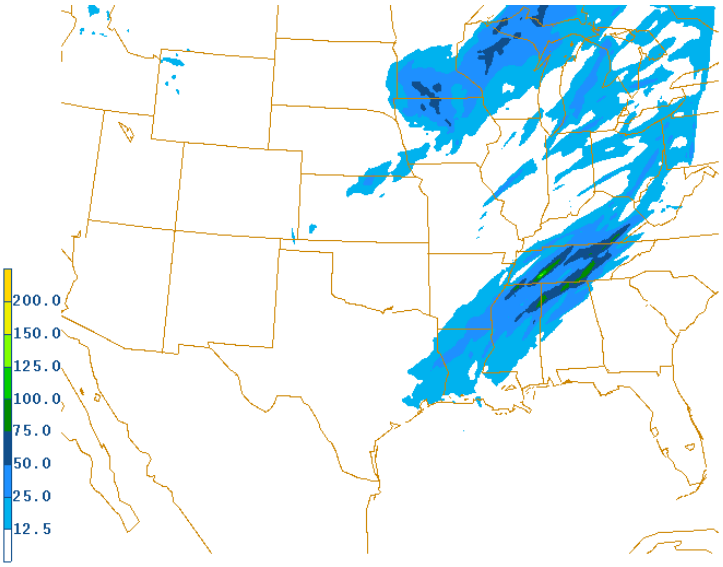

Figure 3.49: Precipitation difference (mm) using the 12km grid spacing for the strongly-forced event for the present-day simulation: (a) F48-F24 precipitation, (b) F72-F48 precipitation.

(a)

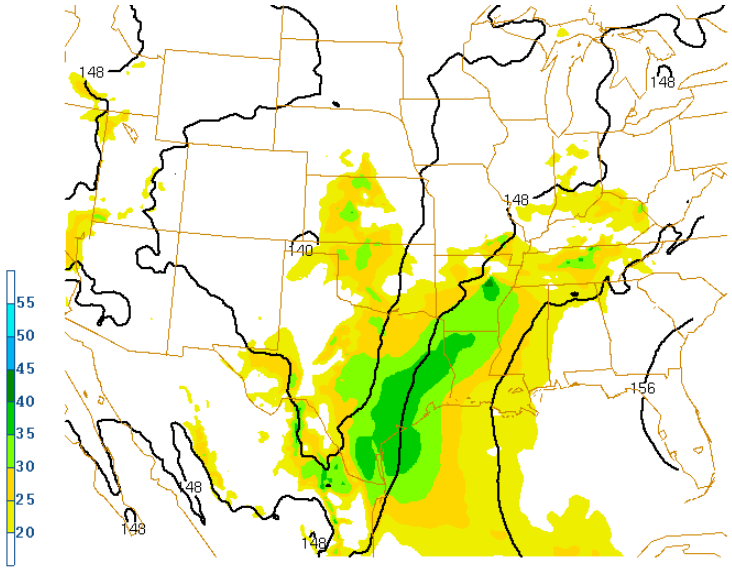

(b)

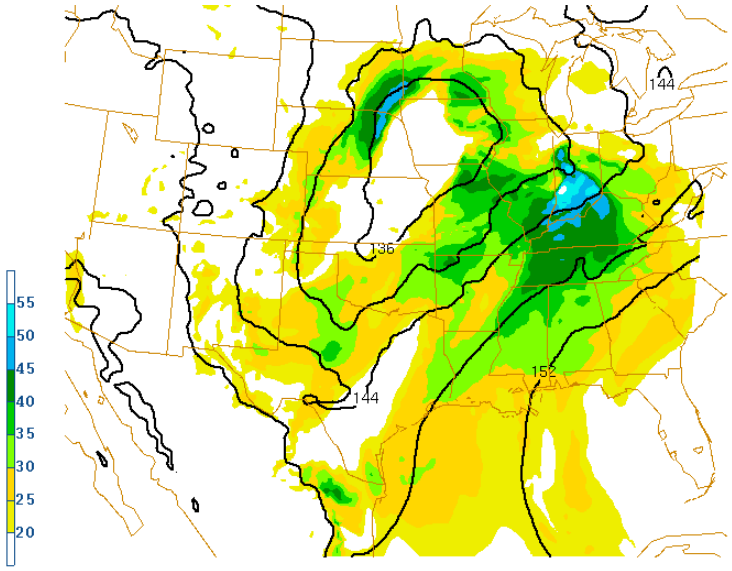

Figure 3.50: Isotachs (kt) at 850mb with the 850mb heights (contour interval of 4 dam) using 12km grid spacing for the strongly-forced event present-day simulation: (a) F24, (b) F48.

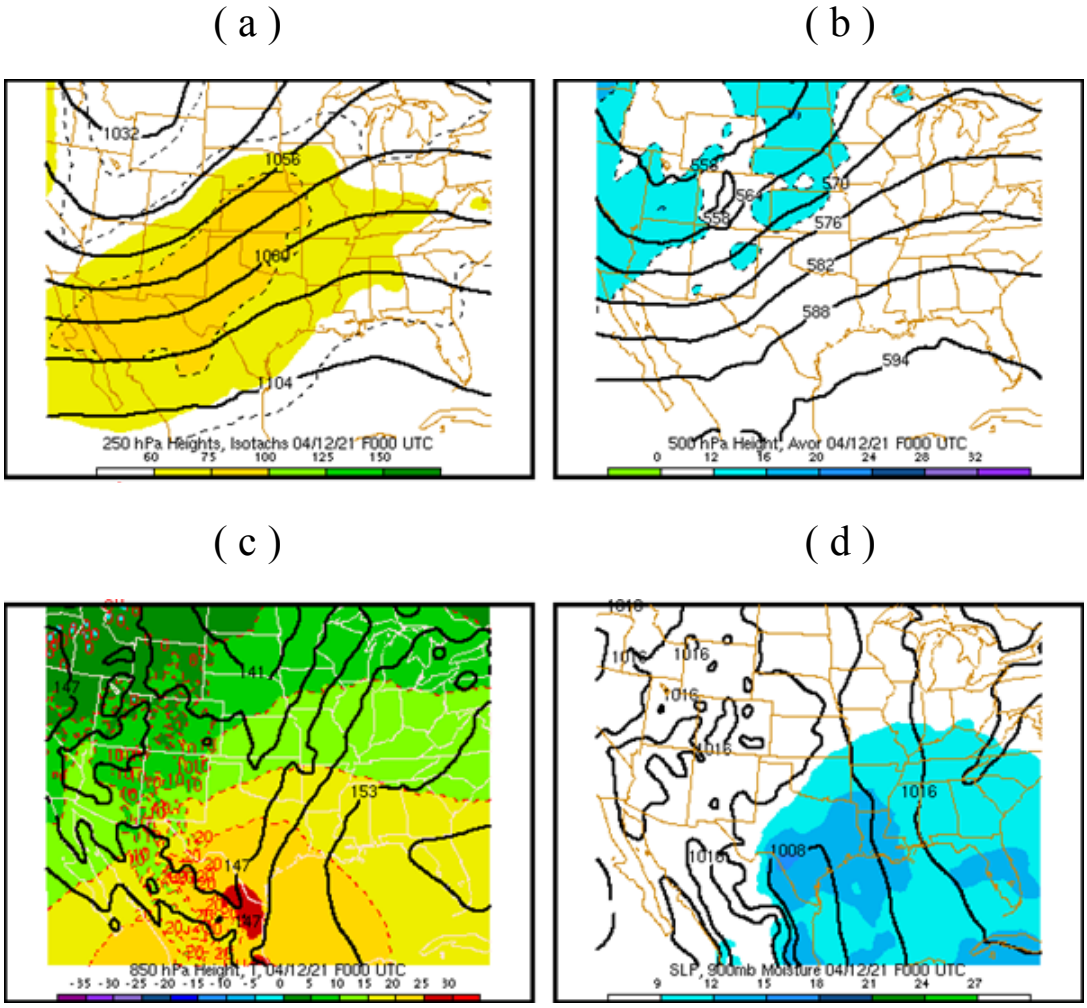

Figure 3.51: Four panel plot of atmospheric parameters at F00 (1200UTC on Day 1) for the strongly-forced event future simulation using 36km grid spacing.

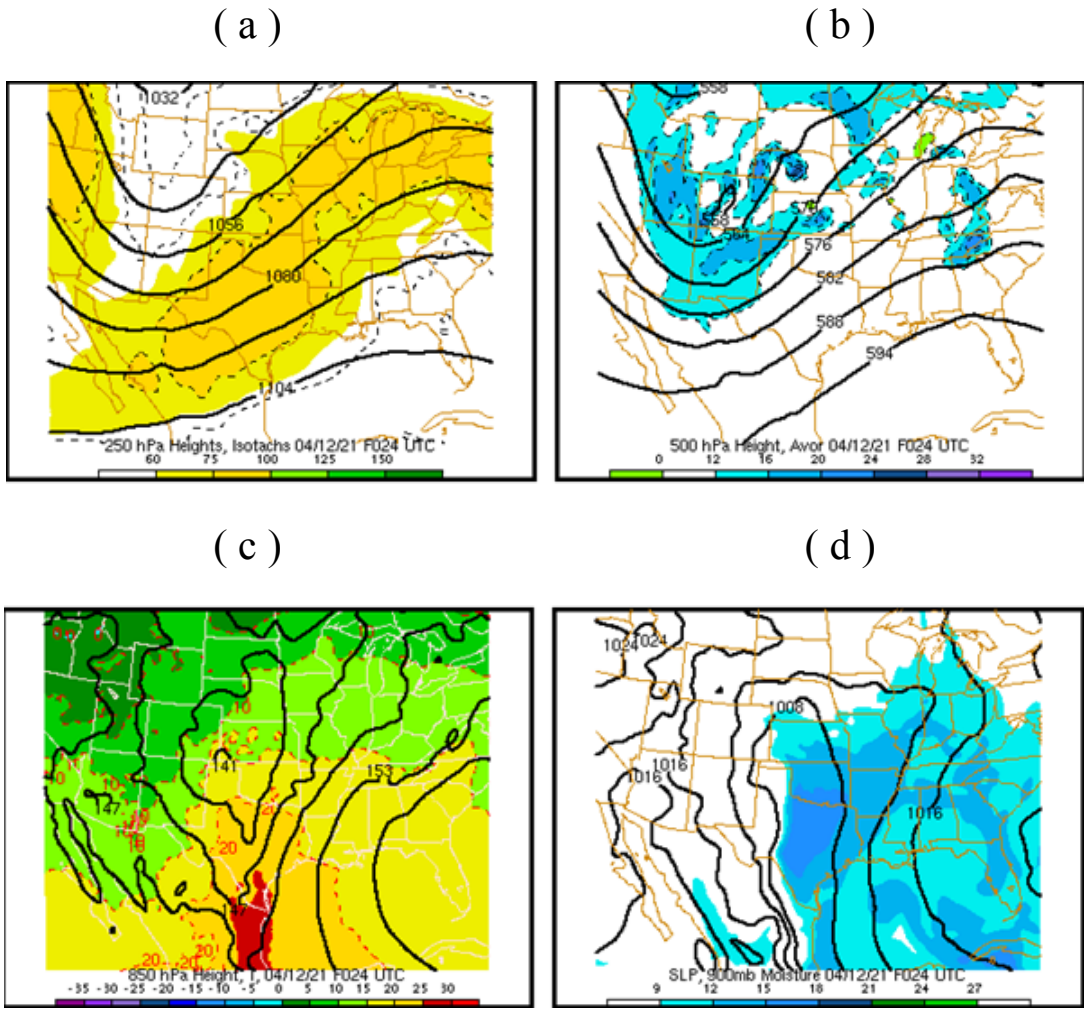

Figure 3.52: Four panel plot of atmospheric parameters at F24 (1200UTC on Day 2) for the strongly-forced event future simulation using 36km grid spacing.

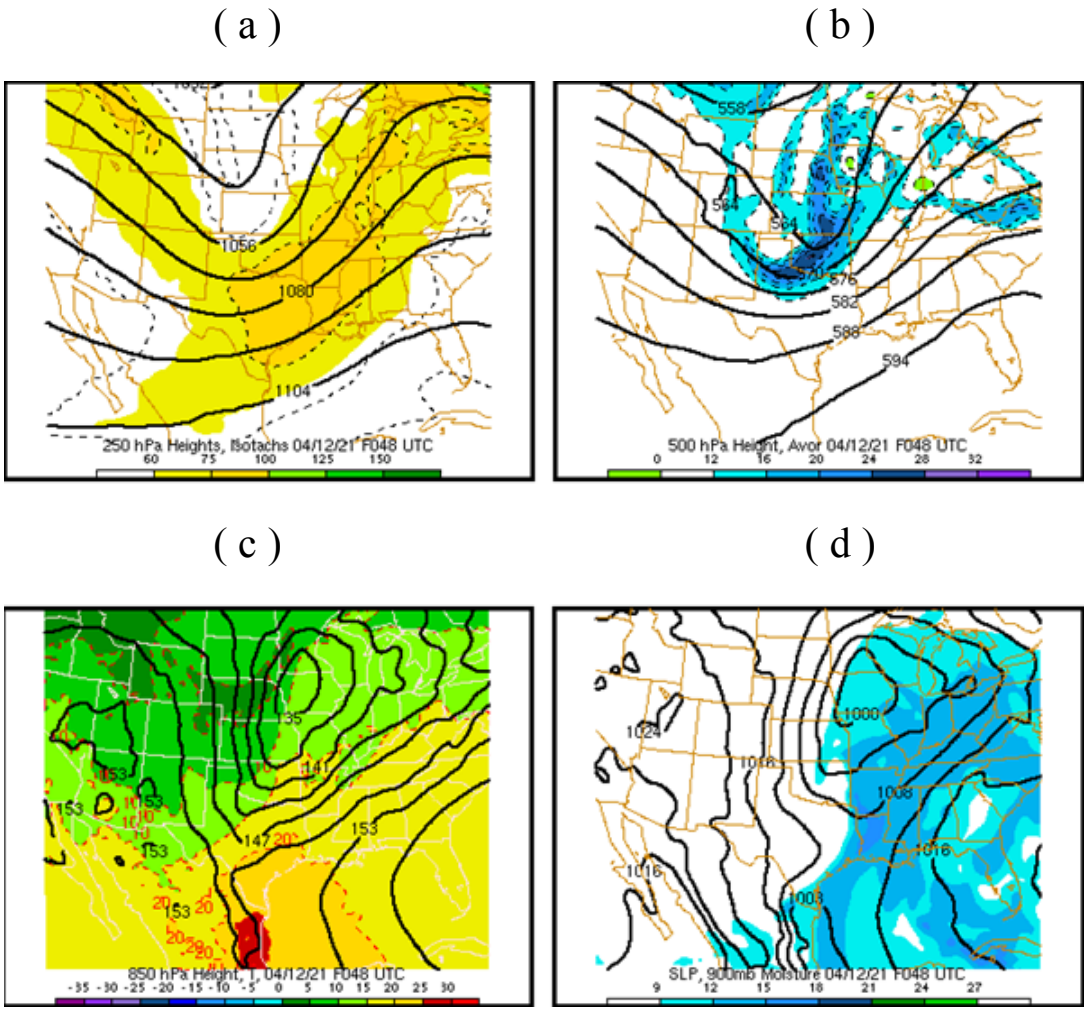

Figure 3.53: Four panel plot of atmospheric parameters at F48 (1200UTC on Day 3) for the strongly-forced event future simulation using 36km grid spacing; can be compared to the F48 four panel plots from strongly-forced event present-day simulation in Figure 3.44.

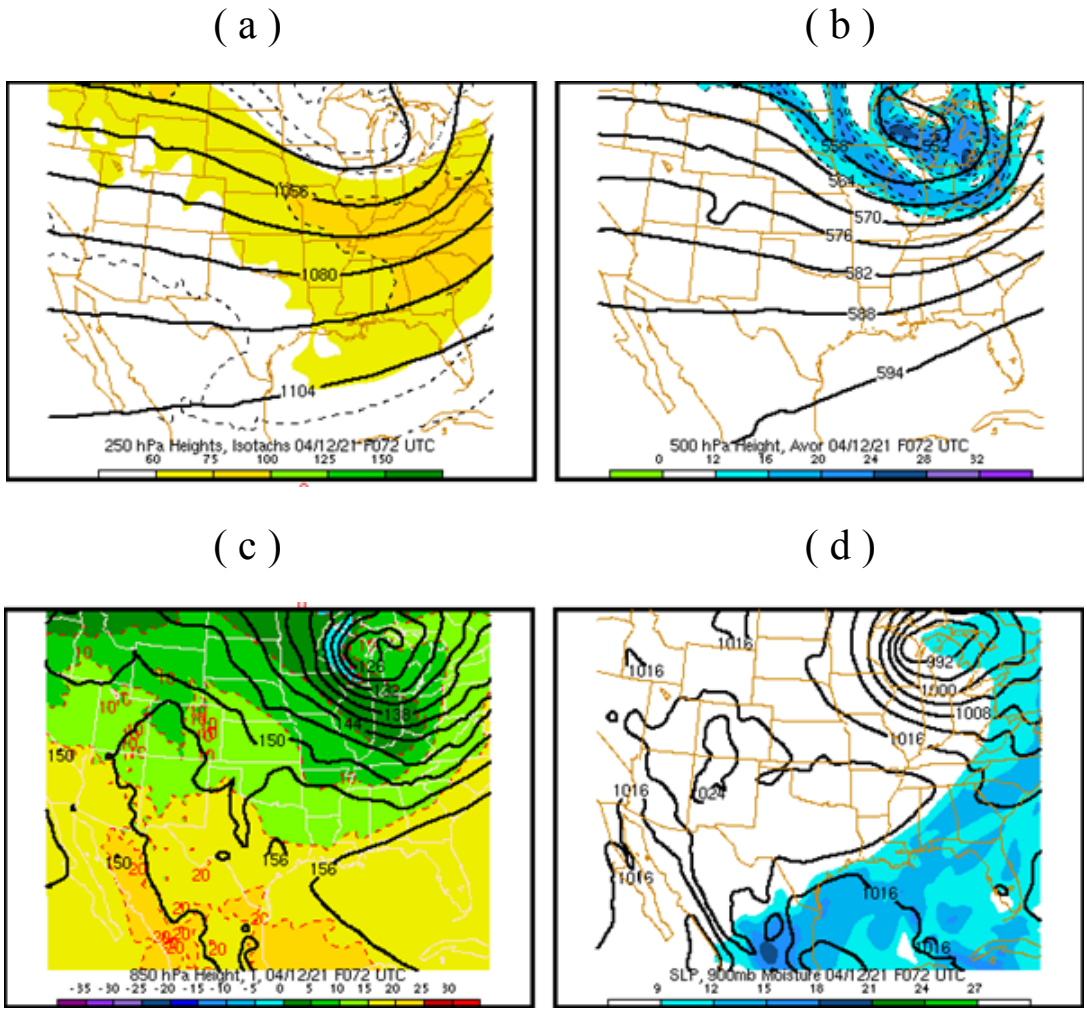

Figure 3.54: Four panel plot of atmospheric parameters at F72 (1200UTC on Day 4) for the strongly-forced event future simulation using 36km grid spacing.

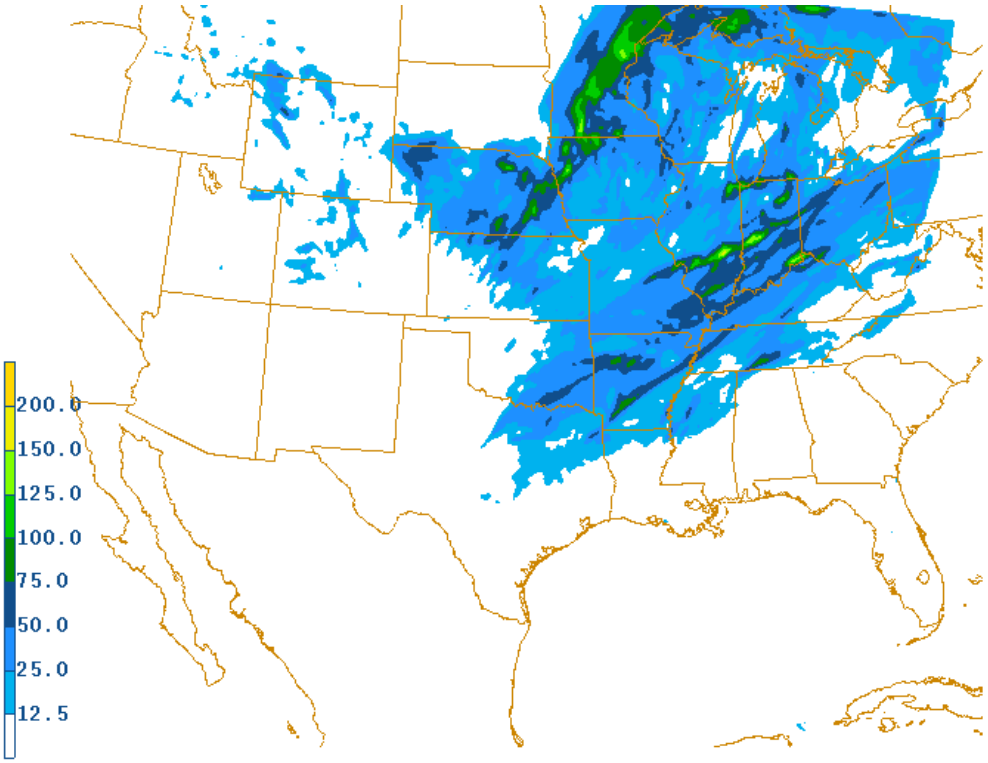

Figure 3.55: Total 72 hour precipitation (mm) for the strongly-forced event future simulation using 12km grid spacing; can be compared to F72 total precipitation from the strongly-forced event present-day run in Figure 3.46.

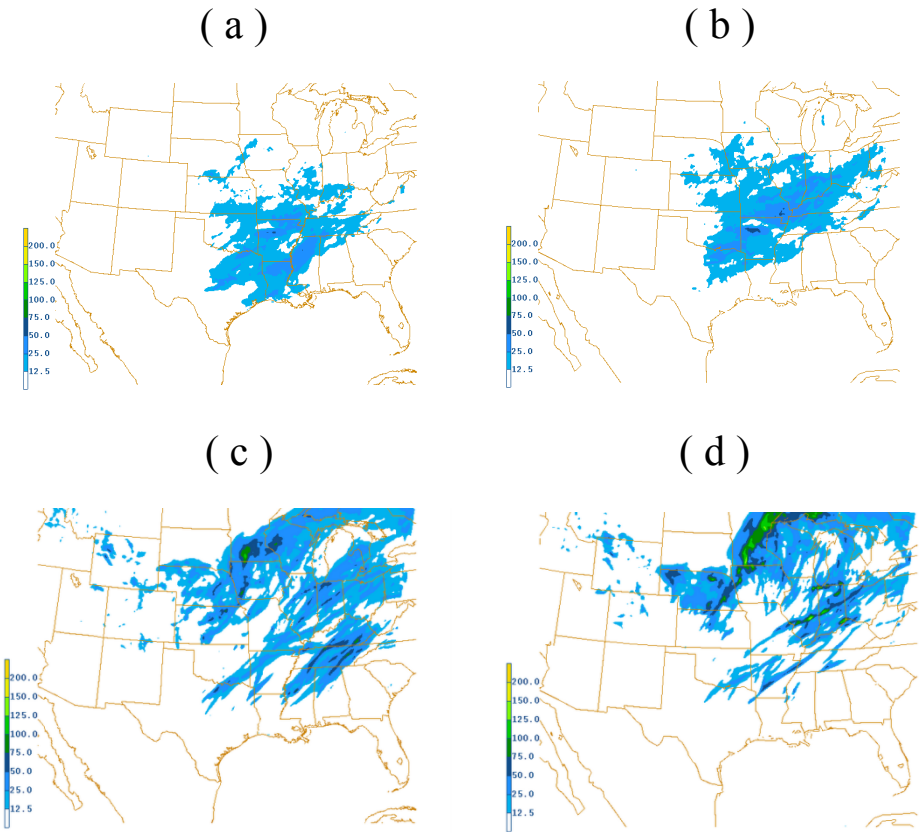

Figure 3.56: The 72 hour total precipitation values for the strongly-forced event: (a) Present-day convective precipitation, (b) Future convective precipitation, (c) Present-day stratiform precipitation, (d) Future stratiform precipitation.

(a)

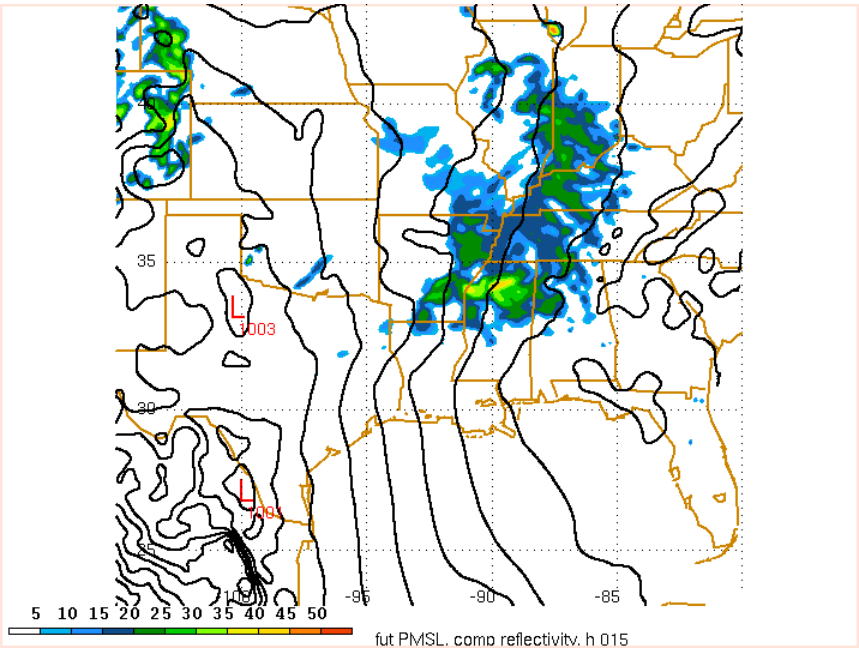

(b)

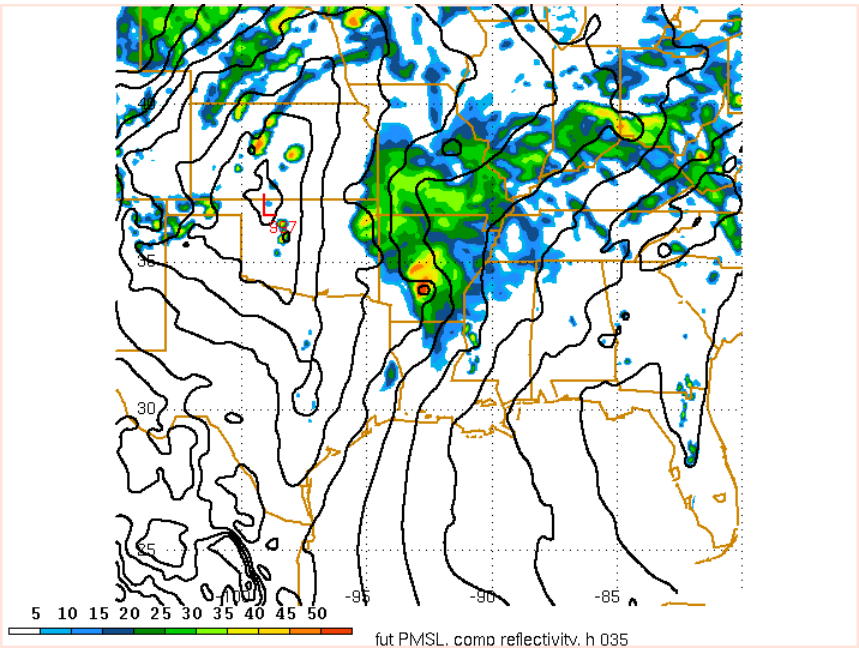

Figure 3.57: Sea level pressure (lowest pressure of 997mb) and reflectivity for the future simulation of the strongly-forced event using 12km grid spacing: (a) F15, (b) F35.

(a)

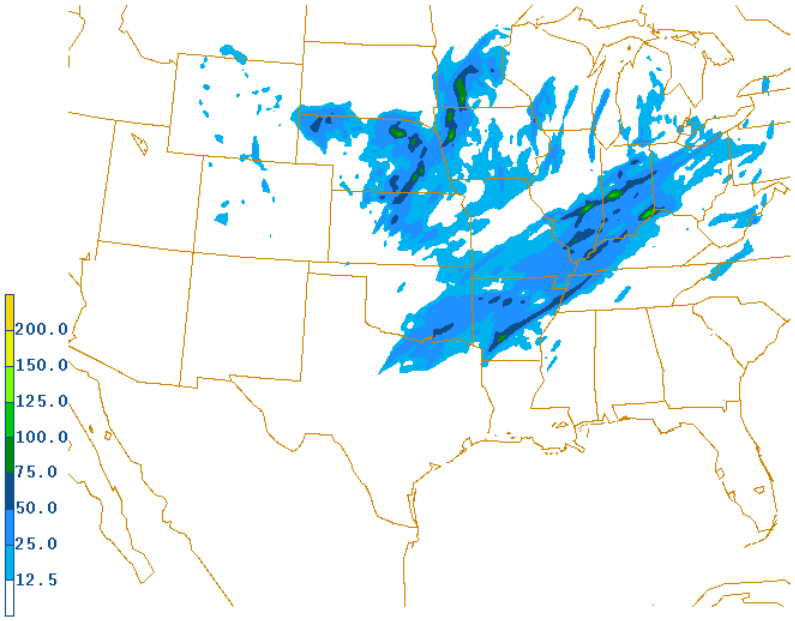

(b)

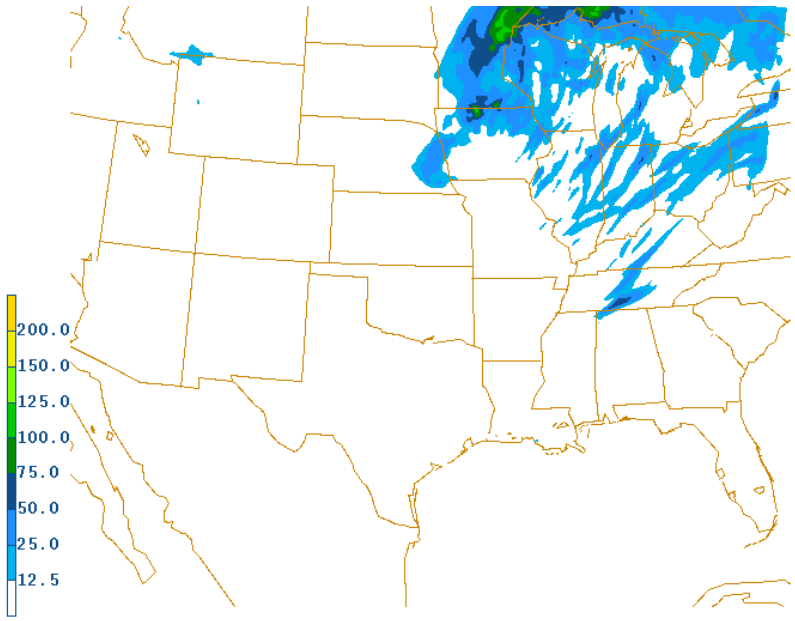

Figure 3.58: Precipitation (mm) difference in the future simulation of the strongly-forced event using 12km grid spacing: (a) F48 – F24, (b) F72-F48.

(a)

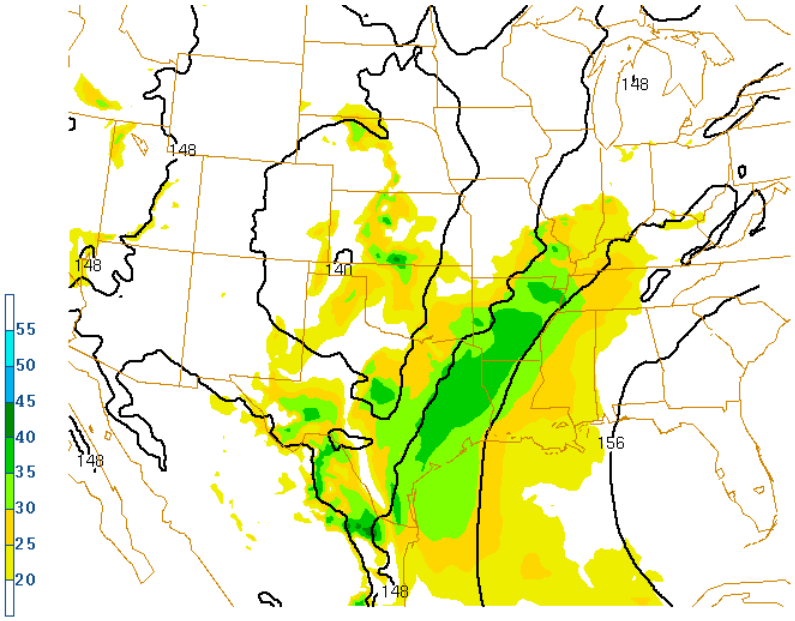

(b)

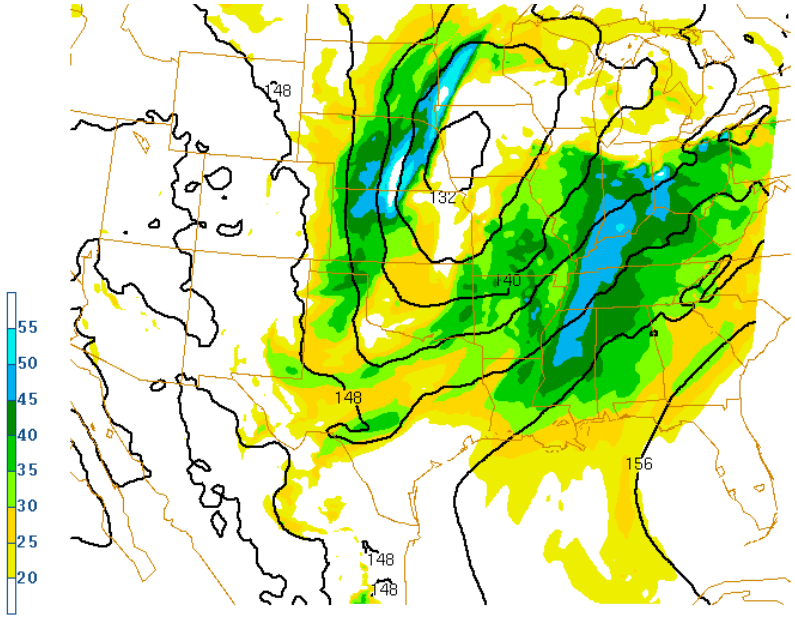

Figure 3.59: Isotachs (kt) at 850mb with the 850mb heights (contour interval of 4 dam) using 12km grid spacing for the strongly-forced event future simulation: (a) F24, (b) F48.

(a)

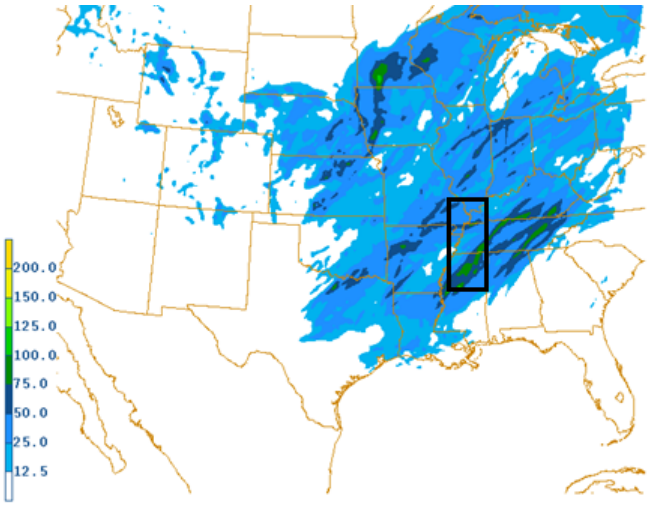

(b)

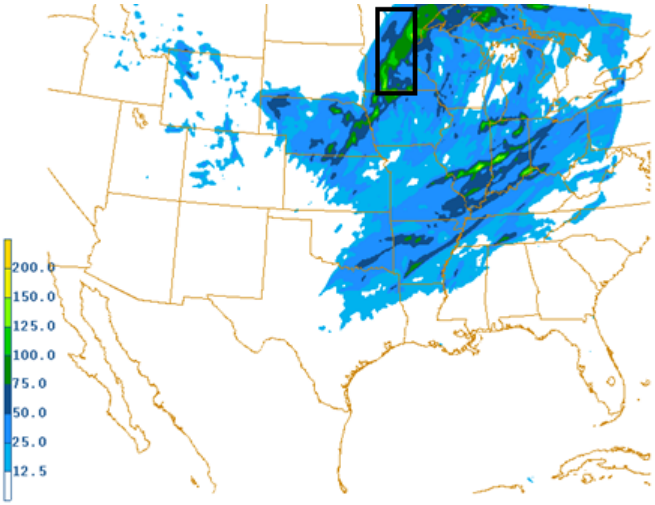

Figure 3.60: Total precipitation averaged over areas of heaviest precipitation for the strongly-forced event: (a) Present-day, (b) Future.

(a)

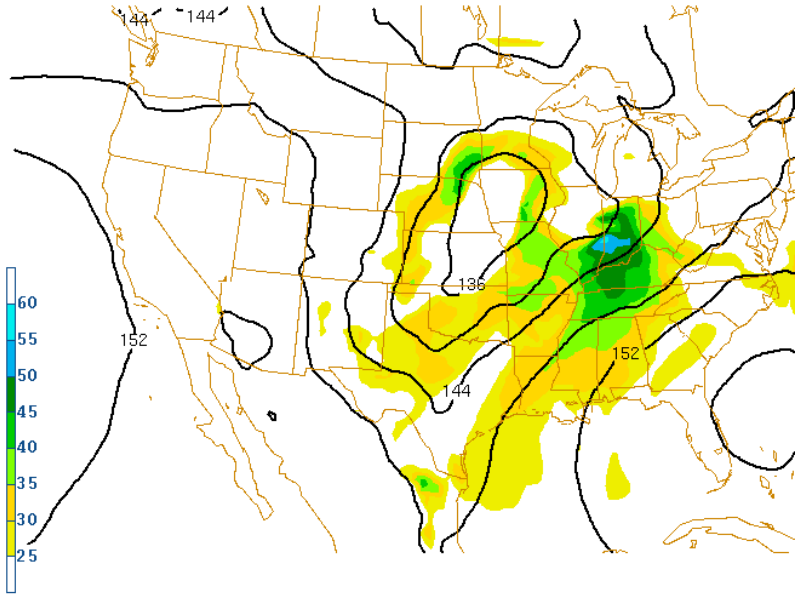

(b)

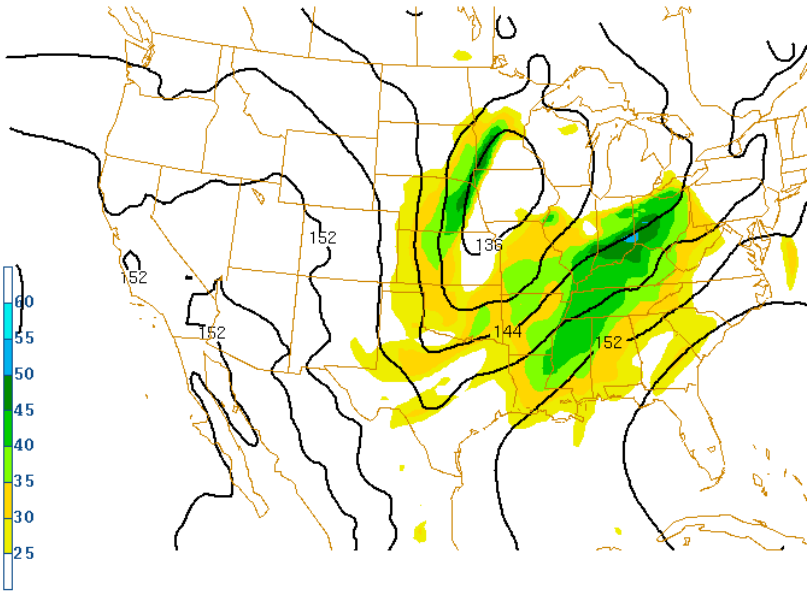

Figure 3.61: 850mb isotachs (kt) at F48 for the strongly-forced event using 36km: (a) present-day simulation, (b) future simulation.

(a)

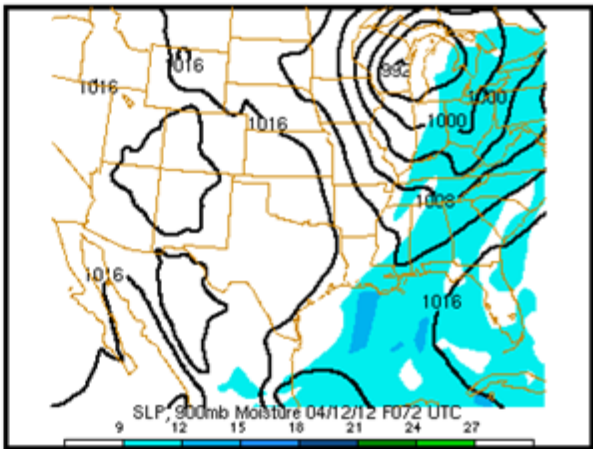

(b)

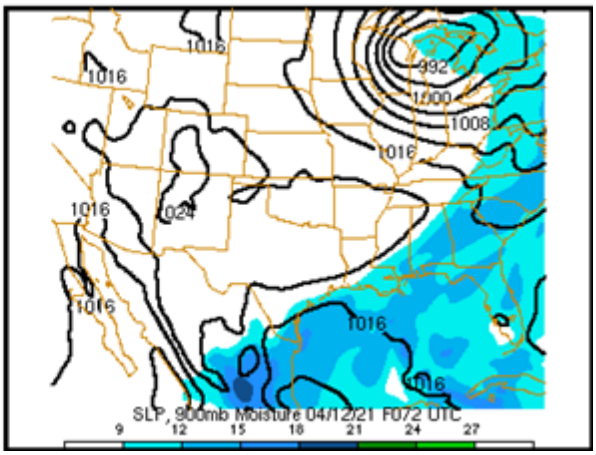

Figure 3.62: Sea-level pressure and 900mb specific humidity at F72: (a) Present-day simulation, (b) Future simulation.

REFERENCES

Ahmadi-givi, F., G. C. Graig, R. S. Plant, 2004: The dynamics of a midlatitude cyclone with very strong latent-heat release. *Q. J. R. Meteorol. Soc.*, 130, 295-323.

Allen, M. R., W. J. Ingram, 2002: Constraints on future changes in climate and the hydrologic cycle. *Nature*, 419, 224-232.

Allen, R. P., B. J. Soden, 2008: Atmospheric warming and the amplification of precipitation extremes. *Science*, 321, 1481-1484.

Boer, G. J., 1995: Some dynamical consequences of greenhouse gas warming. *Atmosphere -Ocean*, 33, 731−751.

Brennan, M. J., G. M. Lackmann, K. M. Mahoney, 2008: Potential vorticity thinking in operations: the utility of nonconservation. *Wea. and Forecast.*, 23, 168-182.

Bukovsky, M. S., D. J. Karoly, 2006: A brief evaluation of precipitation from the North American Regional Reanalysis. *J. Hydrometeor.*, 8, 837-846.

Bukovsky, M. S., D. J. Karoly, 2009: Precipitation simulations using WRF as a nested regional climate model. *J. Appl. Met. Clim.*, 48, 2152−2159.

Chen, G., I. M. Held, W. A. Robinson, 2007: Sensitivity of the latitude of the surface westerlies to surface friction. *J. Atmos. Sci*., 64, 2899−2915.

Chou, C., J. D. Neelin, 2004: Mechanisms of global warming impacts on regional tropical precipitation. *J. Clim.*, 17, 2688-2701.

Chou, C., C. Chen, P. Tan, K. Chen, 2012: Mechanisms for global warming impacts on precipitation frequency and intensity. *J. Clim.*, 25, 3291-3306.

Christensen, O. B., J. J. Christensen, 2004: Intensification of extreme European summer precipitation in a warmer climate. *Glob. and Planet. Change*, 44, 107-117.

Doswell, C. A., et al. 1996 Doswell, C. A., H. E. Brooks, and R. A. Maddox, 1996: Flash flood forecasting: An ingredients-based methodology. Wea. Forecasting, 11, 560–581.

Emore, S., S. J. Brown, 2005: Dynamic and thermodynamic changes in mean and extreme precipitation under changed climate. *Geophys. Res. Lett.*, 32, L17706.

Frei, C., C. Schär, D. Lüthi, and H. C. Davies (1998), Heavy precipitation processes in a warmer climate, Geophys. Res. Lett., 25, 1431–1434.

Gettelman, A., Q. Fu, 2008: Observed and simulated upper-tropospheric water vapor feedback. *J. Clim.*, 21, 3282-3289.

Groisman, P. Y., R. W. Knight, D. R. Easterling, T. R. Karl, G. C. Hegerl, and V. N. Razuvaev, 2005: Trends in intense precipitation in the climate record. J. Climate, 18, 1326–1350.

Held, I. M., B. J. Soden, 2006: Robust responses of the hydrological cycle to global warming. *J. Clim.*, 19, 5686-5699.

Hu, Q., S. Feng, 2001: Climatic role of the southerly flow from the Gulf of Mexico in interannual variations in summer rainfall in the central United States. *J. Clim.*, 14, 3156-3170.

Karl, T. R., and R. W. Knight, 1998: Secular trends of precipitation amount, frequency, and intensity in the USA. Bull. Amer. Meteor. Soc., 79, 231–241.

Kosambi, D. D., 1982: Culture and civilization of Ancient India in historical outline. ISBN 13:9780706913996

Lackmann, G. M., and J. R. Gyakum, 1999: Heavy cold-season precipitation in the Northwestern United States: Synoptic climatology and an analysis of the flood of 17-18 January 1986. Wea. Forecasting, 14, 687-700.

Lackmann, G. M., 2002: Cold-frontal potential vorticity maxima, the low-level jet, and moisture transport in extratropical cyclones. *Mon. Wea. Rev.*, 130, 59-74.

Lackmann, G. M., 2012: The south-central US flood of May 2010, present and future. *Submitted to J. Climate June 2012.*

Lambert, F. H., A. R. Stine, N. Y. Krakauer, J. C. H. Chiang, 2008: How much will precipitation increase with global warming? *EOS*, 89, 193-194.

Lenderink, G., E. van Meijgaard, 2008: Increase in hourly precipitation extremes beyond expectations from temperature changes. *Nat. Geosci.*, 1, 511-514.

Lenderink, G., E. van Meijgaard, 2010: Linking changes in hourly precipitation extremes to the Clausius-Clapeyron relation. *Koninklijk Nederlands Meteorologisch Instituut*.

Li, F., W. Collins, M. Wehner, D. Williamson, J. Olson, C. Algieri, 2011: Impact of horizontal resolution on simulation of precipitation extremes in an aqua-planet version of Community Atmospheric Model (CAM3). *Tellus*, 63, 884-892.

Maddox, R. A., 1979: A methodology for forecasting heavy convective precipitation and flash flooding. *Nat. Wea. Digest*, 4, 30-42.

Maddox, R. A., C. F. Chappell, and L. R. Hoxit, 1979: Synoptic and meso-alpha scale aspects of flash flood episodes. Bull. Amer. Meteor. Soc., 60, 115-123.

Mahoney, K., M. A. Alexander, G. Thompson, J. J. Barsugli, J. D. Scott, 2012: Changes in hail and flood risk in high-resolution simulations over Colorado's mountains. *Nat. Clim. Change*, 2, 125-131.

Milly, P. C., R. T. Wetherald, K. A. Dunne, T. L. Delworth, 2002: Increasing risk of great floods in a changing climate. *Nature*, 415, 514-517.

Mo, C. K., J. Nogues-Paegle, J. Paegle, 1995: Physical mechanisms of the 1993 summer floods. *J. Atmos. Sci.*, 52, 879-895.

Moon-hyon, N., 2012: Jang Yeong-sil: Inventor of the striking clepsydra during the reign of King Sejong in Joseon. *Hist. of Mechan. and Mach. Sci.*, 15, 2, 83-105.

Paegle, J., K. C. Mo, J. Nogues-Paegle, 1996: Dependence of simulated precipitation on surface evaporation during the 1993 United States summer floods. *Mon. Wea. Rev.*, 124, 345-361.

Paeth, H., A. Hense, 2006: On the linear response of tropical African climate to SST changes deduced from regional climate model simulations. *Theor. Appl. Climatol.*, 83, 1-19.

Pall, P., M. R. Allen, D. A. Stone, 2007: Testing the Clausius-Clapeyron constraint on changes in extreme precipitation under CO2 warming. *Clim. Dyn.*, 28, 351-363.

Palmer, T. N., J. Raisanen, 2002: Quantifying the risk of extreme seasonal precipitation events in a changing climate. *Nature*, 415, 512-514.

Schumacher, R. S., and R. H. Johnson, 2006: Characteristics of U.S. extreme rain events during 1999-2003. Wea. Forecasting, 21, 69–85.

Seager, R., N. Naik, G. A. Vecchi, 2010: Thermodynamic and dynamic mechanisms for large-scale changes in the hydrologic cycle in response to global warming. *J. Clim.*, 23, 4651-4668.

Shaw, S. B., A. A. Royem, S. J. Riha, 2011: The relationship between extreme hourly precipitation and surface temperature in different hydroclimatic regions of the United States. *J. Hydrometeor.*, 12, 319-325.

Soden, B. J., D. L. Jackson, V. Ramaswamy, M. D. Schwarzkopf, X. Huang, 2005: The radiative signature of upper tropospheric moistening. *Science*, 4, 841-844.

Skamarock, W. C., J. B. Klemp, J. Dudhia, D. O. Gill, D. M. Barker, M. Duda, X.-Y. Huang, W. Wang and J. G. Powers, 2008: A description of the Advanced Research WRF Version 3. *NCAR Tech. Note*, 1-105.

Solomon, S., D. Qin, M. Manning, Z. Chen, M. Marquis, K.B. Averyt, M. Tignor and H.L. Miller, 2007: Contribution of Working Group I to the Fourth Assessment Report of the Intergovernmental Panel on Climate Change, 2007. *Cambridge Univ. Press*, 1-996.

Stensrud, D. J., 1996: Importance of low-level jets to climate: a review. *J. Clim.*, 9, 1698 -1711.

Sugiyama, M., H. Shiogama, S. Emori, 2010: Precipitation extreme changes exceeding moisture content increases in MIROC and IPCC climate models. *PNAS*, 107, 571-575.

Symons, G. J., 1891: A contribution to the history of rain gauges. *Quart. Jour. of the Royal Met.Soc.*, 17, 79, 127-142.

Trenberth, K. E., 1999: Conceptual framework for changes of extremes of the hydrological cycle with climate change, Clim. Change, 42, 327– 339.

Trenberth, K. E., A. Dai, R. M. Rasmussen, and D. B. Parsons, 2003:, The changing character of precipitation, Bull. Amer. Meteor. Soc., 84, 1205–1217.

Willett, K. M., N. P. Gillett, P. D. Jones, and P. W. Thorne, 2007: Attribution of observed surface humidity changes to human influence. Nature, 449, 710.

Zhao, L., J. Jin, S. Wang, M. B. Elk, 2012: Integration of remote-sensing data with WRF to improve lake-effect precipitation simulations over the Great Lakes region. *J. Geophys. Res.*, 117, D09102, doi:10.1029/2011JD016979.

APPENDIX

Appendix A

Appendix A: Extreme Precipitation Event Classification

The extreme precipitation events are classified based on region of the United States in which they occurred, the season, and the flooding type. There are 136 total extreme precipitation cases consisting of six mesohigh, seven frontal, 32 tropical, and 91 synoptic events. North American Regional Reanalysis (NARR) data are used to determine which category each event fell in based on the four panel plots of the atmospheric conditions. These are displayed in the table below along with the region in which they occurred. Some events have multiple dates and for those events, the day with the most precipitation is selected.

Figure A. 1: Table showing all 136 extreme precipitation events in chronological order from 1985 to 2011 categorized by region in the United States in which they occur and the flooding-type category.

Dates of the Precipitation Event	**Geographical Region**	**Synoptic/Frontal/ Mesohigh/Tropical**
April 11-12, 1985	South	Synoptic
August 30-September 5, 1985	Southeast	Tropical
October 18-20, 1985	South	Synoptic
October 27-28, 1985	South	Tropical
November 3-5, 1985	East	Synoptic
September 9-17, 1986	North	Synoptic
September 26-October 3, 1986	Central	Mesohigh
November 22-26, 1986	Northwest	Synoptic

July 2-3, 1987	Northeast/Central	Synoptic
December 25-27, 1987	Central/East	Synoptic
September 5-9, 1988	Southeast	Synoptic
March 28, 1989	South	Synoptic
May 17-19, 1989	South	Synoptic
January 9-10, 1990	Northwest	Synoptic
January 25, 1990	South	Synoptic
March 16-17, 1990	South/Southeast	Synoptic
April 26-May 2, 1990	South/Central	Synoptic
September 7-9, 1990	Central/East	Synoptic
April 5-6, 1991	South	Frontal
April 29-30, 1991	South	Synoptic
October 8-13, 1991	Southeast	Mesohigh
December 2-3, 1991	Central	Synoptic
December 19-22, 1991	South	Synoptic
August 23-28, 1992	South	Tropical
September 25-27, 1993	Central	Synoptic
April 9-18, 1994	Central	Synoptic
July 4-7, 1994	Southeast	Tropical
October 17-19, 1994	South	Synoptic
January 9-14, 1995	Northwest	Synoptic
August 24-28, 1995	East	Tropical
October 4-5, 1995	South/Southeast/East	Tropical
November 28-December 10, 1995	Northwest	Synoptic
February 7-9, 1996	Northwest	Synoptic
September 5-12, 1996	East/Northeast	Tropical
October 20-22, 1996	Northeast	Tropical
December 26, 1996-January 2, 1997	Northwest	Synoptic

February 28-March 2,1997	Central	Synoptic
June 21-22, 1997	South	Frontal
December 20-21, 1997	South	Synoptic
February 3-24, 1998	Southeast/Northeast/East	Synoptic
June 14-15, 1998	Northeast	Synoptic
August 22-23, 1998	South	Tropical
August 27-29, 1998	East	Tropical
August 31-September 3, 1998	Southeast	Tropical
September 11-13, 1998	South	Tropical
October 18, 1998	South	Synoptic
November 1, 1998	Central	Synoptic
November 13, 1998	South	Synoptic
December 28-30, 1998	Northwest	Synoptic
January 29-30, 1999	South	Synoptic
July 4-5, 1999	North	Synoptic
September 14-October 5, 1999	East	Tropical
November 2-6, 2000	South	Synoptic
June 6-12, 2001	South	Tropical
November 15-16, 2001	South	Frontal
November 28-29, 2001	South	Synoptic
December 17-25, 2001	Central	Synoptic
March 17-24, 2002	South/East	Synoptic
June 3-4, 2002	Central	Synoptic
June 9-10, 2002	North	Synoptic
July 14-16, 2002	South	Frontal
September 7-8, 2002	South	Tropical
September 26-27, 2002	South	Tropical
October 20-November 5, 2002	South	Synoptic
December 14-24, 2002	West/Northwest	Synoptic
January 1-6, 2003	Southeast	Synoptic

February 12-13, 2003	West/Southwest	Synoptic
June 21-24, 2003	Southeast	Mesohigh
August 30-31, 2003	Central	Mesohigh
September 1-2, 2003	Central	Tropical
September 19-24, 2003	East/Northeast	Tropical
October 11-12, 2003	South	Mesohigh
October 19-21, 2003	Northwest	Synoptic
March 4-5, 2004	Central	Synoptic
April 23-24, 2004	Central	Synoptic
May 1, 2004	South	Synoptic
May 13-14, 2004	South	Synoptic
May 22-23, 2004	Central	Synoptic
May 27-June 1, 2004	Central	Synoptic
June 5-10, 2004	South	Frontal
June 12-14, 2004	Northeast	Synoptic
August 30-September 1, 2004	East	Tropical
September 5-9, 2004	East	Tropical
September 17-18, 2004	Northeast	Tropical
November 14-24, 2004	South	Synoptic
January 8-11, 2005	West	Synoptic
April 3-6, 2005	Northeast	Synoptic
August 29-September 19, 2005	South	Tropical
September 24-28, 2005	South/Southeast	Tropical
October 8-9, 2005	Northeast	Tropical
October 13-16, 2005	Northeast	Synoptic
December 30-31, 2005	West	Synoptic
March 20-22, 2006	South	Synoptic
May 14-17, 2006	Northeast	Mesohigh
May 28-June 2, 2006	South	Frontal
June 26-29, 2006	East	Tropical
July 26-27, 2006	South	Frontal
July 28, 2006	Central	Synoptic
September 23-24, 2006	Central/East	Synoptic
October 16-17, 2006	South	Synoptic
November 5-8, 2006	Northwest	Tropical

March 11-13, 2007	South	Frontal
April 14-17, 2007	Central/Eastern	Synoptic
May 6-10, 2007	Central	Synoptic
May 25-29, 2007	South	Frontal
June 17-22, 2007	South	Synoptic
June 27-July 2, 2007	South	Frontal
August 23-25, 2007	Central	Synoptic
December 3-4, 2007	Northwest	Tropical
March 18-19, 2008	South/Central	Synoptic
4-Apr-08	Central	Synoptic
10-Apr-08	Central	Synoptic
May 12-13, 2008	East	Synoptic
August 19-20, 2008	South	Frontal
August 20-28, 2008	Southeast	Tropical
September 1-2, 2008	South	Tropical
September 12-14, 2008	South	Tropical
November 7-12, 2008	Northwest	Synoptic
December 26-28, 2008	Northwest	Synoptic
January 2, 2009	Northwest	Synoptic
January 8, 2009	Northwest	Synoptic
April 2-3, 2009	Southeast	Synoptic
May 2-4, 2009	South/Central	Synoptic
May 19-22, 2009	Southeast	Synoptic
August 4-5, 2009	Central	Synoptic
September 21-26, 2009	Southeast/East	Synoptic
November 10-13, 2009	Southeast/East	Tropical
December 2-3, 2009	South/Southeast	Synoptic
December 15, 2009	South	Synoptic
March 15, 2010	Northeast	Synoptic
March 29-31, 2010	Northeast	Synoptic
May 1-5, 2010	Central/South	Synoptic
June 9-10, 2010	South	Frontal
September 7-11, 2010	South	Tropical
December 18-23, 2010	West	Synoptic

April 24-28, 2011	Central	Synoptic

These events are also mapped using Google maps to identify the areas where the extreme precipitation events occur according to the extreme event categorization discussed above. This map is shown below.

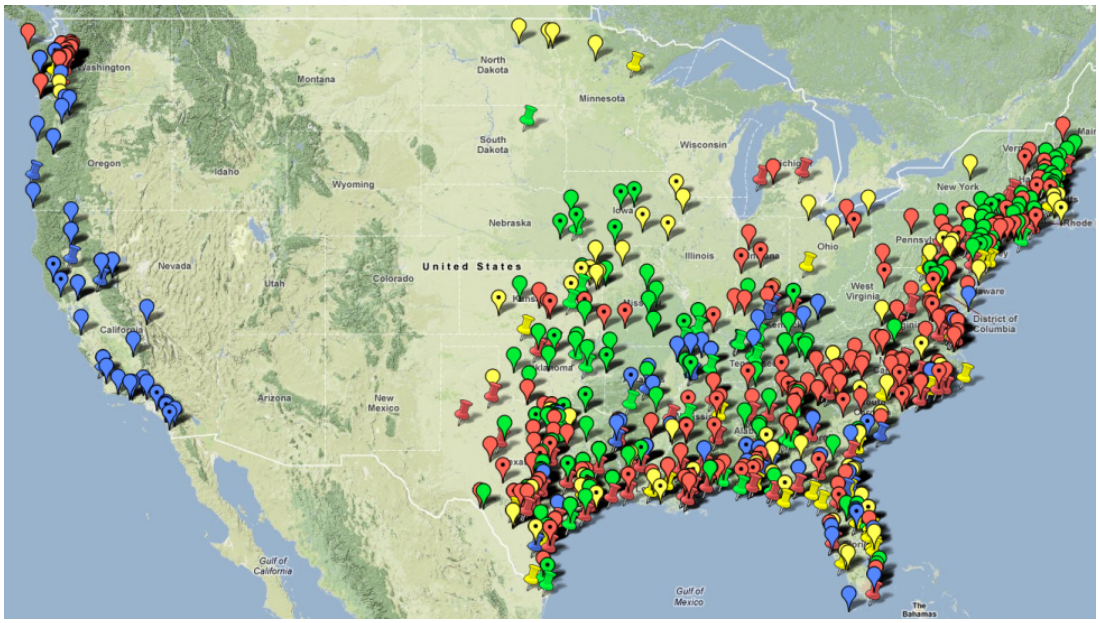

Figure A.2: Map showing the rain gauge stations where extreme precipitation amounts were recorded for the events used in this research. The placemarkers are color-coded seasonally; blue for winter, green from spring, yellow for summer, and red for fall. The placemarkers with no dot in the middle and a round top represent events with 3-4 inches of precipitation, the placemarkers with a dot in the middle and a rounded top represent events with 4-5 inches of precipitation, and the placemarkers with no dot in the middle and a flat top represent events with more than 5 inches of precipitation.